3805 Old Easton Road
Doylestown, PA 18902 USA

[redacted] **ANNUAL REPORT FOR 2023**

Dear Evrys Bio Investor:

Hello! I hope that you and your families are doing well. The Company has done quite well in the recent macroeconomic environment that has been unfavorable for biotechnology companies. As you know, the bottom fell out of the biotech IPO market at the end of 2021. This continued to have a trickle-down effect through all of 2022 and 2023 as public and private investors reassessed their positions.

Despite these unfavorable conditions, the Company completed a [redacted] financing in September 2022, to help fund Evrys' first IND for EV-100 to treat opportunistic infections in transplant recipients. In addition, in the first half of 2023, Evrys satisfied certain scientific milestones and provided the Department of Defense (DoD) an alternate human clinical path that reduces the timeline to register a medical countermeasure (MCM) by 3 or more years. Therefore, DoD promoted EV-100 to Drug Prototype status for the MCM contract. EV-100 promotion to Drug Prototype has a significant positive impact for our investors: EV-100 is now robustly funded with non-dilutive moneys through the end of its first phase 1 human clinical trial in 2025. Indeed, Evrys is projecting to operate with a minimal cash burn into 2025 while progressing a pipeline of innovative antivirals. We are also actively working on a contract application for an additional non-dilutive government contract for hemorrhagic fever viruses.

The Company is growing its management team with laser focus to achieve our next key inflection point, namely our IND. We hope this inflection and other scientific achievements will pave the path to one or more strategic pharma partnerships. As you know, Evrys was founded in 2012 based on groundbreaking basic research at Princeton University. While our innovation journey has taken longer than expected, we continue to benefit from the significant non-dilutive support of the major infectious disease stakeholder during COVID, the U.S. Government. The government has been our partner since our first awarded grant in 2014, only one year after opening our laboratory doors, de-risking our innovation to realize the potential to transform patient care.

Research and Development Summary

Transplant infectious disease:

- **Preclinical research to support translation to the clinic for cytomegalovirus (CMV) prophylaxis:** We have made significant progress to further understand the host-targeted mechanism for Evrys' first-in-class SIRT2 allosteric modulators. For the intended first indication in the clinic, CMV prophylaxis, SIRT2 modulation is effective against diverse clinical isolates of human cytomegalovirus (CMV) including drug resistant isolates. In cell-based assays, EV-100 demonstrates superior virologic control compared to standard-of-care direct-acting antivirals for CMV. Importantly, [redacted]

[redacted] when EV-100 is combined with direct-acting antivirals (Fig. 1); the preclinical data comprises proof-of-concept (PoC) that EV-100 can improve clinical outcomes and provide a high barrier to acquired drug resistance as stand-alone and/or when administered with marketed direct-acting antivirals in combination therapy. Noteworthy achievements in 2023 were two publications in high impact journals of Evrys translational research: "An allosteric inhibitor of sirtuin 2 deacetylase activity exhibits broad-spectrum antiviral activity" in The Journal of Clinical Investigation; and "Inhibition of SIRT2 promotes death of human cytomegalovirus-infected peripheral blood monocytes via apoptosis and necroptosis" in Antiviral Research (both publications attached; the described compound, FLS-359, is a precursor to EV-100).

Figure 1. EV-100 [redacted] with Direct-Acting Antivirals. In cell-culture experiments, different concentrations of two drugs are tested in a grid with increasing drug concentrations of one drug shown along the x-axis and the other on the y-axis. In the 3-D plots, gray represents the result if a purely additive effect is observed; below the gray plane on the z-axis, red, represents antagonism between the two drugs in the combination (at the x/y-axis concentration of each drug tested); above, green, represents synergy. The observed antagonism of maribavir (MBV) versus ganciclovir (GCV), two direct-acting antivirals is known in the literature. This antagonism contraindicates combination dosing of MBV and GCV in the clinic, due to less than an additive effect if each drug were dosed alone. EV-100 was tested in combination with 3 direct-acting antivirals, [redacted]

- **Preclinical research to support translation to the clinic to treat Lassa Fever Virus (LASV) infection:** Validation that Evrys' host targeted SIRT2 modulators simultaneously confer antiviral effectiveness against filoviruses, arenaviruses, and alphaviruses had been achieved in the DoD sponsored MCM program in 2022. Lead optimization for the MCM continued in 2023. Independent of DoD funding, Evrys Bio had started development activities in 2022 for EV-100 civilian use to address CMV infection. At the

beginning of 2023, Nigeria experienced a large outbreak of Lassa fever through April 2023 with a 20% increase in confirmed cases in comparison with cases reported during the same period in 2022; Equatorial Guinea and Tanzania experienced their first recorded outbreaks of Marburg virus disease starting in January and March 2023, respectively.

In May 2023, Evrys Bio opportunistically proposed to our DoD sponsors that EV-100 be promoted to Drug Prototype status for MCM use (Table 1). [redacted] By pulling forward DoD contract Options 1, 2, and 3 funds, ~$17 M in total, for CMC, IND-enablement, and the phase 1 clinical trial, we could accelerate EV-100 development for MCM use, by leveraging the IND for CMV infection. The desired outcome is to accelerate EV-100 through the completion of the phase 1 clinical trial as soon as possible in time for the following seasonal outbreak of LASV. This provides a human clinical development path for the DoD sponsored MCM product registration that is > 3-years faster than the originally contracted Animal Rule strategy. As a result of this buy-in, DoD additionally reaped the benefit of Evrys investment into EV-100 development prior to July 1, 2023 (when cost-recovery on EV-100 Drug Prototype activities was shifted to DoD). This was a watershed moment for Evrys during the recent industry contraction because the Company reaps the benefit of significant non-dilutive de-risking of EV-100 for civilian (CMV prophylaxis) use, to the end of our first-in-human clinical trial.

Table 1. Pan-Viral Effectiveness of EV-100 Including Biothreat Pathogens. Missing data for EV-100 represents viruses yet to be tested.

Virus	Virus Family	Cell Line (CC50)	FLS-359* EC_{50}	EV-100 EC_{50}	Comparator EC_{50}	Comparator Standard of Care (SOC)
Zika	flavivirus	human MRC5 (> 25)	0.4	[redacted]	3.9	amodiaquine
HCoV-OC43	beta coronavirus	human MRC5 (> 25)	0.5	0.4	1.6	hydroxychloroquine
CMV	beta herpesvirus	human MRC5 (> 25)	0.6	0.7	1.4	ganciclovir (SOC)
SARS-CoV2	beta coronavirus	human Calu 3 (16)	0.6	0.4	0.07	remdesivir (SOC)
Influenza A	orthomyxovirus	human HNBE (> 100)	1.2		0.71	ribavirin
Influenza B	orthomyxovirus	canine MDCK (> 5)	1.2		> 25	oseltamivir (SOC)
HCoV-229E	alpha coronavirus	human MRC5 (> 25)	1.6		0.04	remdesivir
Ad5	adenovirus	human MRC5 (> 25)	1.6		3.1	cidofovir
LASV (Lassa)	arenavirus	[redacted]				
Marburg	filovirus					
VEEV (TC-83)	alphavirus					
Ebola (Sudan)	filovirus					
Influenza A^R	orthomyxovirus	canine MDCK (> 5)	2.5		9	oseltamivir (SOC)
HBV	hepadnavirus	human PHH	5.2	3.2	0.03	tenofovir (SOC)
Epstein-Barr	gamma herpesvirus	human Akata (>100)	3.8		43	ganciclovir
RSV	orthopneumovirus	human MRC5 (> 25)	6.7		16.1	ribavirin

*Shown EC_{50} concentration in μM providing 50% maximal antiviral effectiveness. Underlined indicates EC_{90} reported. CC_{50} drug concentration across assays was ≥ 10-100 μM, the highest concentrations tested. *FLS-359 is structurally similar to EV-100, works through the same mechanism-of-action but is unsuitable for drug development (due to poor in vitro ADME profile).*

- **Chemical manufacturing and controls (CMC):** Pilot-scale (200-gram) process development consisting of six convergent steps was completed for EV-100 drug substance. Evrys also manufactured its first large-scale, > 3-kilogram, batch and initiated a second large batch for Good Laboratory Practice (GLP) toxicity studies in 2024. The Good Manufacturing Practice (GMP) batch will be started in Q2 2024 to provide drug substance material for Evrys first-in-human dosing. Completing CMC for the IND has been slower than anticipated, but our team has stayed on top of the challenges and will continue to do so. To further solidify our path forward, we are evaluating qualifications for an additional, second manufacturer.
- **IND-enabling studies:** Rat and mini pig were selected as the rodent and non-rodent species for the EV-100 IND. We initiated preparation of the FDA Pre-IND meeting package in 2023 and will submit in 2024. DoD backing and financial de-risking allows Evrys to prepay and reserve animals and testing facilities at our favored contract research organizations (CROs). As a result, the 28-day rodent and non-rodent GLP toxicity studies will proceed immediately following receipt of FDA Pre-IND feedback. Evrys expects to submit the IND for EV-100 in Q4 2024.

Viral hepatitis:

- **Preclinical drug discovery:** In our hepatitis B (EV-200) program, we have identified 3 lead compounds, potent with sufficient oral bioavailability. In 2024, we plan to test these in mouse models of chronic hepatitis B infection to achieve animal model PoC.

Medical Counter Measure program for biological threats and emerging infectious diseases:

- **Preclinical drug discovery:** As discussed above, Evrys' clinical stage drug EV-100 was promoted to Drug Prototype to treat LASV infection in the DoD sponsored medical countermeasure (EV-300) program. In parallel, the drug discovery effort continues with further lead optimization in the EV-300 program to identify a Back-Up. [redacted]

  Finding a Back-Up is standard industry practice to proactively de-risk potential yet to be identified "NOGO's" downstream in the clinical development program for EV-100.

Exploratory Research:

- Human SIRT2 modulation is implicated in the literature as a potential therapeutic mechanism to address infection by intracellular *Mycobacterium tuberculosis* (Bhaskar *et al.,* 2020, 2023). Evrys signed a material transfer agreement with a non-governmental organization, the TB Alliance, to test Evrys SIRT2 modulators in bacterial MIC_{90} assays, in bacterial challenge of human macrophage assays, and in a mouse model of bacterial challenge. Successful PoC in the mouse model may lead to (an EV-400) program to treat tuberculosis funded by the TB Alliance.

Figure 2. Five MCM leads dosed at 100 mg/kg/day [redacted] Ebola challenge in mice. Three studies were performed on different days in BSL4 laboratories.

[redacted]

2024 Pipeline Summary: At the start of 2024, Evrys is well positioned with respect to progressing a pipeline of transformative therapies to treat viral infection. We are in a strong scientific position, and our work is drawing attention. Black arrows below represent current and anticipated non-dilutive revenue from government contracts and grants already awarded to Evrys. White and gray arrows represent future studies required for FDA approval. If EV-100 clinical development for CMV prophylaxis were fully funded, *e.g.,* via a co-development partnership with a large pharmaceutical company, an aggressive product registration could be achieved by the end of 2027. Evrys' products for chronic hepatitis B and viral respiratory infections are projected to follow in 2029 and 2030.

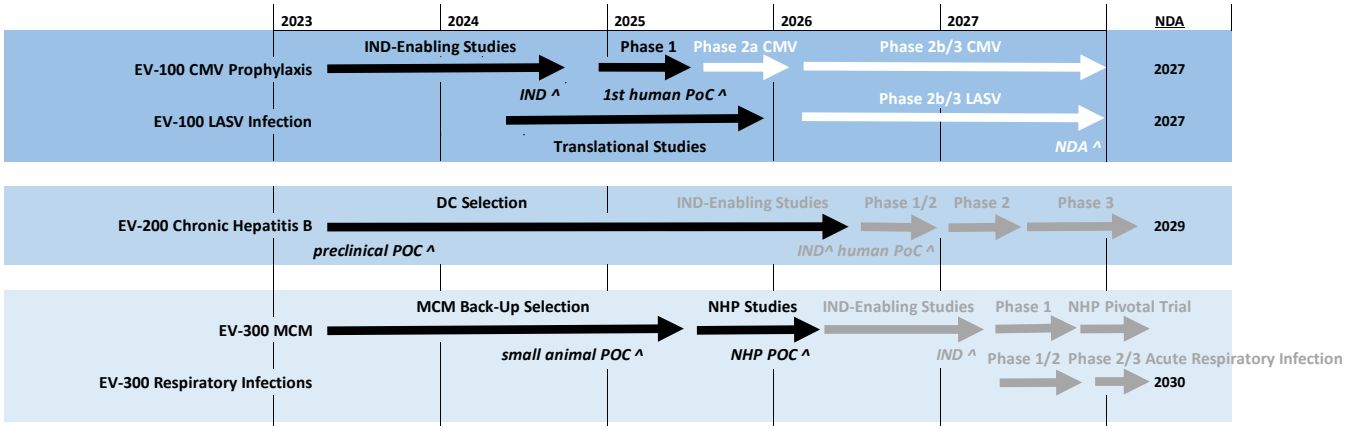

Intellectual Property (I.P.): Evrys Bio I.P. strategy has generated a portfolio of globally filed applications and issued patents to protect our innovation, and we will continue to expand our intellectual property position.

- EV-100 composition-of-matter to treat viral infection was issued with a term until 2038* (U.S. Patent 11,459,321).
- Evrys continues to create additional patent coverage, including method-of-use, formulation or combinations that will extend the market exclusivity of EV-100 beyond the term of the composition-of-matter patent. We are currently in the early stages of preparing applications directed towards the chosen clinical salt form of EV-100.
- Evrys Bio has additional composition-of-matter filings to the same chemical scaffold as EV-100. These are important to prevent "me-too" products from other companies and/or for the protection of Evrys products beyond EV-100, *e.g.,* EV-200. One was issued with terms to 2035*. Another international PCT patent application was filed in December 2021, and the term of national patents issuing from these applications will have terms to 2041*. We anticipate more in the future.
- Evrys licensed from Princeton a patent family directed to methods of modulating virus production by the inhibition of two or more sirtuins. This patent issued in Europe with broad method claims that will likely cover our envisioned products and a term to 2032*.

** A note on patent terms: All patent terms mentioned above are in the absence of any patent term extension granted in the U.S. (or SPC in the EU) at the time of new drug approval. Those terms are not readily predictable, at this time. Patent term extensions are commonly several years.*

Evrys Bio 2023 Financials and Operations

The Appendix provides summary level unaudited financial statements for the years ended 2021, 2022, and 2023 are provided in the Appendix. Find below, highlights and general commentary on operations and finance.

- **Personnel and management team:** We are growing the Evrys team, both in the number of people as well as in experience and expertise to ensure successful transition from drug discovery to a clinical-stage company with multiple prospects for strategic partnering and/or IPO. We started on January 1, 2023, with 6.1 in-house FTEs; we grew in size to 9.7 FTEs on December 31, 2023. To support the progression of our pipeline and platform while building for future success in partnering and commercialization, Evrys Bio is growing our team with top talent. We continue to foster our onsite culture dedicated to "actualizing innovation". Two key hires in the last year are Robert Besthof, Chief of Operations and Strategy, and Jens Knudsen, CFO, from Ambler and Maple Glen, PA, respectively. Robert joined Evrys in September with 25^{+} years of global commercial experience at Lilly, Wyeth, and Pfizer; Robert is a hands-on operational leader in Commercial Assessment, Business Development and Licensing, and most recently, as interim CEO of NRx Pharmaceuticals. Jens Knudsen joined in November also with 25^{+} years of experience building and leading international finance and operations teams at different stages of company development, primarily in the life sciences sector; he has completed multiple forms of financing including IPO, PIPES, Rights Issue, Bank Financing, and Debt Financing raising over $100 million, most

recently as CFO of AMRA Medical, Inc. Both join Evrys with enthusiastic support for our successful non-dilutive strategy to optimize innovation and value creation. Furthermore, both bring to Evrys a range of industry contacts & consultants that we have already started to leverage.

- **2023 Final Budget Debrief** (Table 2)**:** As you know, since inception, we have raised $12.5 M from you, our investors, and > $50 M from the government. Evrys Bio continues to operate much larger than our relatively small team. We continue to grow our government grants and contracts with a significant increase in DoD revenue due to EV-100 Drug Prototype reimbursement starting in June 2023. Monthly spend in 2023 was $590 K, a significant increase from previous years due to EV-100 development costs. Net burn was lower than last year at $67 K compared to $158 K / month in 2022. Net burn in 2021 was lower at $51 K / month but at a monthly spend rate of $330 K when Evrys was still a drug discovery company. In fact, we showed a profit of $137,512 for June to December 2023 - after DoD started to fund EV-100 development. The terms of the DoD cost-plus contract allow us to recover direct costs, indirect costs for contract overhead and G&A, plus a 10% fee. Much of the fee covers non-reimbursable costs to run Evrys Bio including intellectual property expense, business development, and unfunded and ex-U.S. Research and Development. The $2.9 M cash at the end of December 2022 represented remaining cash from the 2022 Series B raise that was earmarked for EV-100 CMC and IND enablement. Table 2 demonstrates how the DoD promotion of EV-100 to Drug Product status in June 2023 positively impacts our financials. We ended 2023 with $2.2 M in cash and DoD reimbursing us for EV-100 development through the end of our first phase 1 clinical trial in 2025. Our Quarterly Spend is shown graphically in Figure 3 (Pg. 8).

Table 2: Operations Comparison: 2021, 2022, 2023.

	2021	2022	2023	2023 Pre-DoD EV-100 de-risk (Jan to May)	2023 Post-DoD EV-100 de-risk (Jun to Dec)
U.S. Govt. Grant/Contracts	$ 3,179,623	$ 3,799,201	$ 6,241,993	$ 1,161,602	$ 5,080,391
Other Revenue	$ 208,216	$ 8,277	$ 65,206	$ 49,267	$ 15,939
TOTAL REVENUE	$ 3,387,839	$ 3,807,478	$ 6,307,199	$ 1,210,869	$ 5,096,330
Salaries & Benefits	$ 1,731,809	$ 1,620,985	$ 1,403,714	$ 605,854	$ 797,860
Consultants	$ 333,559	$ 397,262	$ 886,545	$ 252,272	$ 634,273
Research Supplies	$ 209,461	$ 219,354	$ 127,363	$ 36,786	$ 90,577
Equipment & Repairs	$ 25,071	$ 22,044	$ 16,775	$ 12,226	$ 4,549
External Contracted Research	$ 1,323,198	$ 2,821,606	$ 4,000,334	$ 997,585	$ 3,002,749
Rent & Utilities	$ 156,221	$ 268,273	$ 270,023	$ 112,788	$ 157,235
Financial Services	$ 34,350	$ 31,446	$ 23,112	$ 14,312	$ 8,800
Insurance	$ 11,835	$ 12,989	$ 15,490	$ 7,596	$ 7,894
Legal & Intellectual Property	$ 128,424	$ 234,031	$ 247,519	$ 64,616	$ 182,903
Other G&A	$ 48,588	$ 73,064	$ 115,161	$ 43,183	$ 71,978
TOTAL EXPENSES	$ 4,002,516	$ 5,701,054	$ 7,106,036	$ 2,147,218	$ 4,958,818
NET INCOME/LOSS	$ (614,677)	$ (1,893,576)	$ (798,837)	$ (936,349)	$ 137,512
Cash Available 12/31/2022			$ 2,879,842		
Cash Available 12/31/2023			$ 2,200,521		
Monthly Spend	$ 333,543	$ 475,088	$ 592,170	$ 429,444	$ 708,403
Monthly Net Burn	$ 51,223	$ 157,798	$ 66,570	$ 187,270	$ (19,645)

Figure 3. Quarterly Spend Chart. Each quarterly summary bar is labelled with average headcount. We started 2023 with a quarterly average of 6.7 FTE's and ended with 9.0. Orange CRO activities continue to grow. Gray G&A spend fell to 17.1% of total but in absolute amount increased 24% over 2022.

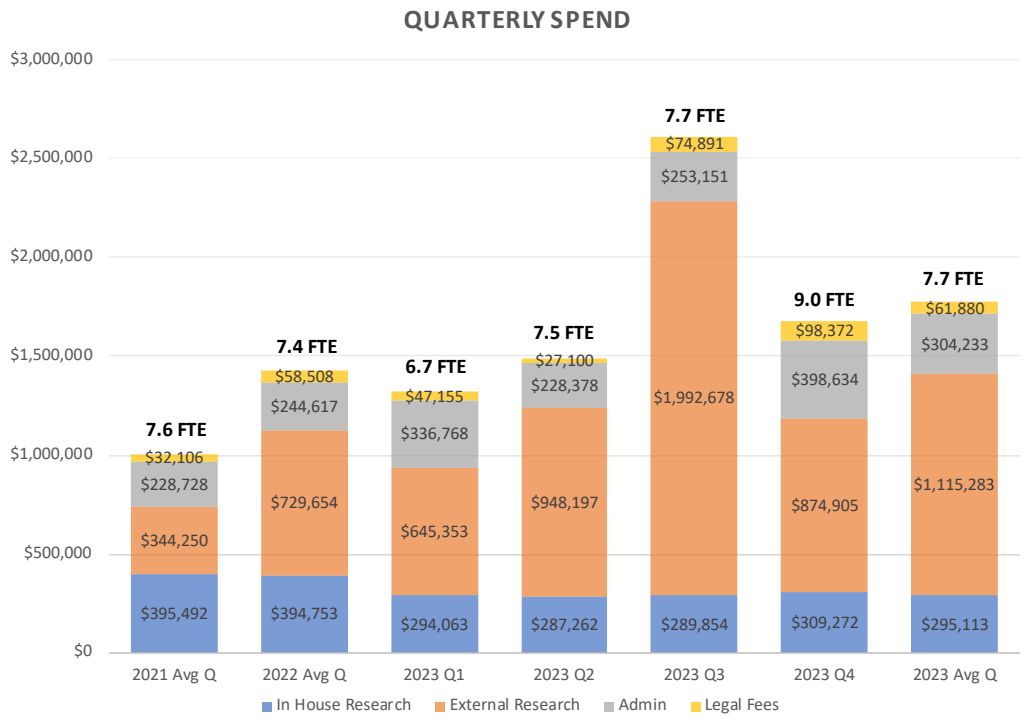

2023 Summary and 2024 Strategy

Evrys has achieved three key value inflection points: 1) we entered development with our first clinical-stage product EV-100, 2) we continue to operate in a capital efficient manner building value for our investors with non-dilutive moneys financing nearly all of our current operations, and 3) we are building our team for the next growth trajectory as a clinical-stage company positioning ourselves for strategic partnering.

Evrys Bio 2024 Goals – Corporate Pillars for Success

1. Development: File Evrys' first IND. Prep for clinical phase 1.
2. Discovery: Maintain strong support at DoD Defense Threat Reduction Agency with world-class translation including combination therapy PoC. Achieve major value inflection points (PoC and Lead Identification) for chronic HBV program.
3. Exploratory: Strategically extend value proposition of Evrys SIRT2 platform beyond treatment of viral infection.
4. Financing: Provide Evrys a path to Clinical Success
5. Infrastructure: Expand infrastructure to support project management across all projects

- **Summary of 2024 Budget to support goals:** The budget for 2024 is $14.59 M (Table 3). The budget includes salaries for new FTE's to be hired or onboarded in 2024: Project Manager, Caitlin Angelo, Senior Research Associate Eva Veriga, Chief of Operations and Strategy Robert Besthof who will convert from consultant, a To Be Hired (TBH) Chemist, and a TBH Operations Associate. The yearly salary of CFO Jens Knudsen was only partially realized in 2023 as he joined in November 2023. In addition, increased consulting expense is anticipated for IND and government contract procurement.

Table 3: Pro Forma Budget.

	2023 Actual	2024 Budget	Notes
U.S. Govt. Grant/Contracts	$ 6,241,994	$ 14,251,739	
Other Revenue	$ 65,205	$ -	
TOTAL REVENUE	$ 6,307,199	$ 14,251,739	
Salaries & Benefits	$ 1,403,712	$ 2,521,862	6 FTE's including CFO, COO
Consultants	$ 886,544	$ 1,424,284	IND and contract management
Research Supplies	$ 127,362	$ 204,000	
Equipment & Repairs	$ 11,142	$ 22,335	
External Contracted Research	$ 4,000,334	$ 9,583,494	See external research details
Rent & Utilities	$ 270,023	$ 288,000	
Financial Services	$ 23,112	$ 95,000	Tax advice
Insurance	$ 15,491	$ 18,000	
Legal & Intellectual Property	$ 247,518	$ 284,000	
Other G&A	$ 87,942	$ 113,400	
Interest Expense	$ 5,632	$ 5,774	
Depreciation	$ 27,220	$ 27,219	
TOTAL EXPENSES	$ 7,106,032	$ 14,587,368	
NET INCOME/LOSS	$ (798,833)	$ (335,629)	

Cash Available 12/31/2023	$ 2,200,510
Cash Available 12/31/2024	$ 1,920,162

Monthly Spend	$ 1,215,617
Monthly Net Burn	$ 23,362

- **External contract research** comprises 65.7% of the entire budget and is further broken out in the External Contract Research Detail (Table 4). EV-100 activities include $5.64 M in CMC, IND-enabling studies, and regulatory activities covered by the DoD contract, and $0.99 M in translational pharmacology studies covered by our NIH SBIR Phase IIB grant. Activities for the EV-200 HBV program are focused on drug discovery for new compounds and achieving small animal proof of concept. Separately is shown EV-300 MCM spend covered by DoD that is distinct from EV-100 CMC and IND-enabling activities. The goal is to identify a Back-Up for EV-100.

Table 4: Exernal Contract Research Detail **Total: $ 9,583,494**

EV-100 (CMV and LASV Infection)		EV-200 Chronic HBV		EV-300 MCM Back-Up		Exploratory Research	
CMC	$ 2,356,723	Pharmacology	$ 380,343	Pharmacology	$ 1,292,153	Pharmacology	$ 200,000
IND enablement	$ 2,963,513	Chemistry	$ 348,000	Chemistry	$ 454,248		
Pharmacology	$ 985,481		$ 728,343	DMPK	$ 288,033		
Phase 1 Trial Prep	$ 315,000				$ 2,034,434		
	$ 6,620,717						

- **The revenue projection** for 2024 is $14.25 M (Table 3) with $12.25 M coming from the DoD contract, $1 M from the National Institute of Allergy and Infectious Disease (NIAID) Small Business Innovation Research (SBIR) Phase IIB grant, and $1 M from Phase II of the HBV NIAID Fast-Track SBIR grant. The 2024 budgeted revenue and expenses will result in a monthly cash burn of $23 K ($280 K annually) which will be covered by available cash.
- **Risk assessment:** The biggest risk is reaching a NOGO on EV-100 drug candidate in 2024. Should we determine not to go forward with EV-100, all development activity will be paused until a Back-Up is identified. While this scenario is undesirable due to the delay for Evrys to become a clinical stage company, the impact on Evrys cash will not be catastrophic: spend will go down but we assume we will keep all our current contracts and grants. Intermediate risks are manufacturing delays. In 2023, we worked with our Contract Manufacturing Organization (CMO) to troubleshoot the EV-100 scale-up process, but also to remediate errors introduced by the CMO deviating from standard protocols. The outcome was a 5-month delay to hold our FDA Pre-IND meeting. The issues have been worked out and we see our current CMO as the most direct path to deliver the material to meet our 2024 goals. To hedge, we are evaluating alternative CMO partners. However, if our current CMO is unable to provide drug substance and we transfer the manufacturing process to the alternate CMO, timelines to IND-filing could be delayed again by as much as 6-9 months. Finally, revenue may not be realized from our awarded HBV NIAID Fast-Track SBIR grant in 2024 until animal PoC is achieved. This would result in up to $1 M less grant revenue in 2024 while the planned spend on activities will continue, not only to meet the phase transition milestones of the grant, but also, to significantly increase the value of Evrys' HBV program for pharma partners and investors. If the HBV grant revenues are delayed, Evrys can cover the additional cash needs with current available cash.
- **Fundraising Overview:** Evrys Bio can support its current operations well into the end of 2025. That said, we will need more funds to progress EV-100 beyond the completion of our first clinical phase 1 trial, and the rest of our pipeline into the clinic. The fundraising goals in 2024 are three-pronged: (1) enable our next significant tranche(s) of non-dilutive government funding; (2) enable a strategic industry collaboration; (3) continue to foster discussions with deep pocket investors.

  From non-dilutive government resources, we will apply for grants/contracts to continue identification of back-up sirtuin-targeted, broad-spectrum antivirals from a distinct chemical scaffold with at least 100-fold improvement in antiviral potency.

  We will also look for non-dilutive moneys to fund EV-100 phase 2 clinical development. The lead government agencies are Department of Defense Joint Program Executive Office for Chemical, Biological, Radiological and Nuclear Defense (DoD JPEO-CBRN) and Department of Health and Human Services Biomedical Advanced Research and Development Authority (DHHS BARDA). While EV-100 is currently too early, JPEO and BARDA will fund medical technologies at the Technical Readiness Level 6 (TRL6) with completed phase 1 clinical trial(s) that establish initial safety and pharmacokinetics. Therefore, in 2024, our goal is to foster continuing contact with these agencies to

familiarize them with EV-100 progress and our host-targeted broad-spectrum technology for future funding.

Once we submit our IND package for EV-100, we will be in a good position to begin directed reach-outs for strategic industry collaboration. EV-100 can bring multiple attributes to a stand-alone or combination antiviral product.

- Broad-spectrum effectiveness
- High barrier to resistance
- Additivity and/or synergy to direct-acting antiviral effectiveness
- Host environment in neighboring uninfected cells that is unproductive for viral replication
- Sustained antiviral effect after drug-block release
- Combination therapies

We have also included for 2024, exploratory research goals to extend the application of Evrys sirtuin modulators to non-antiviral applications. An extended platform to include non-viral indications has the potential to grow both industry and investor interest in Evrys Bio. After 12 years, the greatest value Evrys has built lies in our portfolio and experience base in sirtuin-targeted allosteric modulators with good pharmaceutical properties. The timing may be right for Evrys to grow from a host-targeted antiviral company to a sirtuin small-molecule drug company with a pipeline of infectious disease, cancer, and other indications. Expanding indications is a strategic pillar to increase our attractiveness for pharma partnering; large pharma prefers to partner with companies whose drug platform allows for expansion. Overall, our goal is to build momentum to achieve a pharma partnering event and/or investor financing in early 2025.

Appendix Items

- Roche, K. L., S. Remiszewski, M. J. Todd, J. L. Kulp III, L. Tang, A. V. Welsh, A. P. Barry, C. De, W. W. Reiley, A. Wahl, J. V. Garcia, M. A. Luftig, T. E. Shenk, J. R. Tonra, E. A. Murphy, and L. W. Chiang. 2023. An allosteric inhibitor of sirtuin 2 de-acetylase activity exhibits broad-spectrum antiviral activity. *Journal of Clinical Investigation* **133**: e158978.
- Cheung, J., S. Remiszewski, L. W. Chiang, E. Ahmad, M. Pal, S. A. Rahman, Z. Nikolovska-Coleska, and G. C. Chan. 2023. *Antiviral Research* **217**: 105698.
- Statement of Income
- Statement of Financial Position
- Summary Capitalization Table

Please contact Lillian Chiang with questions about this information.

Forward Looking Statements

This Report contains forward-looking statements. Forward-looking statements do not relate strictly to historical or current facts and anticipate results based on management's plans that are subject to uncertainty. Forward-looking statements may be identified by the context or content and by the use of words like "plans," "expects," "will," "anticipates," "estimates" and other words of similar meaning in conjunction with, among other things, discussions of future operations, research, financial performance, Evrys Bio's strategy for growth, product development, and other matters.

Forward-looking statements are based on current expectations of future events. Evrys Bio cannot guarantee that any forward-looking statement will be accurate, although Evrys Bio believes that it has been reasonable in its expectations and assumptions. Shareholder members and other readers should realize that, if underlying assumptions prove inaccurate or unlikely or unknown or unexpected risks or uncertainties materialize, actual results could vary materially from Evrys Bio's expectations and projections. Shareholder members and other readers are therefore cautioned not to place undue reliance on any forward-looking statements. Furthermore, Evrys Bio assumes no obligation to update any forward-looking statements as a result of new information or future events or developments.

This Report does not set forth the assumptions made in preparing this information and does not set forth the factors that could affect Evrys Bio's ability to achieve results or goals described in any forward-looking statements. Shareholder members and other readers should understand that it is not possible to predict or identify all such factors.

JCI The Journal of Clinical Investigation

An allosteric inhibitor of sirtuin 2 deacetylase activity exhibits broad-spectrum antiviral activity

Kathryn L. Roche, … , Eain A. Murphy, Lillian W. Chiang

J Clin Invest. 2023;133(12):e158978. https://doi.org/10.1172/JCI158978.

Research Article | Infectious disease | Virology

Graphical abstract

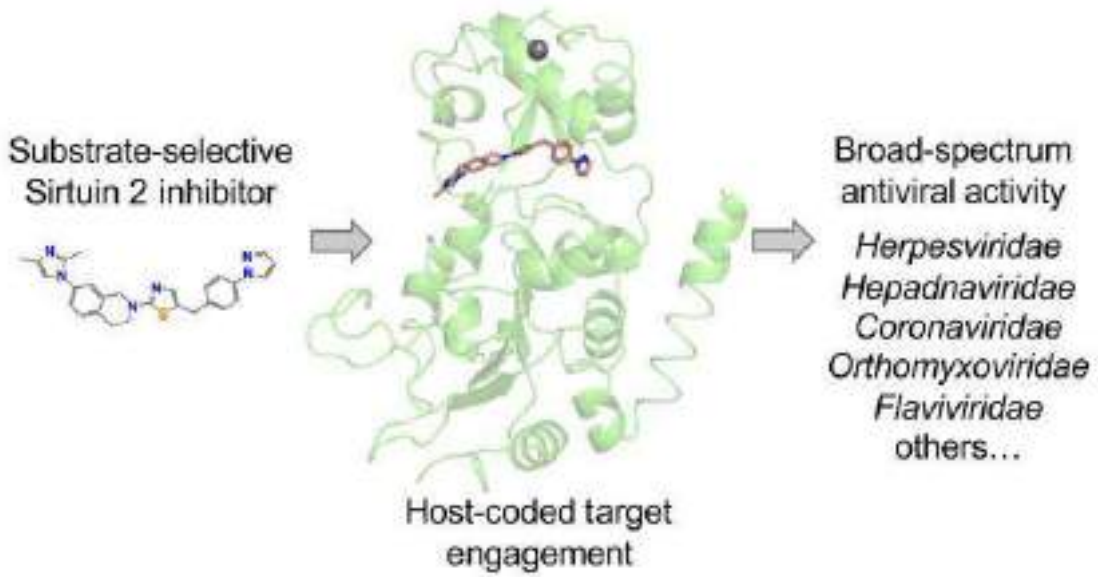

An allosteric inhibitor of sirtuin 2 deacetylase activity exhibits broad-spectrum antiviral activity

Kathryn L. Roche,[1] Stacy Remiszewski,[1] Matthew J. Todd,[1] John L. Kulp III,[1] Liudi Tang,[1] Alison V. Welsh,[1] Ashley P. Barry,[2] Chandrav De,[3] William W. Reiley,[4] Angela Wahl,[3] J. Victor Garcia,[3] Micah A. Luftig,[2] Thomas Shenk,[1,5] James R. Tonra,[1] Eain A. Murphy,[1,6] and Lillian W. Chiang[1]

[1]Evrys Bio LLC, Pennsylvania Biotechnology Center, Doylestown, Pennsylvania, USA. [2]Department of Molecular Genetics and Microbiology, Duke Center for Virology, Duke University School of Medicine, Durham, North Carolina, USA. [3]International Center for the Advancement of Translational Science, Division of Infectious Diseases, Center for AIDS Research, University of North Carolina, School of Medicine, Chapel Hill, North Carolina, USA. [4]TICRO Bioservices, Trudeau Institute, Saranac Lake, New York, USA. [5]Department of Molecular Biology, Princeton University, Princeton, New Jersey, USA. [6]Microbiology and Immunology Department, SUNY Upstate Medical University, Syracuse, New York, USA.

Most drugs used to treat viral disease target a virus-coded product. They inhibit a single virus or virus family, and the pathogen can readily evolve resistance. Host-targeted antivirals can overcome these limitations. The broad-spectrum activity achieved by host targeting can be especially useful in combating emerging viruses and for treatment of diseases caused by multiple viral pathogens, such as opportunistic agents in immunosuppressed patients. We have developed a family of compounds that modulate sirtuin 2, an NAD^+-dependent deacylase, and now report the properties of a member of that family, FLS-359. Biochemical and x-ray structural studies show that the drug binds to sirtuin 2 and allosterically inhibits its deacetylase activity. FLS-359 inhibits the growth of RNA and DNA viruses, including members of the coronavirus, orthomyxovirus, flavivirus, hepadnavirus, and herpesvirus families. FLS-359 acts at multiple levels to antagonize cytomegalovirus replication in fibroblasts, causing modest reductions in viral RNAs and DNA, together with a much greater reduction in infectious progeny, and it exhibits antiviral activity in humanized mouse models of infection. Our results highlight the potential of sirtuin 2 inhibitors as broad-spectrum antivirals and set the stage for further understanding of how host epigenetic mechanisms impact the growth and spread of viral pathogens.

Introduction

Direct-acting antivirals (DAAs) target virus-coded products and are a highly successful therapeutic paradigm. The sofosbuvir/velpatasvir combination, which inhibits the hepatitis C virus polymerase complex, is a case in point. It cures a high proportion of patients with chronic hepatitis C (1). However, DAAs suffer from 2 principal limitations. First, viruses develop resistance, as is well documented for influenza M2 ion channel and neuraminidase inhibitors (2). Second, although there are exceptions (3), DAAs generally target only one virus or virus family.

In contrast to DAAs, host-targeted antivirals (HTAs) inhibit a host product that supports viral replication or enhance the activity of a defensive network. With no selective pressure for the accumulation of mutations in host cell antiviral targets, viral resistance should not develop. Further, since different viruses use overlapping cellular pathways and factors to support their replication (4) and antiviral defense systems often target these common pathways, HTAs can exhibit broad-spectrum activity (5). Thus, HTAs have potential to treat categories of viral disease where the causative agents span multiple virus families. Importantly, broad-spectrum HTAs have potential to provide a rapid therapeutic solution at the onset of a pandemic, reducing the time between novel virus identification and pharmacological intervention (6, 7). Beyond this periodic need, HTAs can treat patients at risk for infection with viruses of different families, such as transplant patients who are at elevated risk for herpesvirus, paramyxovirus, polyomavirus, hepadnavirus, and coronavirus infections during immunosuppressive therapy (8, 9).

One intriguing network of targets for the development of HTAs are the proteins that create and read the cellular acetylome. Lysine N-ε-acetylations are found on thousands of proteins (10). Histone acetyltransferases (HATs) transfer an acetyl group from acetyl-coenzyme A to a target lysine, bromodomain-containing proteins read these modified lysine residues to regulate diverse cellular processes, and histone deacetylases (HDACs) remove the marks. The dynamic interplay between HATs and HDACs specifies the acetylome, which impacts chromatin structure and transcriptional activity, protein-protein interactions, protein localization, and metabolic processes (11, 12).

Conflict of interest: KLR, SR, MJT, JLK, LT, AVW, JRT, EAM, and LWC are or have been employees of Evrys Bio, receiving income from the company and owning company stock. TS is a founder of Evrys Bio and owns company stock, and MAL is a member of the Evrys Bio Scientific Advisory Board and owns company options. Evrys Bio has issued patents and pending applications claiming composition of matter for SIRT2 modulators (US Patents: US-11459321-B2, US-11358961-B2, US-10723708-B2, US-10556894-B2).

Submitted: February 2, 2022; **Accepted:** May 2, 2023; **Published:** June 15, 2023.
Reference information: *J Clin Invest*. 2023;133(12):e158978.
https://doi.org/10.1172/JCI158978.

Not surprisingly, given their broad impact on cellular processes, lysine N-ε-acetylations modulate factors critical for viral replication. For example, transcription of the HIV genome is influenced by histone acetylation, the viral integrase and transactivator of transcription (Tat) proteins are regulated by acetylation, and HIV latency is modulated by drugs that inhibit deacetylation (13). Likewise, influenza A proteins are regulated by acetylation (14), and human cytomegalovirus (HCMV) infection profoundly impacts the cellular and viral acetylomes (15). In addition to supporting viral processes, lysine acetylation also impacts cellular antiviral defense systems. For example, the location of the DNA sensor protein IFN-γ–inducible protein 16 (IFI16) is controlled by acetylation (16), and the activity of nuclear factor-κB (NF-κB), which regulates numerous elements of immune responses, is modulated via acetylations within its p65 subunit (17).

The inhibition of deacetylation has been explored as an antiviral mechanism. HDACs form 2 major families: Zn^{++}-dependent HDACs and NAD^+-dependent HDACs, also termed sirtuins (SIRTs). The seven SIRTs (SIRT1–SIRT7) (18) transfer an acyl group from an acylated lysine of a protein substrate to the ADP-ribose moiety of NAD^+, deacylating the protein and producing nicotinamide plus 2′-*O*-acyl-ADP-ribose (19). Deacetylation is most commonly studied, but SIRTs also remove longer-chain acyl groups (20). The NAD^+ requirement ties SIRT activity to the metabolic state of cells, and infection significantly disrupts cellular metabolism (21, 22). The human SIRTs are localized to distinct cellular compartments (23), and knockdown of each human SIRT, as well as the *E. coli* SIRT CobB, modulates the growth of multiple viruses (24), underscoring their evolutionarily conserved roles in the control of viral replication. The dual SIRT1/2 inhibitors tenovin-1 and sirtinol inhibit the growth of both RNA and DNA viruses (25, 26); and the SIRT2-selective inhibitor AGK2 (27) antagonizes the replication of hepatitis B virus (28, 29). SIRT2-knockout mice are healthy and immunocompetent (30, 31), arguing that selective SIRT2 inhibitors are likely to be well tolerated as antiviral therapeutics.

Here we explore the utility of small molecules targeting SIRT2 as broad-spectrum antivirals with potential to treat opportunistic infections. We demonstrate that the compound FLS-359 binds to SIRT2 and allosterically inhibits its deacetylase activity. Broad-spectrum antiviral activity of the drug is evident across multiple DNA and RNA virus families, including the herpesviruses, human cytomegalovirus (HCMV), and Epstein-Barr virus (EBV), which are of particular concern in immunosuppressed patients (32–36). The drug reduces the accumulation of HCMV RNAs and DNA, substantially decreasing virus spread and infectious yield in human fibroblasts. FLS-359 also reduced virus production in 2 humanized mouse models of HCMV infection. These results highlight SIRT2 as a host target, and support further development of drugs targeting SIRT2 as broad-spectrum antivirals.

Results

FLS-359 binds SIRT2, selectively reducing deacetylase activity. Starting with a hit from a small-molecule screen designed to identify compounds that altered SIRT2 activity in vitro, we developed a portfolio of molecules targeting SIRT2 using anti-HCMV activity as a primary criterion in our lead optimization campaign. FLS-359, 7-(2,4-dimethyl-1*H*-imidazol-1-yl)-2-(5-{[4-(1*H*-pyrazol-1-yl) phenyl]methyl}-1,3-thiazol-2-yl)-1,2,3,4-tetrahydroisoquinoline (Figure 1A), is a representative lead.

An in vitro thermal shift assay (37) was used to test for FLS-359–SIRT2 binding by quantifying the compound-dependent increase in protein thermal stability (Figure 1B). SIRT2 underwent thermal denaturation with a midpoint transition temperature (T_m) of approximately 48°C. FLS-359 increased the T_m by 1.4°C (6.25 μM) or 2.0°C (12.5 μM), demonstrating that the drug engages and stabilizes the purified protein.

The effect of FLS-359 on deacetylation of a peptide containing a histone H3 acetylation site (Ac-H_3K_9WW) was assayed in vitro, using mass spectrometry to quantify deacetylated peptide. The concentration for half-maximal inhibition (IC_{50}) in this assay was about 3 μM for SIRT2 and more than 100 μM for SIRT1 and SIRT3 (Figure 1C). When the NAD^+ concentration was increased from 50 to 100, 200, and 500 μM, more deacetylated product was generated, but the IC_{50} remained essentially the same (Figure 1, D and E). The IC_{50} was about 3 μM for all NAD^+ concentrations when the peptide was used at 5 μM. The IC_{50} was about 7 μM for all NAD^+ concentrations at 50 μM peptide. Therefore, FLS-359 is not competitive with NAD^+. When the peptide concentration was increased from 5 μM (1× K_m; Figure 1D) to 50 μM peptide (10× K_m; Figure 1E), the IC_{50} increased from about 3 μM to about 7 μM, or about 2-fold. If FLS-359 binding was fully competitive with the peptide, an approximately 10-fold increase in IC_{50} would be expected. In addition, saturating compound decreased SIRT2 activity to a lower but residual value. Both of these observations are consistent with partial inhibition, seen with other SIRT2 inhibitors, e.g., AGK2 (27) and MIND4 (38). Since SIRT2 is important to cellular metabolic homeostasis, the observed partial inhibition may prove to be a positive attribute that supports cell viability in uninfected cells while providing an antiviral effect in infected cells.

SIRT2 has deacylation activities in addition to deacetylation (20, 39), including demyristoylation, and several SIRT2 inhibitors are acyl group selective, blocking deacetylation but not demyristoylation (40–43). When tested for inhibition of demyristoylation using the same peptide backbone (Myr-H_3K_9WW) used to assay deacetylation (Ac-H_3K_9WW), neither FLS-359 nor tool compounds (AGK2 and SirReal2) showed activity (Figure 1F and Supplemental Table 1; supplemental material available online with this article; https://doi.org/10.1172/JCI158978DS1). Thus, FLS-359 is substrate selective, inhibiting deacetylation but not demyristoylation.

FLS-359 induces known activities of SIRT2 modulators within cultured cells. SIRT2 deacetylates α-tubulin K40 (44); and, as expected, treatment of cultured HepG2 hepatocellular carcinoma cells with FLS-359 for 24 hours increased the level of acetylated α-tubulin in HepG2 cells by a factor of about 3 (Supplemental Figure 1A). SIRT2 knockdown or inhibition induces degradation of c-Myc protein in tumor cells by inducing its ubiquitination (45, 46), and treatment with FLS-359 for 72 hours dramatically reduced the level of the oncoprotein in MDA-MB-231 breast adenocarcinoma cells (Supplemental Figure 1B). Notably, c-Myc levels were not changed by treatment of MRC-5 human diploid fibroblasts with the drug (Supplemental Figure 1C). Thus, treatment with FLS-359 induces known consequences of SIRT2 inhibition in tumor cells.

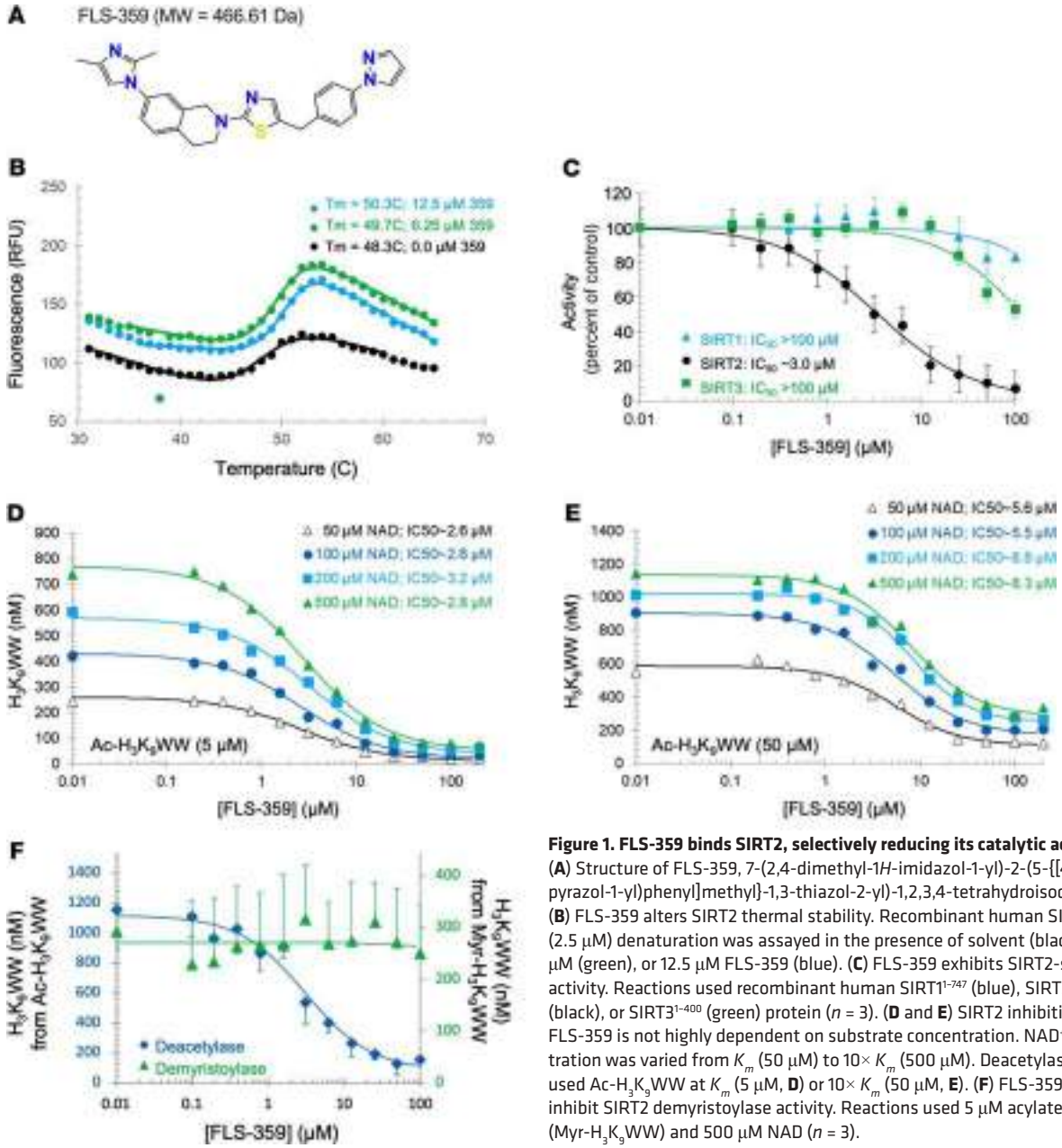

Figure 1. FLS-359 binds SIRT2, selectively reducing its catalytic activity. (**A**) Structure of FLS-359, 7-(2,4-dimethyl-1*H*-imidazol-1-yl)-2-(5-{[4-(1*H*-pyrazol-1-yl)phenyl]methyl}-1,3-thiazol-2-yl)-1,2,3,4-tetrahydroisoquinoline. (**B**) FLS-359 alters SIRT2 thermal stability. Recombinant human SIRT2$^{2-389}$ (2.5 μM) denaturation was assayed in the presence of solvent (black), 6.25 μM (green), or 12.5 μM FLS-359 (blue). (**C**) FLS-359 exhibits SIRT2-selective activity. Reactions used recombinant human SIRT1$^{1-747}$ (blue), SIRT2$^{2-389}$ (black), or SIRT3$^{1-400}$ (green) protein (n = 3). (**D** and **E**) SIRT2 inhibition by FLS-359 is not highly dependent on substrate concentration. NAD$^+$ concentration was varied from K_m (50 μM) to 10× K_m (500 μM). Deacetylase assays used Ac-H_3K_9WW at K_m (5 μM, **D**) or 10× K_m (50 μM, **E**). (**F**) FLS-359 does not inhibit SIRT2 demyristoylase activity. Reactions used 5 μM acylated peptide (Myr-H_3K_9WW) and 500 μM NAD (n = 3).

X-ray structure confirms FLS-359 engagement of SIRT2. X-ray crystallographic structures have been determined for human SIRT1, 2, 3, 5, and 6 (47). The structures consist of 2 domains: an upper Zn^{++}-binding domain and a lower catalytic domain with a Rossmann fold (48, 49). The 2 domains behave as a clamshell, accommodating varying acyl-Lys modifications within a flexible pocket between the 2 clamshell domains. This area is above the C pocket of the NAD$^+$-binding site and is termed the extended C (EC) pocket (49). SIRT1, SIRT2, and SIRT3 are about 70%–80% conserved around the NAD$^+$ and nearby EC pockets, where natural and synthetic small-molecule ligands that affect activity have been resolved (47, 49).

We produced crystals of FLS-359 bound to SIRT2 that diffracted to 1.8 Å resolution and determined the structure of the complex (Supplemental Table 2). FLS-359 sits in the SIRT2 EC pocket (Figure 2, A and B). In comparison with the unliganded SIRT2 apo structure (ref. 50; Protein Data Bank [PDB] ID 3ZGO), the clamshell has opened and an ordered α-helix has shifted to an unstructured loop (residues 294–304); in addition, a loop over the drug binding site is rearranged (Supplemental Figure 2). The 2 substrates, acetyl-Lys (PDB ID 4RMI) and NAD$^+$ (PDB ID 4RMG), are computationally superimposed in Figure 2B. NAD$^+$ binding is not predicted to be affected by FLS-359 binding. In contrast, the FLS-359 dimethylimidazole moiety resides in the same location as the peptidic acetyl group, but computational superpositioning predicts that the pocket can accommodate both FLS-359 and the peptide. The binding interactions of FLS-359 with SIRT2 include π-π interactions with residues F119, F190, and Y139 (Figure 2C). Water residue 566 bridges FLS-359 and SIRT2 with one hydrogen bond to the thiazole of FLS-359 and another hydrogen bond to the backbone

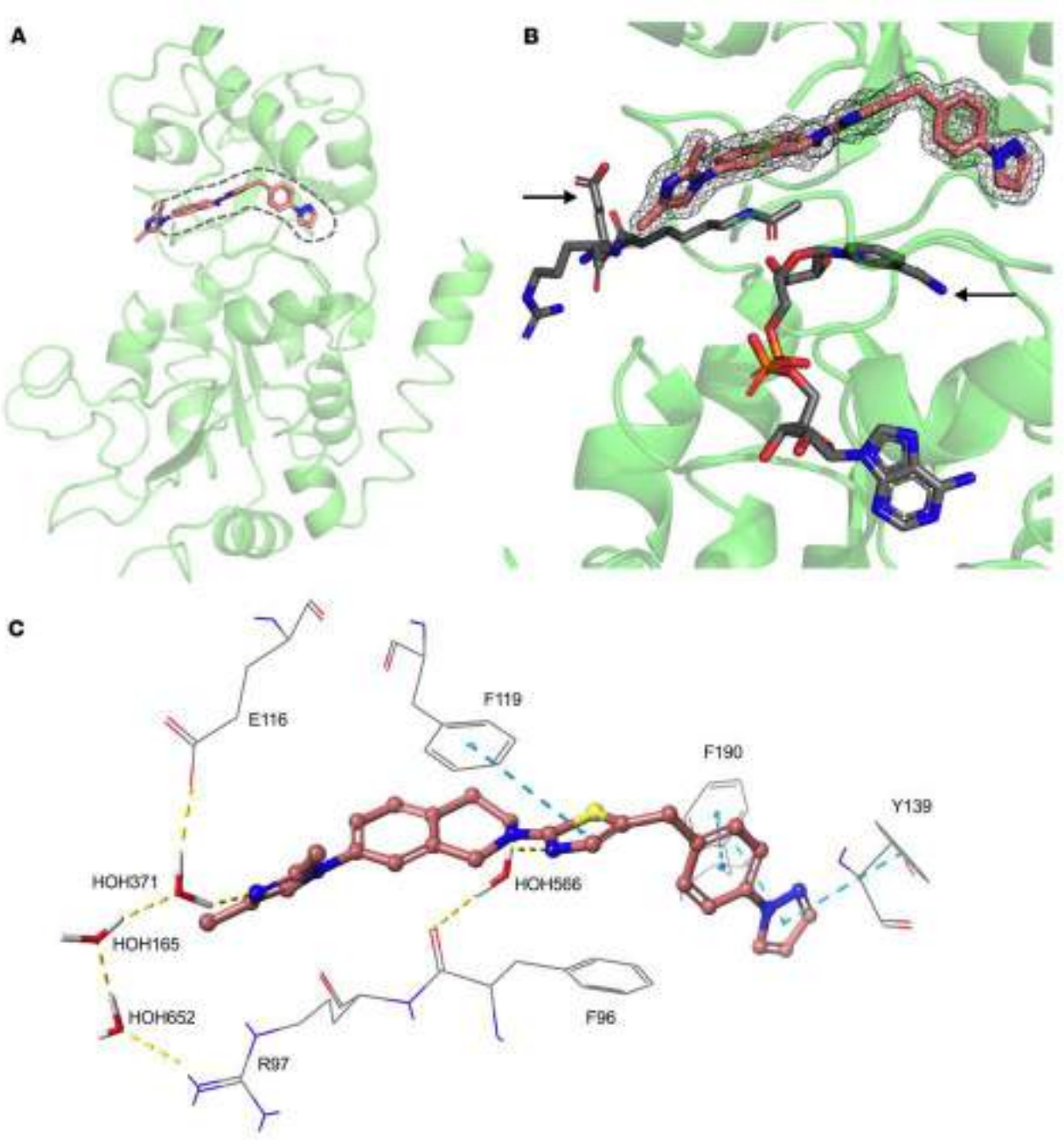

Figure 2. Co-crystal structure of FLS-359 bound to human SIRT2. (**A**) SIRT2 (green ribbon) with FLS-359 (pink carbon atoms in stick display) bound to its EC site (dashed lines). (**B**) Superposition of SIRT2-359 with an Ac-Lys peptide (right-pointing arrow; PDB ID 4RMI) plus NAD^+ (left-pointing arrow; PDB ID 4RMG). The gray mesh over FLS-359 marks the $2F_o–F_c$ electron density map (contoured at 1.5 σ) resulting from refinement of the final model with REFMAC5. (**C**) Close-up view of the SIRT2 EC site focusing on the key FLS-359–SIRT2 interactions. Yellow-highlighted dashed lines indicate hydrogen bonds, and blue dashed bonds represent π-π interactions.

carbonyl of residue F96. A multi-body water network in the peptide channel connects, via a hydrogen bond network, the dimethyl imidazole of FLS-359 to E116 through water residue 371 and to the side chain of R97 through water residues 371, 165, and 652. These water-mediated hydrogen bonds could be key interactions that drive binding affinity to SIRT2 in the hydrophobic EC site.

The FLS-359/SIRT2 structure was used to probe the substrate-selective activity of the drug. Flexible protein docking confirmed that acetyl-Lys (PDB ID 4RMI) and FLS-359 can simultaneously bind within the SIRT2 EC pocket (Supplemental Figure 3A), whereas peptides with thiomyristoyl lysine (PDB IDs 4R8M and 4X3P) are predicted to compete for binding with the drug (Supplemental Figure 3, B and C). Thus, myristoylated peptides have potential to exclude FLS-359 binding, providing an explanation for the drug's substrate-selective activity.

In sum, enzyme thermal denaturation and kinetics studies (Figure 1), as well as co-crystal structure determination (Figure 2), argue that FLS-359 binds selectively to SIRT2 and induces an allosteric

Table 1. FLS-359 exhibits broad-spectrum antiviral activity

Virus/ host cell	Virus family	FLS-359 IC_{50} (μM)	Host cell CC_{50} (μM)	SI[A] CC_{50}/IC_{50}	SOC/C[B] IC_{50} (μM)	SOC/C
SARS-CoV-2/ human Calu3	Betacoronavirus	0.3	15.8	52.7	0.4	Remdesivir (C)
Zika/ human HFF	Flavivirus	0.4	41.6	104.0	2.8	Amodiaquine (C)
HCMV/ human MRC-5	Betaherpesvirus	0.5	>15.8	>40	2.7	Ganciclovir (SOC)
Influenza A/ human dNHBE	Orthomyxovirus	1.2[C]	>100	>83.3	0.7[C]	Ribavirin (C)
HCoV-OC43/ human MRC-5	Betacoronavirus	1.7	>50	>30.1	0.1	Remdesivir (C)
Junin/ human HFF	Arenavirus	3.2	>25	>7.8	0.2	RIID E-1 (C)
Hepatitis B/ human PHH	Hepadnavirus	4.8	>10	>2.1	0.03	Tenofovir (SOC)
Epstein-Barr/ human Akata	Gammaherpesvirus	3.8	>100	>26.3	43	Ganciclovir (C)
RSV/ human MRC-5	Orthopneumovirus	6.7	>12.5	>1.9	16.1	Ribavirin (SOC)

Results are shown for representative assays (details in Methods). ASI, selectivity index. BSOC, standard of care, or C, comparator compound. CIC90. dNHBE, differentiated normal human bronchial epithelial cells; HFF, human foreskin fibroblasts; PHH, primary human hepatocytes; RSV, respiratory syncytial virus.

rearrangement of the active site, reducing the rate of deacetylation. It is a substrate-selective inhibitor, blocking deacetylation but not demyristoylation.

FLS-359 exhibits broad-spectrum antiviral activity. FLS-359 was tested for activity against multiple RNA and DNA viruses in cultured cells. The drug inhibited the growth of each pathogen shown (Table 1). The IC_{50} varied across the viruses, but the differences must be interpreted with caution, because the assays were performed at different research sites and used a variety of host cells. Nevertheless, in multiple cases, the antiviral IC_{50}s were in the range of current standards of care, with acceptable half-maximal cytotoxic concentrations (CC_{50}s). Most assays were performed in primary cells or diploid cell lines, because SIRT2 inhibition is antiproliferative or cytotoxic to many tumor cell lines (46, 51).

Given the importance of EBV and HCMV as adventitious agents in immunosuppressed patients (32–36), the effects of FLS-359 were examined in greater detail for these viruses. A broad-spectrum antiviral able to treat both infections has substantial potential utility.

FLS-359 inhibits EBV lytic reactivation and/or replication. The Akata Burkitt lymphoma cell line is permissive for EBV lytic reactivation through activation of the B cell receptor (52). As expected, 24 hours after receptor engagement with anti-IgG, 30% of Akata cells induced surface expression of the late EBV gene gp350, which serves as a proxy for cells that are replicating viral DNA and forming new virions (Figure 3A). In the presence of the viral DNA replication inhibitor phosphonoacetic acid (PAA), $gp350^+$ cells were reduced to about 11% (Figure 3A). FLS-359 treatment led to a dose-dependent decrease in $gp350^+$ cells with 10 μM drug, inhibiting EBV reactivation at a similar level to PAA (Figure 3, A and B). The FLS-359 CC_{50} for Akata cells was greater than 100 μM (Table 1), so the inhibition of gp350 accumulation was not due to drug-induced cytotoxicity. The drug also inhibited the accumulation of viral immediate-early (BZLF1), early (BMRF1), and late (BLLF1) mRNAs (Figure 3C). We conclude that FLS-359 markedly reduces EBV lytic activation in Akata cells.

FLS-359 inhibits HCMV spread in diploid fibroblasts. The antiviral activity of a drug is generally measured by assaying of its effect on the production of infectious viral progeny. However, many viruses spread via 2 modes, either by release of a particle that eventually infects a new cell or by direct cell-to-cell transfer (53, 54). HCMV can move by either mechanism, and subviral particles can move from cell to cell, allowing the virus to spread without producing infectious particles (55). To capture the effect of drugs on HCMV movement and amplification by either mechanism, we used a spread assay. It uses a clinical isolate, TB40/E-mCherry-UL99eGFP (56), containing 2 reporters to monitor infection of MRC-5 fibroblasts: mCherry controlled by the SV40 early promoter, expressed with immediate-early kinetics, and eGFP fused to the viral UL99 coding region, expressed with late kinetics. The assay protocol is simple: infect confluent fibroblasts at a low input multiplicity (0.01 IU/cell), add drug immediately following infection, and quantify the area expressing fluorescent markers after 7 days (Figure 4A). The extended, 7-day assay reflects the fact that HCMV replicates and spreads slowly, with a single cycle of growth extending over 72–96 hours in MRC-5 cells. FLS-359 was well tolerated by confluent MRC-5 cells over 7 days, when assayed by counting of nuclei (Figure 4B) or neutral red uptake (Figure 4C); and it was also tolerated by dividing MRC-5 cells over 6 days (Supplemental Figure 4). FLS-359 reduced the total infected cell area marked by mCherry expression in confluent fibroblasts (Figure 4, D and E). Reduced mCherry expression was also evident when monitored by Western blot assay (Supplemental Figure 5), mimicking expression of the viral immediate-early protein IE1. This assay indicates that FLS-359 inhibits HCMV spread with an IC_{50} of 0.466 ± 0.203 μM (Figure 4F). Control anti-HCMV drugs acting at different steps in the viral replication cycle, ganciclovir and letermovir, exhibited IC_{50}s of 1.7 and 0.003 μM, respectively, consistent with literature reports (57, 58). The potencies measured by the spread assay were similar to potencies determined by 50% tissue culture infectious dose ($TCID_{50}$) assay of virus in the medium (Figure 4G).

Although letermovir efficiently reduced extracellular infectivity (Figure 4G), it reduced infected cell area (Figure 4F) to a lesser extent (4-fold) than ganciclovir (33-fold) or FLS-359 (>100-fold). Part of this effect could result from a failure of letermovir to eliminate originally infected cells. However, letermovir blocks at a late point in the viral replication cycle, inhibiting the virus-coded terminase subunit pUL56 (59, 60), which cleaves a unit genome of viral DNA as it enters the capsid. Earlier work has shown that HCMV capsids can spread directly from cell

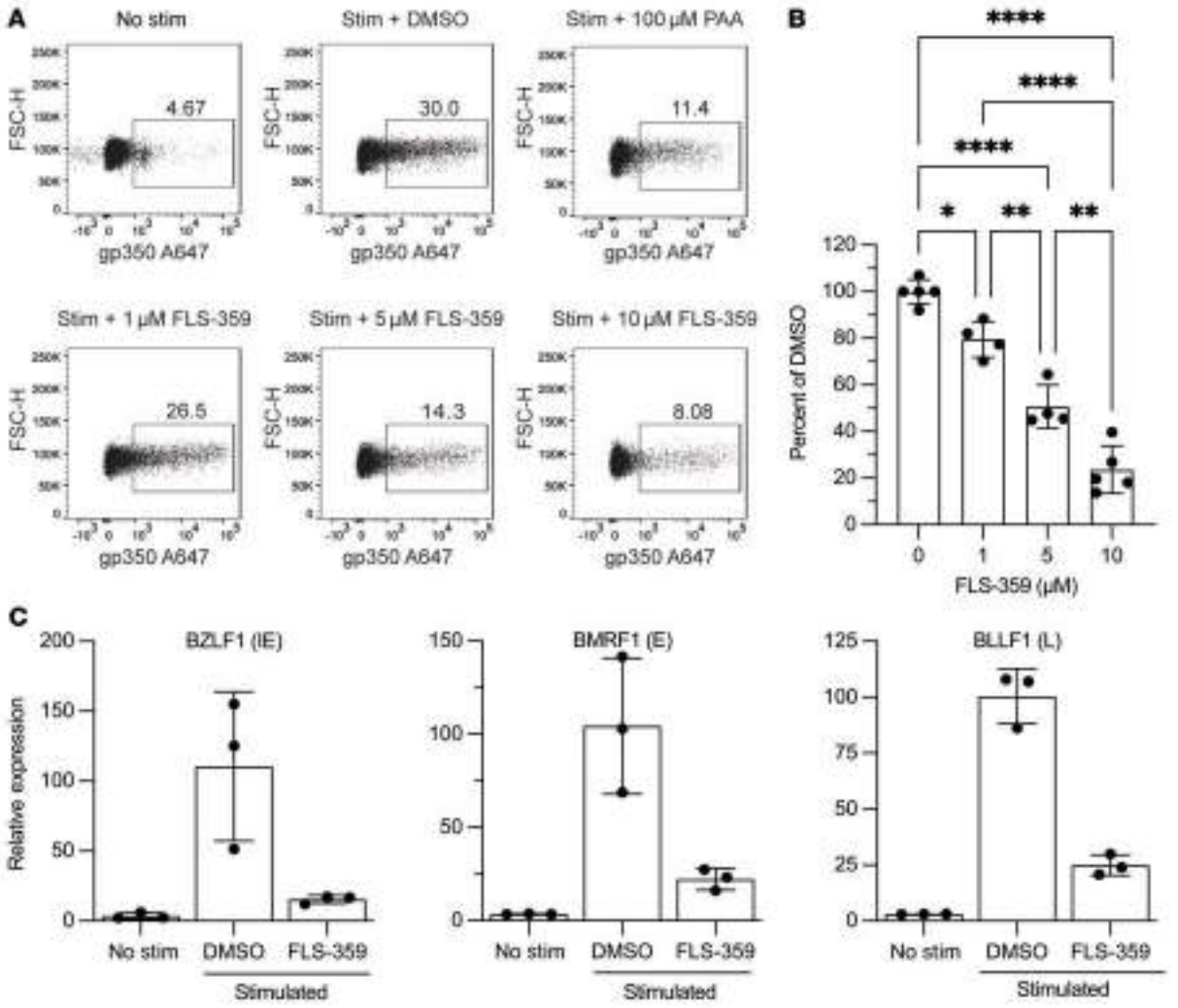

Figure 3. FLS-359 suppresses EBV lytic reactivation. (**A**) Akata BL cells were stimulated with 10 μg/mL anti-IgG and simultaneously treated with DMSO, 100 μM phosphonoacetic acid (PAA; positive control), or increasing concentrations of FLS-359 (1, 5, and 10 μM). Surface expression of the viral late gene gp350 was measured at 24 hours after induction by flow cytometry. (**B**) Dot plots reporting experiments in **A**, shown with mean ± SD (n = 4). *P < 0.05, **P < 0.01, and ****P < 0.0001. (**C**) Dot plots reporting quantitative reverse transcriptase PCR (qRT-PCR) measurement of BZLF1 (IE, immediate early), BMRF1 (E, early), and BLLF1 (L, late) gene expression suppressed by FLS-359 (10 μM) in Akata BL cells induced with anti-IgG. Mean ± SD is shown (n =3).

to cell (55), and a portion of the residual spread observed with letermovir might result from movement of partially assembled DNA-capsid complexes.

To test whether inhibition of HCMV is a general feature of SIRT2 inhibitors, we assayed tool compounds with chemical structural diversity: AGK2 (27), AK-7 (61), SirReal2 (49), MIND4 (38), and TM (46). Although they were less potent than FLS-359, all of the SIRT2 inhibitors reduced HCMV spread (Table 2 and Supplemental Figure 6). Since the inhibitors have very different structures, this result argues that they all inhibit HCMV at least in part through targeted modulation of SIRT2.

Having demonstrated the broad-spectrum antiviral attributes of FLS-359, including anti-herpesvirus activity, we focused on the drug's parameters as an anti-HCMV agent.

FLS-359 reduces HCMV spread when administered after an infection has been initiated. To model the ability of FLS-359 to control an established infection in comparison with current standards of care, MRC-5 fibroblasts were infected (0.1 IU/cell) and treated with drug either immediately or after a delay of 1–4 days (Figure 5A). Drug treatment was maintained for 5 days, and then the effect of the delay was assayed by monitoring of viral spread. FLS-359, ganciclovir, and letermovir each exhibited antiviral activity when administered after a delay (Figure 5B) without inducing toxicity at effective doses (Figure 5C). Indeed, the antiviral IC_{50}s remained essentially unchanged as the addition of drug was delayed over increasing intervals (Supplemental Table 3). At each delayed time of drug addition, a greater maximal fold reduction of infected cell area was achieved by treatment with FLS-359, compared with ganciclovir or letermovir (Supplemental Table 3). Thus, FLS-359 maintains its antiviral potency when administered at 4 days after the initiation of infection, while demonstrating superior control of viral spread compared with standards of care.

FLS-359 induces an antiviral state that persists after the drug is withdrawn. Long-lasting consequences of SIRT2 modulation could result from a long intracellular half-life of the compound or from modifications to the cellular acylome. Accordingly, we performed

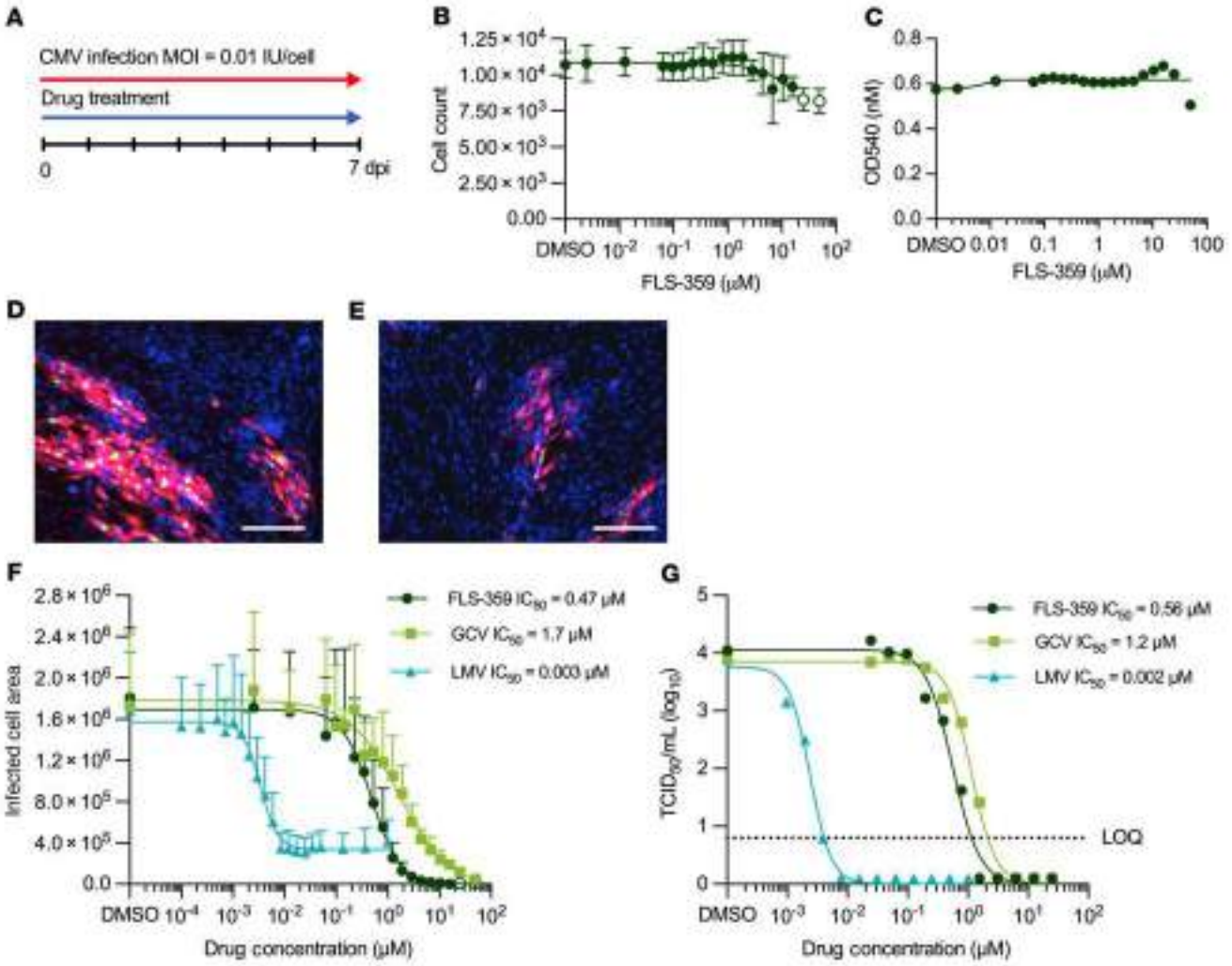

Figure 4. FLS-359 inhibits HCMV spread in fibroblasts. (**A**) Schematic representation of the spread assay. (**B** and **C**) Cytotoxicity was assessed in confluent MRC-5 cells after 7 days of FLS-359 treatment by DAPI staining for cell count (**B**) or neutral red uptake (**C**) (n = 3). (**D** and **E**) Confocal images of MRC-5 cells infected with TB40/E-mCherry-UL99eGFP (0.01 IU/cell) at 7 days post-infection (dpi), treated with vehicle (**D**) or FLS-359 at 0.5 μM (**E**). Fluorescent mCherry (red) is expressed with immediate-early kinetics and eGFP (green) with late kinetics, and DAPI (blue) locates nuclei. Scale bars: 300 μm. (**F**) Virus spread assay. CMV-infected cell area is quantified by mCherry fluorescence and plotted versus FLS-359, ganciclovir (GCV), or letermovir (LMV) concentrations. IC_{50} (mean ± SD) is reported (n = 4). (**G**) Virus yield assay. Cell-free virus at 7 dpi was quantified by $TCID_{50}$. IC_{50} is reported. LOQ, limit of quantification.

a treat-release experiment in which MRC-5 cells were infected (0.5 IU/cell) for 96 hours in the presence of drug, drug was removed, and virus growth was monitored by $TCID_{50}$ assay of culture medium for an additional 96 hours (Figure 6A). Cells treated with vehicle (DMSO) lacking drug served as a control, and continued to produce virus throughout the time course (Figure 6B). Release of the letermovir-induced block generated detectable progeny at 24 hours, the first time monitored after release, with a resumption of growth kinetics similar to that in DMSO-treated cultures; release of the ganciclovir block generated detectable progeny at 48 hours; and release from the FLS-359 block did not generate progeny over the full 96-hour period that was monitored. Minimal cellular toxicity was evident in FLS-359–treated cultures at 96 hours after removal of the drug (Figure 6, C and D), arguing against a nonspecific toxic effect.

The long-term efficacy of FLS-359 after washout in the treat-release protocol with only a portion of cells infected suggested that the drug might protect uninfected cells from subsequent infection. This possibility was tested in a treat-release-infect experiment in which MRC-5 cells were treated with drug for 24 hours, drug was removed for 72 hours, and then cells were infected (0.5 IU/cell) and infected cell area was measured at 72 hours post-infection (hpi) (Supplemental Figure 7A). Whereas 24-hour pretreatment with FLS-359 followed by a 72-hour washout inhibited viral spread (IC_{50} = 4.8 μM), ganciclovir had no activity in the same pretreatment regimen (Supplemental Figure 7B). In a control experiment, both drugs were active when readministered at the time of infection (Supplemental Figure 7C). This indicates that FLS-359 alters the susceptibility of cells to infection, but does not speak to the mechanism.

The long-term efficacy of FLS-359 could also result from a prolonged intracellular half-life. Therefore, we monitored its half-life in uninfected MRC-5 cells by treating them with drug for 24 hours, removing medium with drug and washing the cells, and then quantifying drug levels by mass spectrometry

Table 2. Multiple SIRT2 inhibitors reduce HCMV spread

Compound	HCMV IC_{50} (μM)	MRC-5 CC_{50} (μM)	SI[A] CC_{50}/IC_{50}	SIRT2[B] IC_{50} (μM)
FLS-359	0.5	>15.8	>31.6	3.0
AGK2	3.4[C]	>100	>29.4	3.5
AK-7	8.2	>25	>3	15.5
MIND4	14.4	19.8	1.4	3.5
SirReal2	14.9[C]	>20	>1.3	0.14–0.44
TM	26.0	46.3	1.8	0.028

Nonlinear regression analysis was used to calculate IC_{50}s from infected MRC-5 cell area measured at 7 dpi (n = 2). CC_{50}s for uninfected MRC-5 cells were determined by DAPI cell count after a 7-day treatment. Underlying data are shown in Supplemental Figure 6. [A]SI, selectivity index. [B]Reported SIRT2 IC_{50}s are from literature cited in the text, except FLS-359 (Figure 1, C and D). [C]Infected cell area did not reach 0 at the highest drug concentration tested.

(Supplemental Figure 8A). A reduced but significant level of FLS-359 was detected in cells (~5 μM) and supernatant (~0.4 μM) at 72 hours after drug removal, whereas the control drug, letermovir, was effectively removed from supernatant and cells by washing (Supplemental Figure 8, B and C). As a control, FLS-359 was added to medium in cell culture dishes without cells, and it was efficiently removed by washing (Supplemental Figure 8, D and E), ruling out the possibility that the drug was simply sticking to the plastic dishes. FLS-359 induces a relatively long-lasting pharmacodynamic effect in both infected and uninfected cells that inhibits HCMV replication, at least in part due to an extended intracellular half-life.

FLS-359 inhibits the accumulation of intracellular HCMV RNAs and DNA and reduces the infectivity of virus progeny. To evaluate the site in the viral replication cycle that is sensitive to SIRT2 inhibition, we monitored the accumulation of representative immediate-early, early, and late HCMV protein-coding RNAs. MRC-5 cells were infected (3 IU/cell), cells were harvested, and RNAs were quantified by quantitative reverse transcriptase PCR (qRT-PCR) assay at 72 hpi (Figure 7A). All of the viral protein-coding RNAs tested were reduced by the SIRT2 inhibitor, and in most cases, the reduction was dose dependent (Figure 7B). The immediate-early UL123 (IE1) and UL122 (IE2) RNAs encode master regulators that modulate expression of the other viral genes (62, 63), so it is possible that an inhibitory event reducing their levels propagates to reduce accumulation of the remaining genes that were assayed.

FLS-359 also reduced the level of HCMV-coded long noncoding RNAs, including RNA4.9, which crosses the viral origin of DNA replication (oriLyt), as well as the UL57 and UL69 protein-coding RNAs that flank the oriLyt (Figure 7C). Reduced accumulation of RNA4.9 restricts HCMV DNA accumulation (64). In addition, UL44, UL54, and UL57 — all of which are reduced by drug treatment — encode products that function directly in viral DNA replication (65). UL44 and UL54 encode subunits of the viral DNA polymerase, and UL57 encodes a single-stranded DNA-binding protein. Not surprisingly, then, intracellular viral DNA accumulation was compromised by treatment with FLS-359 for 72 hours (Figure 8A) in a dose-dependent manner (Figure 8B). As expected, ganciclovir, a 2′-deoxyguanosine analog, also inhibited intracellular viral DNA accumulation, when tested using doses equivalent to its IC_{50} and IC_{90}. In contrast, letermovir, which acts at a post-replication step, did not have a significant effect on DNA accumulation. FLS-359 reduced the production of infectious virus to below the limit of quantification, whereas ganciclovir and letermovir reduced virus yield to a more limited extent, as expected for the doses tested (Figure 8C). To further evaluate the effect of FLS-359 on virus production, cells were infected, drug treatment was initiated at 2 hpi and maintained until 96 hpi, and then the infectivity of progeny virus particles was evaluated (Figure 8D). As seen for the 72-hour treatment (Figure 8C), virus infectivity was dramatically reduced by the 96-hour drug treatment (Figure 8E). At 1.0 μM FLS-359, the particle/infectious unit ratio was reduced by a factor of 14.5, while 2.5 or 5.0 μM drug reduced infectivity more than 1,690-fold. In a control experiment, incubation of a virus stock with FLS-359 (1 or 5 μM) for 96 hours at 37°C had no significant effect on infectivity (Figure 8F), ruling out the possibility that the drug inactivates virions. Thus, FLS-359 reduces the accumulation of intracellular viral nucleic acids, the production of extracellular virus particles, and the infectivity of the virus particles that are generated.

FLS-359 inhibits HCMV infection in 2 humanized mouse models. FLS-359 pharmacokinetics was assessed in female BALB/c mice (Supplemental Table 4). After a single 50 mg/kg oral (p.o.) dose, the drug exhibited an approximately 6-hour plasma half-life, achieving maximal plasma concentrations (C_{max}) of 89 μM, substantially exceeding the in vitro IC_{50}s. The relatively long half-life and high C_{max} resulted in good exposure, with an AUC of 713 μM·h/mL. FLS-359 was also administered to NOD/Shi-scid/IL-2Rγ^{null} (NOG) mice at 50 mg/kg p.o. twice per day (b.i.d.) for 14 days. No weight loss and no adverse clinical signs were observed, indicating that FLS-359 is well tolerated at this dose and schedule.

The inhibitory activity of FLS-359 was tested in 2 humanized models of HCMV infection. The first (58, 66) used TB40/E virus–infected MRC-5 fibroblasts (0.05 IU/cell), seeded into a collagen matrix (gelfoam) and then implanted subcutaneously (1×10^6 infected cells) into immunodeficient mice. FLS-359 (50 mg/kg, p.o., b.i.d.), valganciclovir (50 mg/kg, p.o., daily), or diluent was administered beginning immediately after implantation. Implants were recovered on day 11 after infection, and $TCID_{50}$ assays revealed that both drugs significantly reduced virus production (Figure 9A). We also tested the efficacy of FLS-359 in humanized lung-only mice, generated by subcutaneous implantation of human lung tissue into immune-deficient mice (67). In this model, the human lung tissue expands to form a highly vascularized palpable implant that contains human fibroblast, epithelial, endothelial, and mesenchymal cells, which form lung-like structures that support HCMV replication and in vivo efficacy testing of antiviral agents (67, 68). Administration of FLS-359 (50 mg/kg, p.o., b.i.d.), ganciclovir (100 mg/kg, i.p., daily), or diluent was initiated 2 hours before infection of human lung implants by direct inoculation of TB40/E virus (4.25×10^5 IU/implant). Drug treatments were continued until the lung implants were removed on day 17 after infection, and virus was quantified by $TCID_{50}$ assay. Both drugs again significantly reduced the production of infectious HCMV progeny (Figure 9B), confirming in vivo activity of the SIRT2-targeted drug.

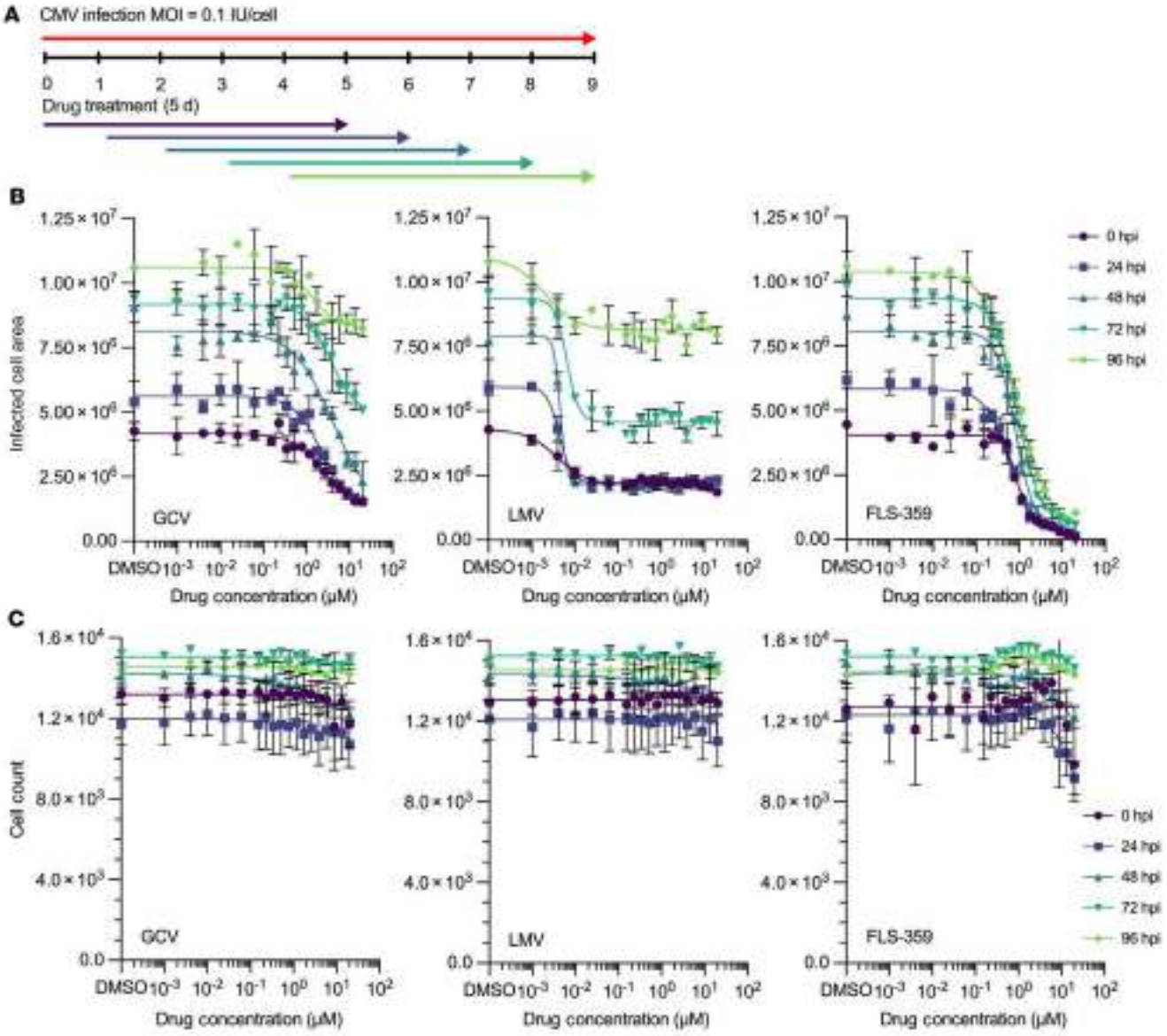

Figure 5. FLS-359 is effective in a delayed treatment protocol. (**A**) Confluent MRC-5 cells were infected with TB40/E-mCherry-UL99eGFP (0.1 IU/cell). FLS-359, ganciclovir (GCV), or letermovir (LMV) was added at 0 hpi, or delayed for 24, 48, 72, or 96 hours. (**B** and **C**) After 5 days of drug treatment, infected cell area was quantified by mCherry fluorescence (**B**) and cell counts by nuclear DAPI stain (**C**). Mean ± SD is shown (n = 3).

Discussion

FLS-359 bound SIRT2 between its Zn^{++}-binding domain and the catalytic Rossmann fold domain (Figure 2), in the EC pocket where other small-molecule ligands have been localized (49). A thermal shift assay (Figure 1B) and inhibition of deacetylase activity (Figure 1, C and D) confirmed drug binding. FLS-359 decreases SIRT2 deacetylase activity, but SIRT2 remains partially active when fully occupied by drug, as seen with other tool compounds, e.g., AGK2 (27) and MIND4 (38), possibly because FLS-359 sits in the EC pocket, but the acetyl-peptide substrate can still bind and undergo catalysis, albeit at a reduced rate. This explanation is consistent with the small decrease in SIRT2 activity at 10× K_m concentration of acetyl-substrate peptide (Figure 1E), and argues that the drug is an allosteric modulator. The movement in the FLS-359/SIRT2 crystal structure (Supplemental Figure 2) when compared with apo structure (ref. 50; PDB ID 3ZGO) is consistent with this allosteric binding mechanism.

FLS-359 binds and modulates SIRT2 in vitro (Figure 1) and within cells (Supplemental Figure 1), but does FLS-359 antiviral activity result from SIRT2 modulation? Although we have documented robust anti-HCMV activity for FLS-359 (Figure 4), it has been reported that knockdown of SIRT2 increases the yield of HCMV by a factor of about 4 at 96 hpi (24). This apparent contradiction likely results from the different functional consequences of a knockout/knockdown that ablates all SIRT2 activities, as compared with SIRT2-modulating drugs that exhibit substrate selectivity (40–43). SIRT2 removes a variety of long-chain acyl groups in addition to acetyl groups in biochemical assays (19, 20), and FLS-359 blocks SIRT2 deacetylation but not demyristoylation (Figure 1F and Supplemental Table 1). Modeling predicts that SIRT2 can accommodate both an

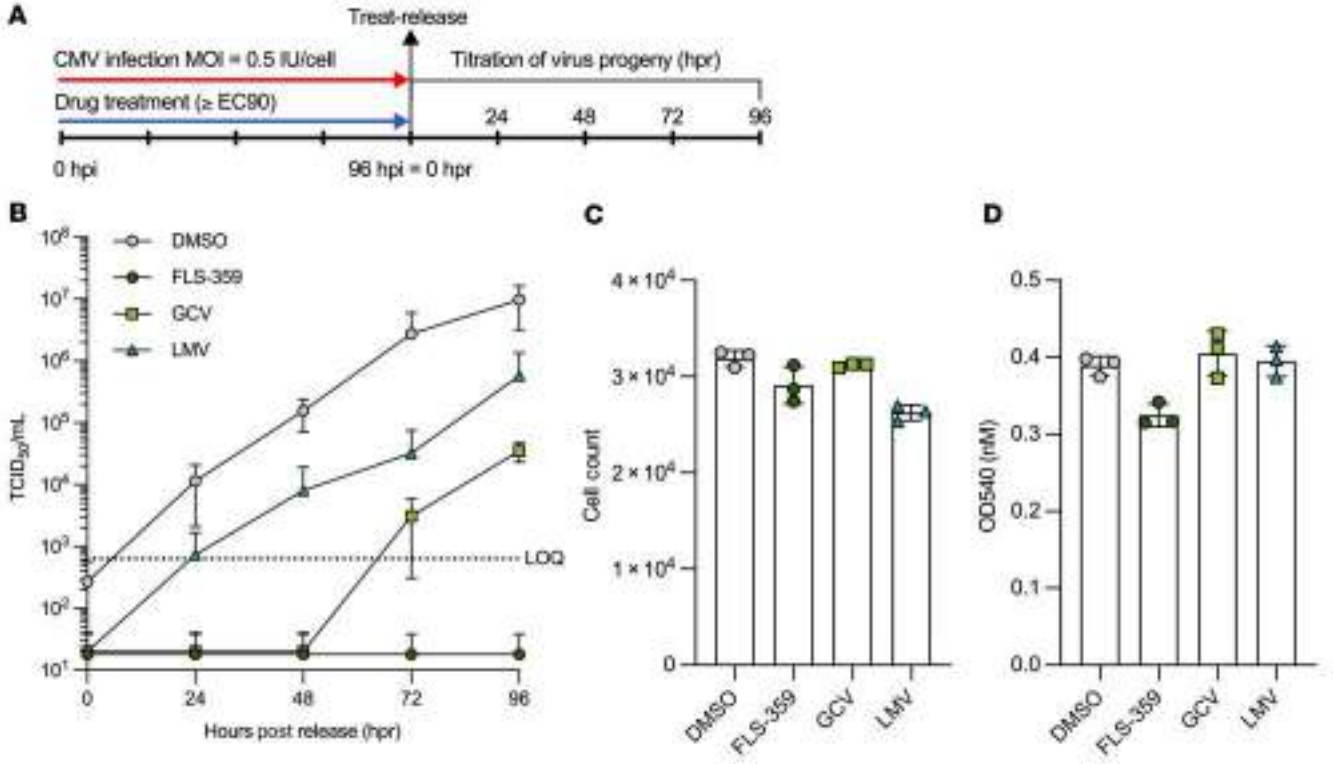

Figure 6. Long-term antiviral activity of FLS-359 following removal of drug. (**A**) Confluent MRC-5 cells were infected with TB40/E-mCherry-UL99eGFP (0.5 IU/cell) in the presence of drugs at their approximate EC_{90}s (FLS-359, 5 μM; ganciclovir [GCV], 20 μM; letermovir [LMV], 0.05 μM). Infection proceeded for 96 hours, monolayers were washed 3 times with buffer (PBS), and drug-free growth medium was added. Supernatant was sampled at 24-hour intervals over 4 days after release, and virus was titered by $TCID_{50}$. (**B**) Cell-free virus titers as a function of time after release of the drug-induced block. LOQ, limit of quantification. (**C** and **D**) Cell viability was assessed at 96 hours after release of the drug block by cell count (**C**) or lactate dehydrogenase activity (**D**). Mean ± SD is shown (n = 3).

acetyl group and FLS-359, whereas the binding of a myristoyl group excludes FLS-359 (Supplemental Figure 3). As a consequence, FLS-359 can modulate SIRT2 deacetylation, but cannot inhibit demyristoylation activity; and it is possible that additional acylations escape inhibition by the drug. Substrate-selective drugs have been described for a variety of enzymes (42), and knockdown/knockout experiments cannot reliably predict the physiological consequences of their activities. One approach that addresses this experimental conundrum is to test the activity of multiple, different drugs that modulate a specific enzymatic activity (42), as we have done for the anti-HCMV activity of SIRT2 inhibitors (Figure 4F, Table 2, and Supplemental Figure 6). Six structurally distinct SIRT2-targeting compounds reduced the yield of HCMV in spread assays, arguing that SIRT2 modulation is a key element of the antiviral activity.

It is conceivable that these compounds have off-target activities that impact viral growth, perhaps via effects on additional members of the SIRT family. However, this possibility seems unlikely, because the thioacyl lysine TM has been tested in vitro against all seven SIRTs and is highly selective for SIRT2 (46). Further, FLS-359 (Figure 1C), AGK2 (69), MIND4 (38), and SirReal2 (49) are highly selective for SIRT2 versus their most closely related family members, SIRT1 and SIRT3 (70).

It is not clear why the anti-HCMV activity of FLS-359 (0.5 μM; Figure 4F) appears to be more potent than its in vitro activity on purified SIRT2 (3.3 μM; Figure 1C). Intracellular SIRT2 is produced from 3 splice variants (71), modified by phosphorylations and acetylations (72–74), and associates with numerous other cellular proteins (75). These variations, modifications, and associations might make SIRT2 more or less susceptible to inhibition by the drug. Alternatively, the compound might accumulate preferentially in a cellular compartment where a key target protein resides. It is also possible that a secondary target of the drug contributes to its antiviral activity or a more active metabolite is generated within cells. Finally, it is conceivable that inhibition of SIRT2 modulates multiple pathways required for efficient viral replication, amplifying the antiviral effect of the drug.

Our work highlights the broad-spectrum antiviral activity of FLS-359 (Table 1), which inhibits the replication of both RNA and DNA viruses. The IC_{50}s for inhibition of the different viruses tested range from 0.3 μM for SARS-CoV-2 to 6.7 μM for respiratory syncytial virus. This range of sensitivities might result from testing in different cell types with different antiviral readouts. It is also possible that different SIRT2-controlled posttranslational modifications impact different viruses to a greater or lesser extent and the antiviral mechanisms vary across a range of pathogens. This data set clearly illustrates the broad-spectrum activity of this class of inhibitors, a potentially invaluable feature of antivirals in immunosuppressed populations and as new pathogens emerge and evolve in the human population.

How does SIRT2 inhibition antagonize HCMV replication? As noted above, HCMV infection induces profound alterations to the cytoplasmic and nuclear acetylomes, including changes

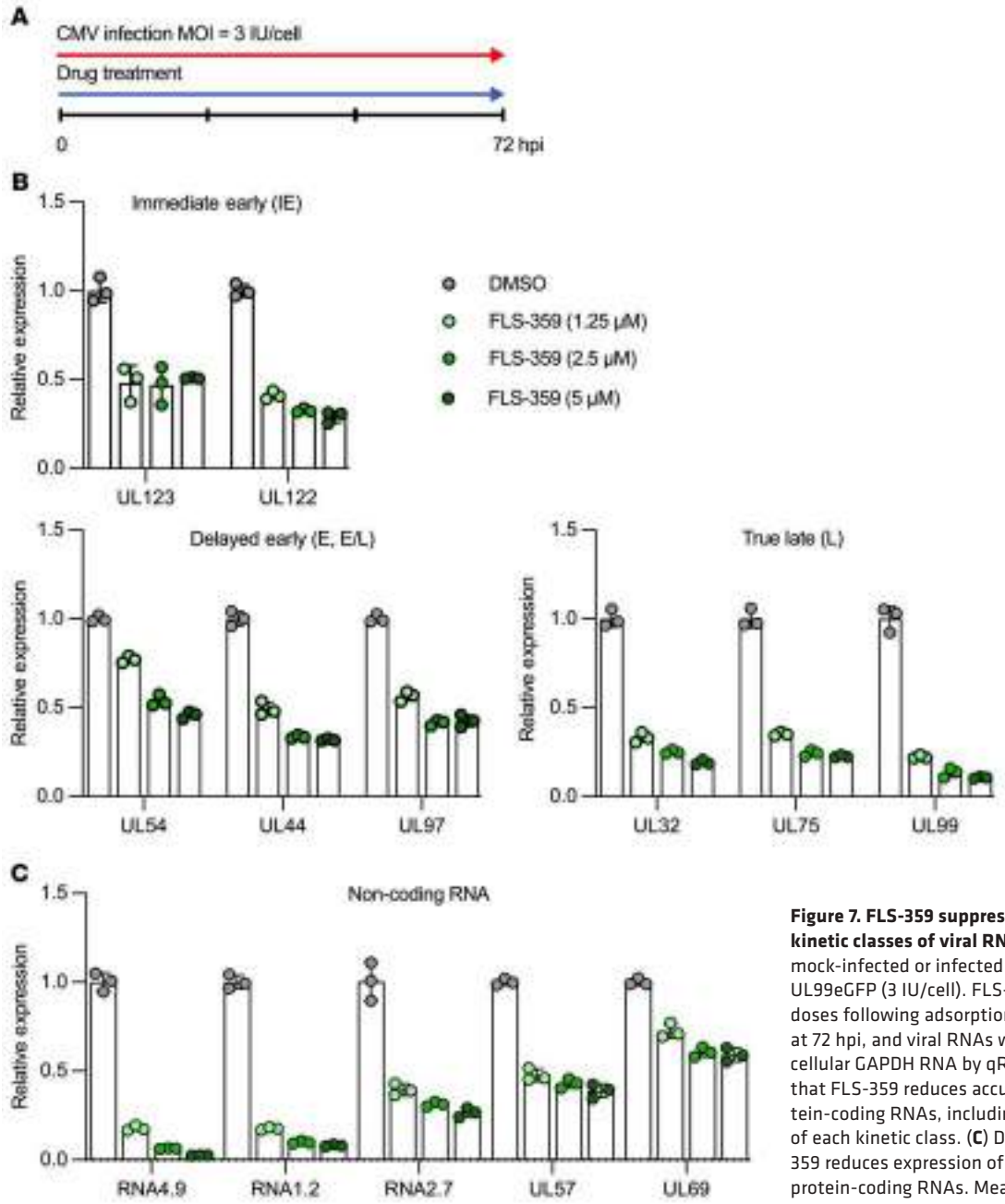

Figure 7. FLS-359 suppresses accumulation of all kinetic classes of viral RNAs. (**A**) MRC-5 cells were mock-infected or infected with TB40/E-mCherry-UL99eGFP (3 IU/cell). FLS-359 was added at indicated doses following adsorption, cell RNA was prepared at 72 hpi, and viral RNAs were quantified relative to cellular GAPDH RNA by qRT-PCR. (**B**) Dot plots showing that FLS-359 reduces accumulation of all tested protein-coding RNAs, including multiple representatives of each kinetic class. (**C**) Dot plots showing that FLS-359 reduces expression of multiple viral noncoding and protein-coding RNAs. Mean ± SD is shown (n = 3).

to viral and cellular transcriptional regulatory proteins (15). Some of these changes likely support viral growth and spread, by facilitating viral replication processes or by reducing the cellular protective response. As a consequence, drugs that modulate the infected-cell acetylome, and more broadly the infected-cell acylome, have potential to create an environment that antagonizes viral replication.

Although SIRT2 is predominantly cytoplasmic, it shuttles between the nucleus and cytoplasm, acting in both compartments (76). FLS-359 modestly reduced the accumulation of all viral RNAs tested, including the UL122 and UL123 RNAs (Figure 7B), arguing that it modulates viral transcription or RNA stability. Expression of the UL122 and UL123 RNAs is controlled by the major immediate-early promoter (MIEP), which is the primary HCMV promoter/enhancer to become active following infection. Numerous cellular factors bind at the MIEP (63), and the activity of any of these factors could potentially be modulated by SIRT2 inhibitors. SIRT2 also acts on transcription by modulating the acetylation state of histones H3 and H4 (77, 78). Although SIRT2 inhibition could lead to hyperacetylation of HCMV chromatin, a state that generally favors transcriptional activation, an indirect consequence, such as enhanced expression of a cell-coded repressor, could inhibit viral transcription. Reduced accumulation of the major immediate-early proteins could then reduce the expression of all downstream viral RNAs — similar to what was observed (Figure 7B). Changes in acetylation status of virus-coded factors, such as pUL26, where an acetylation mimic (K203Q) inhibited virus production (15), could also play a role.

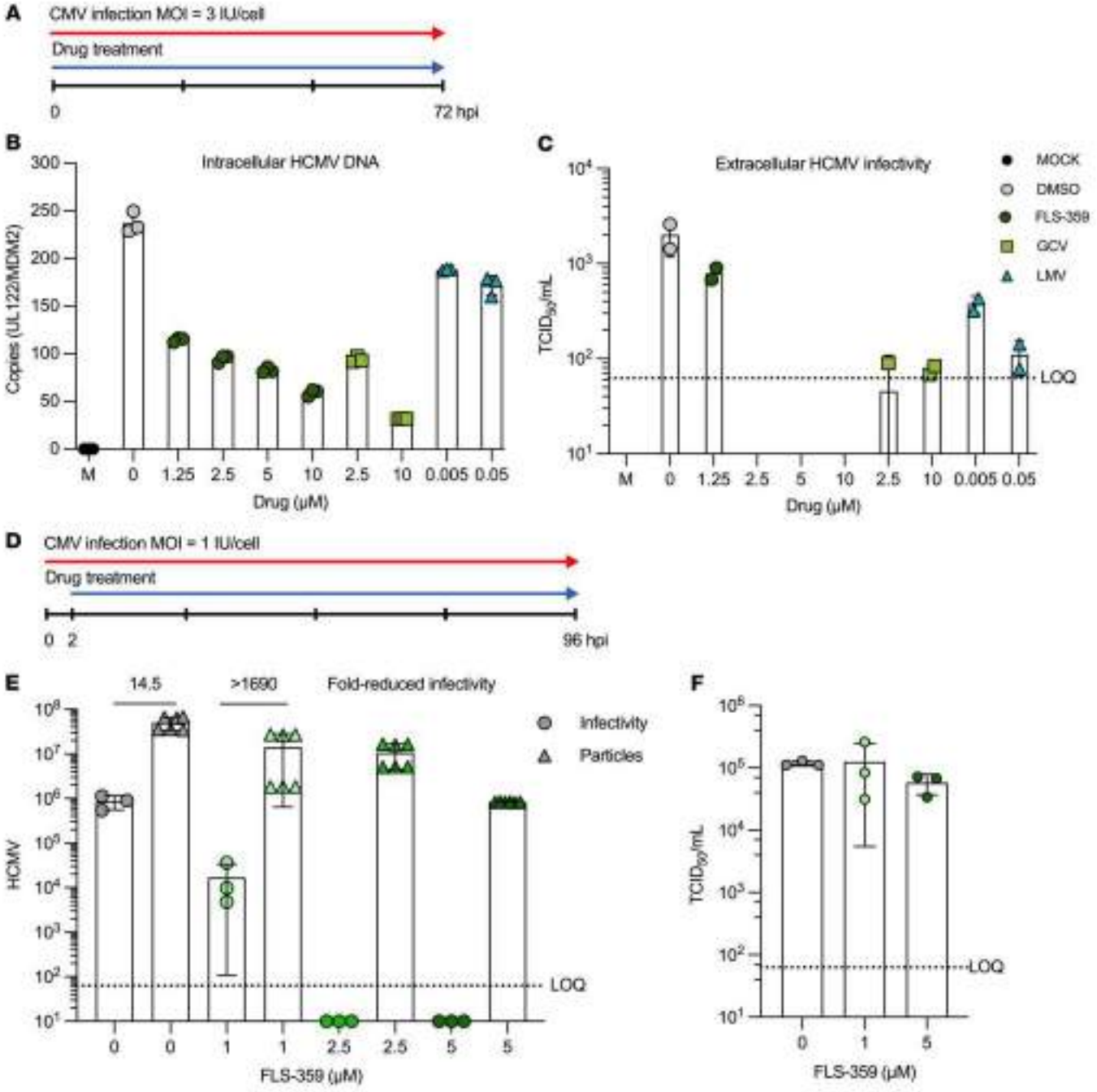

Figure 8. FLS-359 reduces intracellular HCMV DNA accumulation and extracellular virus production. (**A**) MRC-5 cells were mock-infected or infected with TB40/E-mCherry-UL99eGFP (3 IU/cell), treated with the indicated FLS-359, ganciclovir (GCV), and letermovir (LMV) doses, and harvested at 72 hpi. (**B**) Cellular DNA was prepared, and HCMV DNA was quantified by qPCR using UL122-specific probes and normalized to cellular MDM2 DNA (n = 3). (**C**) The effect of drugs on virus yield was monitored by $TCID_{50}$ assay (n = 2). (**D**) MRC-5 cells were infected with TB40/E-mCherry-UL99eGFP (1 IU/cell) and treated with the indicated drug doses from 2 hpi to 96 hpi. (**E**) DNase I–resistant viral DNA was quantified by qPCR (n = 6), and infectious virus was quantified by $TCID_{50}$ assay (n = 3). (**F**) TB40/E-mCherry-UL99eGFP virus (10^5 IU/mL) was incubated with indicated drug doses for 24 hours, and infectious virus was quantified by $TCID_{50}$ assay (n = 3). LOQ, limit of quantification. Mean ± SD is shown.

FLS-359 reduced intracellular viral DNA accumulation (Figure 8B), a likely consequence of reduced UL44, UL54, UL57, and RNA4.9 RNA expression (Figure 7, B and C). pUL44 and pUL54 are subunits of the viral DNA polymerase, pUL57 is a single-stranded DNA-binding protein required for viral DNA replication, and RNA4.9 is a noncoding RNA that forms an R-loop at the viral origin of DNA replication and is required for efficient viral DNA accumulation (64). However, the relatively modest approximately 3-fold reduction in intracellular viral DNA levels (Figure 8B) does not account for the more than 1,000-fold reduction in infectious virus (Figure 8C) caused by treatment with FLS-359 over the course of 72 hours. A second experiment recorded an approximately 70-fold reduction in

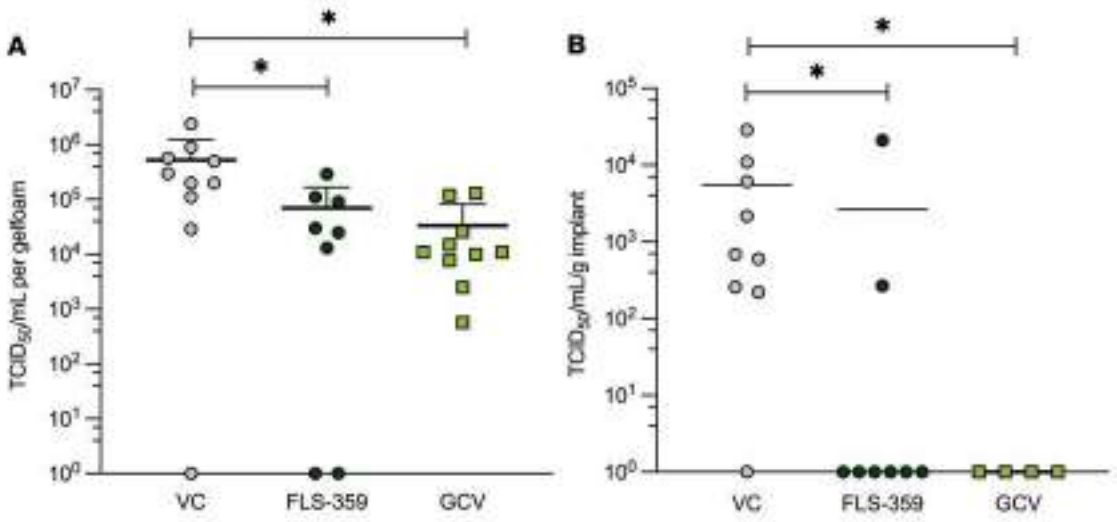

Figure 9. In vivo efficacy of FLS-359. (**A**) Gelfoam/human fibroblast model. MRC-5 cells were infected with TB40/E-mCherry-UL99eGFP (0.05 IU/cell), incubated for 24 hours, harvested, counted, and seeded (1×10^6 cells) into gelfoam plugs. After 3 days of incubation, plugs were implanted subcutaneously on the flanks of CIEA NOG mice. Beginning at 24 hours after implantation, mice were treated with vehicle control (VC; 0.5% methylcellulose + 0.5% Tween-80, p.o., b.i.d.), FLS-359 (50 mg/kg in VC, p.o., b.i.d.), or valganciclovir (GCV; 100 mg/kg in VC, p.o., b.i.d.). After 11 days of treatment, gelfoam plugs were harvested, and virus was quantified by $TCID_{50}$ assay. *$P < 0.03$. (**B**) Human lung-only mouse model. Beginning at 2 hours before infection with TB40/E (4.25×10^5 IU) via direct injection into lung implants, lung-only mice were treated with vehicle control (VC; 0.5% methylcellulose + 0.5% Tween-80 in sterile distilled water, p.o., b.i.d.), FLS-359 (50 mg/kg in VC, p.o., b.i.d.), or ganciclovir (GCV; 100 mg/kg in VC, i.p., daily). After 17 days of treatment, implants were harvested and processed for $TCID_{50}$ determination. *$P < 0.04$. Variance was calculated by 1-sided Kruskal-Wallis test followed by Dunn's multiple-comparison test.

extracellular virus particles, and viral infectivity was again reduced by more than 1,600-fold (Figure 8E). Thus, the number of virus particles and their infectivity are both impacted by the drug. Reduced levels of viral proteins could interfere with efficient DNA packaging into capsids, and export of mature enveloped virions. FLS-359 could also interfere with the production of infectious virions by perturbing the microtubule network. Consistent with the role of SIRT2 in α-tubulin deacetylation (44), FLS-359 can induce hyperacetylation of α-tubulin (Supplemental Figure 1A). Altered acetylation of α-tubulin K40 has potential to modulate microtubule activity (79), which in turn is critical for structure (80) and function (81) of the HCMV assembly zone, the viral organelle in which capsids are assembled into virions (82). Further, very-long-chain fatty acids are required for infectivity of virus particles (83), and SIRT2 inhibition impacts lipid synthesis (84), so it is possible that an effect of FLS-359 on fatty acid synthesis reduces the infectivity of HCMV progeny. Additional viral processes, such as nuclear egress of capsids, which is controlled by lamin B1 acetylation (15), might also be impacted by SIRT2 inhibition. Finally, in stressed tumor cells SIRT2 inhibition has been shown to activate p53 (85), induce degradation of overexpressed c-Myc (45, 46), and block full activation of the PI3K/Akt pathway (86) — any of which could potentially reduce the production of infectious viral progeny. Although further studies are needed to more fully appreciate the mode of FLS-359 antiviral action, it appears likely that its anti-HCMV mechanism is multifactorial, and the multiple components likely speak to its broad-spectrum antiviral activity and strongly predict that drug-resistant mutants will not evolve.

Will SIRT2 inhibitors prove to be well tolerated in humans? Mice appeared healthy and alert and did not lose weight during our anti-HCMV studies; SIRT2-knockout (30) and SIRT2/3-knockout (31) mice are healthy; and EX-527, which is selective for SIRT1 but also has anti-SIRT2 activity (87), is well tolerated in humans (88). Further, the acute nature of many viral infections will require short-term treatments, mitigating possible long-term toxicity.

The broad-spectrum antiviral activity of SIRT2 inhibitors can potentially find utility in multiple clinical applications. Treatment of viral disease in transplant patients is a prime example. These immunosuppressed patients have heightened susceptibility to environmental pathogens as well as adventitious agents traveling with donor tissues or resident in the recipient, including herpesviruses, polyomaviruses, respiratory viruses, hepadnaviruses, and emerging viruses (8, 9, 89, 90). We have already determined that several of these viral agents are inhibited by FLS-359, including HCMV (Figure 4), which continues to threaten transplant recipients in spite of effective direct-acting therapies. EBV (Figure 3), HBV, respiratory viruses that include influenza and now SARS-CoV-2, and other newly emerging agents such as Zika virus are also inhibited by FLS-359 (Table 1). A host-targeted, broad-spectrum drug should improve outcomes, especially for transplant patients undergoing antiviral prophylaxis.

In sum, FLS-359 is a representative of a new family of SIRT2 modulators. Its broad-spectrum and multifaceted antiviral activity illustrates its potential as a host-targeted antiviral with utility in treatment of numerous viral diseases and sets the stage for further understanding of how epigenetic mechanisms impact the growth and spread of multiple viral pathogens.

Methods

SIRT2 thermal stability assay. Equal volumes of 2× FLS-359 and 2× human $SIRT2^{2-352}$ (GenScript) in binding buffer (20 mM PIPES, pH 7.4, 100 mM NaCl, 0.005% Tween, 10 μM 1-anilino-8-naphthalenesulfonate) were added to PCR plates (Hard-Shell 384, black well, Bio-Rad), overlaid with silicon oil, and centrifuged (600*g*, 20 seconds). Thermal melt data were

collected using custom instrumentation (Fluorescence Innovations), with either 405 nm or 532 nm laser excitation and fluorescence lifetime emission to measure total well fluorescence and fluorescence lifetime as a function of temperature. Data were treated as previously described (37) to determine the midpoint transition temperature, T_m.

SIRT deacylase assay. Human SIRT deacylase activity was measured in assay buffer (50 mM Tris, pH 8.0, 137 mM NaCl, 2.7 mM KCl, 1 mM $MgCl_2$, 1 mg/mL BSA) containing purified, recombinant $SIRT2^{2–389}$, $SIRT1^{1–747}$, or $SIRT3^{1–400}$ protein (GenScript); acetylated (Ac-H_3K_9WW: QTARK^{Ac}STGGKAPRWW-NH_2) or myristoylated (Myr-H_3K_9WW: QTARK^{Myr}STGGKAPRWW-NH_2) peptide (GenScript); NAD^+; and inhibitors. Reactions were initiated by addition of SIRT protein, and aliquots were quenched with 1% formic acid after 10 minutes at 37°C. Reaction products (deacetylated peptide ions or Ac-ADP-ribose) were detected using RapidFire High Throughput Mass Spectrometry (PureHoney Technologies). Deacetylated peptide substrate (GenScript) and Ac-ADP-ribose (Toronto Research Chemicals) were used as controls in detection reactions.

X-ray structure determination. The study was performed at Crelux GmbH. $SIRT2^{56–356}$ was used for crystallization; a hexahistidine tag used for purification was removed before crystallization. Crystals of SIRT2 in complex with FLS-359 were obtained using hanging-drop vapor diffusion setups. SIRT2 (21.9 mg/mL; 50 mM HEPES-NaOH, 150 mM NaCl, pH 8.0) was preincubated with 3.6 mM (5.7-fold molar excess) of FLS-359 for 1 hour. A 1 μL aliquot of the protein solution was then mixed with 2 μL of reservoir solution (0.1 M HEPES-NaOH, pH 6.6, 0.3 M Li_2SO_4, 21% [wt/vol] PEG 3350) and streak-seeded before being equilibrated at 20°C over 0.2 mL of reservoir solution. Well-diffracting crystals grew as thick aggregates of thin plates and were mounted within 19 days.

For data collection, crystals were cryoprotected by the addition of ethylene glycol to a concentration of 20% (vol/vol) to the crystallization drop before mounting. Single thin plates were isolated for data collection. A complete 1.8 Å data set of a SIRT2/FLS-359 single crystal was collected at PETRA III (Hamburg, Germany, beamline P11) (Supplemental Table 2), and the data were integrated, analyzed, and scaled by XDS (91) (within the autoPROC pipeline [ref. 92], Pointless (93), and Aimless (94), respectively.

For structure determination and refinement, molecular replacement was done using a Crelux reference structure of SIRT2 as a starting model. Several rounds of alternating manual rebuilding and refinement with REFMAC5 (95) resulted in the final model (Supplemental Table 2). Atomic displacement factors were modeled with a single isotropic B-factor per atom, except for selected cysteine sulfur atoms for which residual electron density after isotropic refinement indicated an anisotropic behavior, as well as for the Zn^{++} atom in chain A. Non-crystallographic symmetry restraints were used throughout the refinement cycles.

Computational superpositioning predictions used the Glide module of Schrödinger, release 2022-4. The following SIRT2 structures were tested for predicted interactions with FLS-359: PDB ID 4RMI and 4RMG (49), 3ZGO (50), 4R8M (96), and 4X3P (97).

Coordinates and structure factors of the SIRT2/FLS-359 complex were deposited in the Protein Data Bank (PDB ID 7T1D).

Cells, viruses, and reagents. Human embryonic lung fibroblasts (MRC-5; ATCC CCL-171) were maintained in DMEM with 10% FBS. The type I B lymphoma cell line Akata (52) and MDA-MB-231 breast adenocarcinoma cells (ATCC HTB-26) were cultured in RPMI 1640 medium with 10% FBS. HepG2 hepatocellular carcinoma cells (ATCC HB-8065) were propagated in DMEM with 10% FBS. TB40/E-mCherry-UL99eGFP virus was described previously (73), and was titered by $TCID_{50}$ assay on MRC-5 cells (98). FLS-359 was synthesized as described in US Patent Application US20210139475A1. ^{1}H NMR was consistent with the structure, and purity was determined to be greater than 97% by reversed-phase HPLC. Ganciclovir and AGK2 (MilliporeSigma), letermovir (MedChem Express), SirReal2 and MIND4 (Chembridge/Hit2Lead), AK-7 (Cayman Chemical), and TM (Abmole) were stored at –20°C as 10 mM stocks in DMSO.

Assays for FLS-359 antiviral activity. SARS-CoV-2 (strain USA-WA1/2020) was assayed on Calu3 cells by qRT-PCR quantitation of extracellular viral genomes using remdesivir as an antiviral control at the United States Army Medical Research Institute of Infectious Diseases (USAMRIID). Zika virus (strain DAK41525) was assayed on human foreskin fibroblasts by immunofluorescence assay detecting a viral antigen using amodiaquine as an antiviral control at USAMRIID. HCMV (strain TB40/E) was assayed on MRC-5 fibroblasts by spread assay using ganciclovir and letermovir as antiviral controls (Figure 4). Influenza A (strain A/California/07/2009) was assayed on differentiated normal human bronchial epithelial cells by yield reduction assay using ribavirin as an antiviral control by a Division of Microbiology and Infectious Diseases contractor. Betacoronavirus 1 (strain OC43) was assayed on MRC-5 fibroblasts in a cytopathic effect (CPE) inhibition assay at Evrys Bio. Junin virus (strain Candid 1) was assayed on MRC-5 fibroblasts by immunofluorescence assay detecting a viral antigen using RIID E-1 as an antiviral control at USAMRIID. Hepatitis B virus (genotype D, subtype ayw) was assayed on primary human hepatocytes by monitoring of viral relaxed circular DNA using tenofovir as an antiviral control at ImQuest Biosciences. Epstein-Barr virus (EBV; strain Akata) was assayed on Akata BL cells activated by treatment with anti-IgG, and then viral gp350 expression was monitored using phosphonoacetic acid (PAA) as an antiviral control (Figure 3). Respiratory syncytial virus (strain Long) was assayed on MRC-5 fibroblasts by immunofluorescence assay detecting multiple viral antigens using ribavirin as an antiviral control at RetroVirox. Assays were performed in triplicate to determine IC_{50}s.

Assay for HCMV spread. Confluent MRC-5 cultures were infected with TB40/E-mCherry-UL99eGFP (0.01 IU/cell). Drugs were added after a 1-hour adsorption period using a Tecan D300e dispenser, and the DMSO concentration was normalized to 0.5% across wells. At 7 days post-infection (dpi), fluorescent images were captured using a BioTek Cytation 3 Multi-Mode Reader and analyzed using Agilent BioTek Gen5 software to calculate infected cell area. Uninfected, drug-treated cultures were fixed with 4% paraformaldehyde, stained with DAPI, imaged, and analyzed to determine nuclei counts.

Protein, RNA, and DNA analysis. Proteins were analyzed by Western blot as previously described (99) using anti-mCherry (1:1,000; EPR20579, Abcam), anti-IE1 (1:100; clone 1B12; ref. 100), anti–acetyl-α-tubulin K40 (1:10,000; T7451, MilliporeSigma), anti–c-Myc (1:2,000; Y69, Abcam), anti–β-actin (1:10,000; A5441, MilliporeSigma), and anti–α-tubulin (1:10,000; DMA1, MilliporeSigma) primary antibodies, plus IRDye 680RD anti-mouse or IRDye 800CW anti-rabbit (1:20,000; LI-COR) secondary antibodies. (See full, uncut gels in the supplemental material.) RNA and DNA were analyzed by qPCR assay as previously described (99) using primers listed in Supplemental Table 5.

Analysis of mouse pharmacokinetic parameters and tolerability. FLS-359 was formulated as a suspension at 5 mg/mL in 0.5% methylcellulose (cP 25) plus 0.5% Tween-80 (MilliporeSigma) in sterile water and vortexed and/or sonicated immediately before p.o. administration. The pharmacokinetics study used fed female BALB/c mice (22 g, n = 3 per time point). Blood samples (~30 μL via saphenous vein puncture) were taken at 0.25, 0.5, 1, 2, 4, 8, and 24 hours. A standard curve was prepared in control plasma using FLS-359 (0.01–10 μg/mL) in terfenadine solvent (50 ng/mL in methanol/acetonitrile 1:1 vol/vol). The lower limit of quantification was 10 ng/mL. An aliquot of 10 μL plasma sample was mixed with 10 μL terfenadine solvent plus 2 μL methanol. An additional 200 μL of terfenadine solvent was added, and the resulting mixture was vortexed for 1 minute and centrifuged at 1,500*g* for 15 minutes. The supernatant was diluted 10× with methanol/water (1:1 vol/vol with 0.1% formic acid), and 2 μL aliquots were analyzed using a QTRAP 4000 LC-MS/MS System (Sciex) with a C18 column (Kinetex). Pharmacokinetic parameters were determined with the noncompartmental analysis tool in WinNonlin (Certara).

To assess the tolerability of FLS-359, female NOD/Shi-scid/IL-2Rγ^{null} (NOG) mice were treated with 50 mg/kg p.o., b.i.d., for 14 days. Mice had free access to food and water and were evaluated for morbidity and mortality twice daily. Body weights and food consumption were recorded once per day before the morning dosing. Detailed clinical observations were made 1–2 hours after the morning compound administration and once 5–6 hours after the morning observation.

Mouse gelfoam-fibroblast model for anti-HCMV activity. For the mouse gelfoam model (58, 66), MRC-5 cells were infected with HCMV TB40/E-mCherry-UL99eGFP (0.05 IU/cell). On the same day, sterile gelfoam (SURGIFOAM Absorbable Gelatin Sponge, USP) was aseptically cut into 1.2 cm × 0.5 cm × 0.7 cm pieces and transferred into a sterile dish containing DMEM. Infected cultures and gelfoam pieces were incubated at 37°C for 24 hours. Then, infected cells were harvested and counted, and 1 × 10^6 cells in medium (30 μL) were slowly added to the gelfoam pieces in a 24-well non–tissue culture–treated plate. Seeded gelfoams were incubated for 3 hours at 37°C, and then 1 mL of medium was added to each gelfoam and incubated at 37°C for 3 days. On the day of gelfoam implant, 18-week-old male and female NOD.Cg-*Prkdc*^{scid}*Il2rg*^{tm1Sug}*/JicTac* mice (CIEA NOG, Taconic Biosciences) were anesthetized using isoflurane (Patterson Veterinary), the dorsal area above the hip region was shaved and sterilized with Betadine (Purdue Products) and 70% ethanol, the gelfoam was inserted beneath the skin, and incisions were closed. FLS-359 (50 mg/kg, p.o., b.i.d.), valganciclovir (50 mg/kg, p.o., daily), or diluent (0.5% methylcellulose plus 0.5% Tween-80) was administered, beginning immediately after implantation. On day 11, mice were euthanized, the gelfoams were harvested, homogenized, and clarified by centrifugation at 17,500*g* for 5 minutes at 4°C, and virus in the supernatant was quantified by $TCID_{50}$.

Human lung-only mouse model for anti-HCMV activity. Lung-only mice (LoM) were generated as previously described (67, 68). In brief, LoM were constructed by implanting of 2 pieces of human lung tissue (Advanced Bioscience Resources) subcutaneously into the back of male and female NOD.Cg-*Prkdc*^{scid}*Il2rg*^{tm1Wjl}*/SzJ* mice (NSG, The Jackson Laboratory). Expansion of the implants was monitored by palpation. Anesthetized mice were exposed to HCMV by direct injection of HCMV TB40/E (4.25×10^5 IU) into the implants in a total volume of 100 μL. Mice received vehicle control (0.5% methylcellulose, 0.5% Tween-80; p.o., b.i.d.), FLS-359 (50 mg/kg in vehicle; p.o., b.i.d.), or ganciclovir (100 mg/kg; i.p., daily) beginning 2 hours before infection. Human lung implants were harvested at 17 dpi and flash-frozen. Subsequently, implants were thawed and homogenized, and virus load was measured by $TCID_{50}$ assay.

Statistics. Quantitative results are shown as mean ± SD of independent experiments as noted in the figure legends. Statistical significance was evaluated using GraphPad Prism 8 (GraphPad Software). Efficacy readouts in animal studies were compared between treatment groups by Kruskal-Wallis test, followed by 1-sided Dunn's multiple-comparison test. A P value of 0.005 was used to determine statistical significance.

Study approval. Mouse studies were carried out in compliance with the NIH *Guide for the Care and Use of Laboratory Animals* (National Academies Press, 2011) according to protocols approved by Institutional Animal Care and Use Committees of Bioduro Beijing Co. (protocol BD-201709136, mouse pharmacokinetics), the Trudeau Institute (protocol 19-002, HCMV gelfoam), and the University of North Carolina at Chapel Hill (protocol 20-235, HCMV LoM).

Author contributions

KLR, SR, MJT, JLK, LT, APB, CD, WWR, AVW, JVG, MAL, TS, EAM, and LWC designed research studies. KLR, SR, MJT, LT, APB, AVW, and CD conducted experiments and acquired data. KLR, SR, MJT, JLK, LT, APB, CD, WWR, AVW, JVG, MAL, TS, EAM, and LWC analyzed data. KLR, SR, MJT, JLK, LT, AVW, APB, WWR, AW, JVG, MAL, TS, JRT, EAM, and LWC contributed to writing the manuscript and/or preparing figures.

Acknowledgments

We thank Emre Koyuncu (Cresenta Biosciences) for insights into the antiviral activities of sirtuins; John Denu (University of Wisconsin) for advice on the biochemistry of sirtuin 2; Quint Kückelhaus (Crelux) for running SIRT2/FLS-359 crystallizations; Karine Röwer (Crelux) for SIRT2/FLS-359 x-ray structure determination; Nieng Yan (Princeton University and Shenzhen Medical Academy of Research & Translation) for advice on x-ray crystallography; Youngwok Kim (Evrys Bio) and Sheli Radoshitsky (USAMRIID) for performing in vitro antiviral assays; Deborah Duso and Tricia Hart (Trudeau Institute) for implanting and harvesting gelfoams, gavaging mice, and doing $TCID_{50}$ assays; and Matthew Cole (Trudeau Institute) for preparing virus stocks and infecting fibroblasts for implantation in gelfoams. Evrys Bio utilized the nonclinical and preclinical services program offered by the National Institute of Allergy and Infectious Diseases. These studies were funded in part by grants from the NIH to Evrys Bio (R43-AI110048, R44-AI122488, R43-AI114079, and R44-AI114079) and to MAL (R01-CA140337) and a contract to Evrys Bio from the Department of Defense (W911QY18P0300). Evrys Bio has issued patents and pending applications claiming composition of matter for SIRT2 modulators.

Address correspondence to: Lillian W. Chiang, Evrys Bio LLC, 3805 Old Easton Road, Doylestown, Pennsylvania 18902, USA. Phone: 267.370.5436; Email: lillian@evrysbio.com.

1. Feld JJ, et al. Sofosbuvir and velpatasvir for HCV genotype 1, 2, 4, 5, and 6 infection. *N Engl J Med*. 2015;373(27):2599–2607.
2. Hussain M, et al. Drug resistance in influenza A virus: the epidemiology and management. *Infect Drug Resist*. 2017;10:121–134.
3. Brown AJ, et al. Broad spectrum antiviral remdesivir inhibits human endemic and zoonotic deltacoronaviruses with a highly divergent RNA dependent RNA polymerase. *Antiviral Res*. 2019;169:104541.
4. Bösl K, et al. Common nodes of virus–host interaction revealed through an integrated network analysis. *Front Immunol*. 2019;10:2186.
5. Ianevski A, et al. Novel activities of safe-in-human broad-spectrum antiviral agents. *Antiviral Res*. 2018;154:174–182.
6. Adalja A, Inglesby T. Broad-spectrum antiviral agents: a crucial pandemic tool. *Expert Rev Anti Infect Ther*. 2019;17(7):467–470.
7. Bekerman E, Einav S. Infectious disease. Combating emerging viral threats. *Science*. 2015;348(6232):282–283.
8. Taneja A, et al. Viral infections after allogeneic hematopoietic stem cell transplant. *Adv Cell Gene Ther*. 2019;2(2):e43.
9. Fishman JA. Infection in organ transplantation. *Am J Transplant*. 2017;17(4):856–879.
10. Svinkina T, et al. Deep, quantitative coverage of the lysine acetylome using novel anti-acetyl-lysine antibodies and an optimized proteomic workflow. *Mol Cell Proteomics*. 2015;14(9):2429–2440.
11. Choudhary C, et al. The growing landscape of lysine acetylation links metabolism and cell signalling. *Nat Rev Mol Cell Biol*. 2014;15(8):536–550.
12. Narita T, et al. Functions and mechanisms of non-histone protein acetylation. *Nat Rev Mol Cell Biol*. 2019;20(3):156–174.
13. Jeng M, et al. Manipulation of the host protein acetylation network by human immunodeficiency virus type 1. *Crit Rev Biochem Mol Biol*. 2015;50(4):314–325.
14. Giese S, et al. Role of influenza A virus NP acetylation on viral growth and replication. *Nat Commun*. 2017;8(1):1259.
15. Murray LA, et al. Orchestration of protein acetylation as a toggle for cellular defense and virus replication. *Nat Commun*. 2018;9(1):4967.
16. Li T, et al. Acetylation modulates cellular distribution and DNA sensing ability of interferon-inducible protein IFI16. *Proc Natl Acad Sci U S A*. 2012;109(26):10558–10563.
17. Chen L, et al. Acetylation of RelA at discrete sites regulates distinct nuclear functions of NF-kappaB. *EMBO J*. 2002;21(23):6539–6548.
18. Sharma A, et al. Shedding light on structure, function and regulation of human sirtuins: a comprehensive review. *3 Biotech*. 2023;13(1):29.
19. Feldman JL, et al. Sirtuin catalysis and regulation. *J Biol Chem*. 2012;287(51):42419–42427.
20. Feldman JL, et al. Activation of the protein deacetylase SIRT6 by long-chain fatty acids and widespread deacylation by mammalian sirtuins. *J Biol Chem*. 2013;288(43):31350–31356.
21. Goodwin ML, et al. Lactate and cancer: revisiting the Warburg effect in an era of lactate shuttling. *Front Nutr*. 2015;1:27.
22. Shenk T, Alwine JC. Human cytomegalovirus: coordinating cellular stress, signaling, and metabolic pathways. *Annu Rev Virol*. 2014;1(1):355–374.
23. Michishita E, et al. Evolutionarily conserved and nonconserved cellular localizations and functions of human SIRT proteins. *Mol Biol Cell*. 2005;16(10):4623–4635.
24. Koyuncu E, et al. Sirtuins are evolutionarily conserved viral restriction factors. *mBio*. 2014;5(6):e02249–14.
25. Hackett BA, et al. Sirtuin inhibitors are broadly antiviral against arboviruses. *mBio*. 2019;10(4):e01446-19.
26. Mao G, et al. Suppressive effects of sirtinol on human cytomegalovirus (hCMV) infection and hCMV-induced activation of molecular mechanisms of senescence and production of reactive oxygen species. *Mech Ageing Dev*. 2016;158:62–69.
27. Outeiro TF, et al. Sirtuin 2 inhibitors rescue alpha-synuclein-mediated toxicity in models of Parkinson's disease. *Science*. 2007;317(5837):516–519.
28. Yu H-B, et al. AGK2, a SIRT2 inhibitor, inhibits hepatitis B virus replication in vitro and in vivo. *Int J Med Sci*. 2018;15(12):1356–1364.
29. Piracha ZZ, et al. Sirtuin 2 isoform 1 enhances hepatitis B virus RNA transcription and DNA synthesis through the AKT/GSK-3β/β-catenin signaling pathway. *J Virol*. 2018;92(21):e00955-18.
30. Ciarlo E, et al. Sirtuin 2 deficiency increases bacterial phagocytosis by macrophages and protects from chronic Staphylococcal infection. *Front Immunol*. 2017;8:1037.
31. Heinonen T, et al. Dual deletion of the sirtuins SIRT2 and SIRT3 impacts on metabolism and inflammatory responses of macrophages and protects from endotoxemia. *Front Immunol*. 2019;10:2713.
32. Limaye AP, et al. Progress and challenges in the prevention, diagnosis, and management of cytomegalovirus infection in transplantation. *Clin Microbiol Rev*. 2020;34(1):e00043-19.
33. Kotton CN. Updates on antiviral drugs for cytomegalovirus prevention and treatment. *Curr Opin Organ Transplant*. 2019;24(4):469–475.
34. Griffiths P, Reeves M. Pathogenesis of human cytomegalovirus in the immunocompromised host. *Nat Rev Microbiol*. 2021;19(12):759–773.
35. San-Juan R, et al. Epstein-Barr virus-related post-transplant lymphoproliferative disorder in solid organ transplant recipients. *Clin Microbiol Infect*. 2014;20(suppl 7):109–118.
36. Bamoulid J, et al. Subclinical Epstein-Barr virus viremia among adult renal transplant recipients: incidence and consequences. *Am J Transplant*. 2013;13(3):656–662.
37. Matulis D, et al. Thermodynamic stability of carbonic anhydrase: measurements of binding affinity and stoichiometry using ThermoFluor. *Biochemistry*. 2005;44(13):5258–5266.
38. Quinti L, et al. SIRT2- and NRF2-targeting thiazole-containing compound with therapeutic activity in Huntington's disease models. *Cell Chem Biol*. 2016;23(7):849–861.
39. Huang H, et al. Lysine benzoylation is a histone mark regulated by SIRT2. *Nat Commun*. 2018;9(1):3374.
40. Galleano I, et al. A continuous, fluorogenic sirtuin 2 deacylase assay: substrate screening and inhibitor evaluation. *J Med Chem*. 2016;59(3):1021–1031.
41. Spiegelman NA, et al. Direct comparison of SIRT2 inhibitors: potency, specificity, activity-dependent inhibition, and on-target anticancer activities. *ChemMedChem*. 2018;13(18):1890–1894.
42. Lin H. Substrate-selective small-molecule modulators of enzymes: mechanisms and opportunities. *Curr Opin Chem Biol*. 2022;72:102231.
43. Kudo N, et al. Identification of a novel small molecule that inhibits deacetylase but not defatty-acylase reaction catalysed by SIRT2. *Philos Trans R Soc Lond B Biol Sci*. 2018;373(1748):20170070.
44. North BJ, et al. The human Sir2 ortholog, SIRT2, is an NAD^+-dependent tubulin deacetylase. *Mol Cell*. 2003;11(2):437–444.
45. Liu PY, et al. The histone deacetylase SIRT2 stabilizes Myc oncoproteins. *Cell Death Differ*. 2013;20(3):503–514.
46. Jing H, et al. A SIRT2-selective inhibitor promotes c-Myc oncoprotein degradation and exhibits broad anticancer activity. *Cancer Cell*. 2016;29(3):297–310.
47. Wang Y, et al. An overview of sirtuins as potential therapeutic target: structure, function and modulators. *Eur J Med Chem*. 2019;161:48–77.
48. Moniot S, et al. Structures, substrates, and regulators of mammalian sirtuins — opportunities and challenges for drug development. *Front Pharmacol*. 2012;3:16.
49. Rumpf T, et al. Selective Sirt2 inhibition by ligand-induced rearrangement of the active site. *Nat Commun*. 2015;6:6263.
50. Moniot S, et al. Crystal structure analysis of human Sirt2 and its ADP-ribose complex. *J Struct Biol*. 2013;182(2):136–143.
51. Wang T, et al. Recent progress on the discovery of Sirt2 inhibitors for the treatment of various cancers. *Curr Top Med Chem*. 2019;19(12):1051–1058.
52. Takada K, et al. An Epstein-Barr virus-producer line Akata: establishment of the cell line and analysis of viral DNA. *Virus Genes*. 1991;5(2):147–156.
53. Cifuentes-Munoz N, et al. Viral cell-to-cell spread: conventional and non-conventional ways. *Adv Virus Res*. 2020;108:85–125.
54. Cifuentes-Muñoz N, et al. Direct cell-to-cell transmission of respiratory viruses: the fast lanes. *PLoS Pathog*. 2018;14(6):e1007015.
55. Silva MC, et al. Human cytomegalovirus cell-to-cell spread in the absence of an essential assembly protein. *Proc Natl Acad Sci U S A*. 2005;102(6):2081–2086.
56. Nukui M, et al. The natural flavonoid compound deguelin inhibits HCMV lytic replication within fibroblasts. *Viruses*. 2018;10(11):614.
57. Plotkin SA, et al. Sensitivity of clinical isolates of human cytomegalovirus to 9-(1,3-dihydroxy-2-propoxymethyl)guanine. *J Infect Dis*. 1985;152(4):833–834.
58. Lischka P, et al. In vitro and in vivo activities of the novel anticytomegalovirus compound AIC246. *Antimicrob Agents Chemother*. 2010;54(3):1290–1297.
59. Razonable R, Melendez D. Letermovir and inhibitors of the terminase complex: a promising new class of investigational antiviral drugs against human cytomegalovirus. *Infect Drug Resist*. 2015;269:269–277.
60. Goldner T, et al. The novel anticytomegalovirus

compound AIC246 (letermovir) inhibits human cytomegalovirus replication through a specific antiviral mechanism that involves the viral terminase. *J Virol*. 2011;85(20):10884–10893.
61. Taylor DM, et al. A brain-permeable small molecule reduces neuronal cholesterol by inhibiting activity of sirtuin 2 deacetylase. *ACS Chem Biol*. 2011;6(6):540–546.
62. Stenberg RM. The human cytomegalovirus major immediate-early gene. *Intervirology*. 1996;39(5–6):393–399.
63. Adamson CS, Nevels MM. Bright and early: inhibiting human cytomegalovirus by targeting major immediate-early gene expression or protein function. *Viruses*. 2020;12(1):110.
64. Tai-Schmiedel J, et al. Human cytomegalovirus long noncoding RNA4.9 regulates viral DNA replication. *PLoS Pathog*. 2020;16(4):e1008390.
65. Pari GS. Nuts and bolts of human cytomegalovirus lytic DNA replication. *Curr Top Microbiol Immunol*. 2008;325:153–166.
66. Bravo FJ, et al. A model of human cytomegalovirus infection in severe combined immunodeficient mice. *Antiviral Res*. 2007;76(2):104–110.
67. Wahl A, et al. Precision mouse models with expanded tropism for human pathogens. *Nat Biotechnol*. 2019;37(10):1163–1173.
68. Wahl A, et al. SARS-CoV-2 infection is effectively treated and prevented by EIDD-2801. *Nature*. 2021;591(7850):451–457.
69. Tatum PR, et al. Identification of novel SIRT2-selective inhibitors using a click chemistry approach. *Bioorg Med Chem Lett*. 2014;24(8):1871–1874.
70. Frye RA. Phylogenetic classification of prokaryotic and eukaryotic Sir2-like proteins. *Biochem Biophys Res Commun*. 2000;273(2):793–798.
71. Rack JGM, et al. Constitutive nuclear localization of an alternatively spliced sirtuin-2 isoform. *J Mol Biol*. 2014;426(8):1677–1691.
72. Choi YH, et al. Src regulates the activity of SIRT2. *Biochem Biophys Res Commun*. 2014;450(2):1120–1125.
73. North BJ, Verdin E. Mitotic regulation of SIRT2 by cyclin-dependent kinase 1-dependent phosphorylation. *J Biol Chem*. 2007;282(27):19546–19555.
74. Pereira JM, et al. Infection reveals a modification of SIRT2 critical for chromatin association. *Cell Rep*. 2018;23(4):1124–1137.
75. Budayeva HG, Cristea IM. Human sirtuin 2 localization, transient interactions, and impact on the proteome point to its role in intracellular trafficking. *Mol Cell Proteomics*. 2016;15(10):3107–3125.
76. North BJ, Verdin E. Interphase nucleo-cytoplasmic shuttling and localization of SIRT2 during mitosis. *PLoS One*. 2007;2(8):e784.
77. Das C, et al. CBP/p300-mediated acetylation of histone H3 on lysine 56. *Nature*. 2009;459(7243):113–117.
78. Vaquero A. SirT2 is a histone deacetylase with preference for histone H4 Lys 16 during mitosis. *Genes Dev*. 2006;20(10):1256–1261.
79. Janke C, Montagnac G. Causes and consequences of microtubule acetylation. *Curr Biol*. 2017;27(23):R1287–R1292.
80. Sanchez V, et al. Accumulation of virion tegument and envelope proteins in a stable cytoplasmic compartment during human cytomegalovirus replication: characterization of a potential site of virus assembly. *J Virol*. 2000;74(2):975–986.
81. Clippinger AJ, Alwine JC. Dynein mediates the localization and activation of mTOR in normal and human cytomegalovirus-infected cells. *Genes Dev*. 2012;26(18):2015–2026.
82. Alwine JC. The human cytomegalovirus assembly compartment: a masterpiece of viral manipulation of cellular processes that facilitate assembly and egress. *PLOS Pathog*. 2012;8(9):e1002878.
83. Koyuncu E, et al. Saturated very long chain fatty acids are required for the production of infectious human cytomegalovirus progeny. *PLoS Pathog*. 2013;9(5):e1003333.
84. Ye X, et al. Sirtuins in glucose and lipid metabolism. *Oncotarget*. 2017;8(1):1845–1859.
85. Hoffmann G, et al. A novel sirtuin 2 (SIRT2) inhibitor with p53-dependent pro-apoptotic activity in non-small cell lung cancer. *J Biol Chem*. 2014;289(8):5208–5216.
86. Ramakrishnan G, et al. Sirt2 deacetylase is a novel AKT binding partner critical for AKT activation by insulin. *J Biol Chem*. 2014;289(9):6054–6066.
87. Napper AD, et al. Discovery of indoles as potent and selective inhibitors of the deacetylase SIRT1. *J Med Chem*. 2005;48(25):8045–8054.
88. Westerberg G, et al. Safety, pharmacokinetics, pharmacogenomics and QT concentration-effect modelling of the SirT1 inhibitor selisistat in healthy volunteers. *Br J Clin Pharmacol*. 2015;79(3):477–491.
89. Clausen ES, Zaffiri L. Infection prophylaxis and management of viral infection. *Ann Transl Med*. 2020;8(6):415–415.
90. Manansala M, et al. Management of immunosuppressants in the era of coronavirus disease-2019. *Curr Opin Pulm Med*. 2021;27(3):176–183.
91. Kabsch W. XDS. *Acta Crystallogr D Biol Crystallogr*. 2010;66(2):125–132.
92. Vonrhein C, et al. Data processing and analysis with the autoPROC toolbox. *Acta Crystallogr D Biol Crystallogr*. 2011;67(4):293–302.
93. Evans P. Scaling and assessment of data quality. *Acta Crystallogr D Biol Crystallogr*. 2006;62(1):72–82.
94. Evans PR, Murshudov GN. How good are my data and what is the resolution? *Acta Crystallogr D Biol Crystallogr*. 2013;69(7):1204–1214.
95. Kovalevskiy O, et al. Overview of refinement procedures within REFMAC 5: utilizing data from different sources. *Acta Crystallogr D Struct Biol*. 2018;74(3):215–227.
96. Teng Y-B, et al. Efficient demyristoylase activity of SIRT2 revealed by kinetic and structural studies. *Sci Rep*. 2015;5(1):8529.
97. Wang Y, et al. Deacylation mechanism by SIRT2 revealed in the 1′-SH-2′-O-myristoyl intermediate structure. *Cell Chem Biol*. 2017;24(3):339–345.
98. O'Connor CM, Shenk T. Human cytomegalovirus pUS27 G protein-coupled receptor homologue is required for efficient spread by the extracellular route but not for direct cell-to-cell spread. *J Virol*. 2011;85(8):3700–3707.
99. Nukui M, et al. Protein S-nitrosylation of human cytomegalovirus pp71 inhibits its ability to limit STING antiviral responses. *J Virol*. 2020;94(17):e00033-20.
100. Zhu H, et al. Human cytomegalovirus IE1 and IE2 proteins block apoptosis. *J Virol*. 1995;69(12):7960–7970.

Antiviral Research 217 (2023) 105698

Contents lists available at ScienceDirect

Antiviral Research

journal homepage: www.elsevier.com/locate/antiviral

Inhibition of SIRT2 promotes death of human cytomegalovirus-infected peripheral blood monocytes via apoptosis and necroptosis

Jennifer Cheung [a], Stacy Remiszewski [b], Lillian W. Chiang [b], Ejaz Ahmad [c], Mohan Pal [c], SM Ashikur Rahman [c], Zaneta Nikolovska-Coleska [c,d], Gary C. Chan [a,*]

[a] Department of Microbiology & Immunology, SUNY Upstate Medical University, Syracuse, NY, 13210, USA
[b] Evrys Bio, LLC, Pennsylvania Biotechnology Center, Doylestown, PA, 18902, USA
[c] Department of Pathology, University of Michigan Medical School, Ann Arbor, MI, 48109, USA
[d] Rogel Cancer Center, University of Michigan Medical School, Ann Arbor, MI, USA

ARTICLE INFO

Keywords:
Cytomegalovirus
Apoptosis
Necroptosis
Small-molecule inhibitor
Sirtuin 2
Monocyte

ABSTRACT

Peripheral blood monocytes are the cells predominantly responsible for systemic dissemination of human cytomegalovirus (HCMV) and a significant cause of morbidity and mortality in immunocompromised patients. HCMV establishes a silent/quiescent infection in monocytes, which is defined by the lack of viral replication and lytic gene expression. The absence of replication shields the virus within infected monocytes from the current available antiviral drugs that are designed to suppress active replication. Our previous work has shown that HCMV stimulates a noncanonical phosphorylation of Akt and the subsequent upregulation of a distinct subset of prosurvival proteins in normally short-lived monocytes. In this study, we found that SIRT2 activity is required for the unique activation profile of Akt induced within HCMV-infected monocytes. Importantly, both therapeutic and prophylactic treatment with a novel SIRT2 inhibitor, FLS-379, promoted death of infected monocytes via both the apoptotic and necroptotic cell death pathways. Mechanistically, SIRT2 inhibition reduced expression of Mcl-1, an Akt-dependent antiapoptotic Bcl-2 family member, and enhanced activation of MLKL, the executioner kinase of necroptosis. We have previously reported HCMV to block necroptosis by stimulating cellular autophagy. Here, we additionally demonstrate that inhibition of SIRT2 suppressed Akt-dependent HCMV-induced autophagy leading to necroptosis of infected monocytes. Overall, our data show that SIRT2 inhibition can simultaneously promote death of quiescently infected monocytes by two distinct death pathways, apoptosis and necroptosis, which may be vital for limiting viral dissemination to peripheral organs in immunosuppressed patients.

1. Introduction

Human cytomegalovirus (HCMV) is a member of the *Herpesviridae* family of viruses with seropositivity rates ranging from 40 to 100% in adults worldwide (Cannon et al., 2010; Zuhair et al., 2019). HCMV infection is typically asymptomatic in immunocompetent individuals but can cause mononucleosis-like symptoms (Fiala et al., 1977). HCMV is also linked to various inflammatory conditions, such as atherosclerosis, and certain cancers, including breast cancer and glioblastomas (Cobbs et al., 2002; Geisler et al., 2019; Nikitskaya et al., 2016; Rahman et al., 2019). However, HCMV is a significant cause of morbidity and mortality in immunocompromised patients (Emery, 2001). Due to the immunosuppression necessary to prevent organ rejection, patients receiving bone marrow or solid organ transplants are among the most vulnerable to severe HCMV disease. HCMV is the most common viral opportunistic infection following hematopoietic stem cell and solid organ transplants, with disease incidence reaching 50–75% of lung transplant and 50% of kidney transplant recipients (Azevedo et al., 2015; Patel and Paya, 1997). In these vulnerable patient populations, HCMV can spread to and trigger inflammation in a multitude of organ systems, including the lungs, brain, esophagus, intestines, and eyes, potentially leading to multi-organ failure, organ rejection, or even death

Abbreviations: MOI, multiplicity of infection; SSC, side scatter; FSC, forward scatter; SRB, Sulforhodamine B; p, phospho; HPI, hours post-infection; DPI, days post-infection; h, hour; RT, room temperature; SEM, standard error of the mean; G, gravitational force; AV, Annexin-V; PI, propidium iodide.

* Corresponding author. Department of Microbiology and Immunology, SUNY Upstate Medical University, 750 East Adams Street, Syracuse, NY, 13210, USA.
E-mail address: chang@upstate.edu (G.C. Chan).

https://doi.org/10.1016/j.antiviral.2023.105698
Received 24 May 2023; Received in revised form 2 August 2023; Accepted 4 August 2023
Available online 9 August 2023

(Azevedo et al., 2015). Preventing systemic dissemination of the virus is an integral component to relieving the disease burden caused by HCMV.

During acute HCMV infection, monocytes are key cells that mediate systemic dissemination (Chan et al., 2012a; Manez et al., 1996; Smith et al., 2004a; Taylor-Wiedeman et al., 1994). HCMV establishes a quiescent infection in monocytes, during which no viral lytic genes are expressed and productive viral replication is stalled (Hargett and Shenk, 2010; Krishna et al., 2017; Rossetto et al., 2013; Sinclair and Sissons, 1996; Smith et al., 2021; Wagenknecht et al., 2015). Subsequently, the virus uses monocytes as "Trojan horses" to disseminate throughout the body while evading the immune system (Elder et al., 2019). Upon extravasation into tissues, infected monocytes differentiate into long-lived, replication-permissive macrophages allowing for infection of organs (Chan et al., 2008a, 2012a, 2012b; Cojohari et al., 2020; Min et al., 2020; Smith et al., 2004a; Soderberg-Naucler et al., 2001). This viral dissemination strategy limits the effectiveness of current HCMV antivirals. At present, the limited repertoire of antiviral therapeutics approved for HCMV—ganciclovir, valganciclovir, maribavir, cidofovir, foscarnet, and letermovir—all exclusively block the lytic phase of HCMV's lifecycle and are unable to target quiescently infected monocytes to prevent spread (Crumpacker, 1992; Kendle and Fan-Havard, 1998; Maertens et al., 2019; Matthews and Boehme, 1988; Patil et al., 2010; Verghese and Schleiss, 2013). Consequently, while prophylactic and pre-emptive use of HCMV antivirals has dramatically reduced the incidence of early HCMV disease, rebound infection and late-onset disease remains a significant issue once antiviral therapy has been discontinued in organ transplant recipients (Boeckh et al., 2003; Singh, 2005). In addition, severe drug-associated toxicities from long-term use of HCMV antivirals and the rise of drug-resistant HCMV strains have further increased the need for novel antiviral therapies to reduce the disease burden of HCMV (Jacobson, 1992; Kendle and Fan-Havard, 1998; Perrottet et al., 2009). One promising avenue of drug development is the targeting of host proteins modulated by HCMV infection and vital to the survival of infected cells.

A key biological hurdle that HCMV must overcome is extending the normally short 48–72 h lifespan of monocytes without the support of viral antiapoptotic proteins (Patel et al., 2017; Whitelaw, 1966). Apoptosis is the major pathway through which surveilling monocytes are programmed to die after entering circulation from the bone marrow in the absence of differentiation stimuli (Mangan et al., 1993). HCMV rapidly blocks the intrinsic biological programming of monocytes to undergo apoptosis (Chan et al., 2010; Cojohari et al., 2016; Collins-McMillen et al., 2018; Collins-McMillen et al., 2015; Peppenelli et al., 2016; Peppenelli et al., 2018; Reeves et al., 2012). HCMV-induced antiapoptotic mechanisms triggered within infected monocytes occur through binding of viral glycoproteins to host cellular receptors (Chan et al., 2010; Mahmud et al., 2020; Peppenelli et al., 2016; Yurochko et al., 1992, 1997). The distinct receptor combination and subsequent kinetics of activation following engagement of the virion to the cell surface initiates a noncanonical PI3K/Akt signaling cascade, which leads to the preferential phosphorylation of Akt at residue S473 (Cojohari et al., 2016; Mahmud et al., 2020; Peppenelli et al., 2018). This unique Akt phosphorylation signature mediates an HCMV-specific transcriptional and translational profile, leading to the upregulation of a distinct subset of antiapoptotic proteins necessary for the survival of HCMV-infected monocytes (Cojohari et al., 2016; Mahmud et al., 2020; Peppenelli et al., 2018). However, once apoptosis is inhibited, infected monocytes initiate necroptosis, a "trapdoor" cell death pathway as an antiviral countermeasure (Mocarski et al., 2015), which can be rapidly suppressed by HCMV in monocytes (Altman et al., 2020), and in other cell types (Fletcher-Etherington et al., 2020; Upton and Chan, 2014; Upton et al., 2008, 2010, 2012). Akt is a known regulator of necroptosis and in certain cases is required for its suppression (Liu et al., 2014; McNamara et al., 2013). Together, these studies suggest that targeting the Akt pathway could prevent HCMV from impeding both apoptosis and necroptosis, thus destining infected monocytes for cell death.

Sirtuins (SIRTs) are a family of seven evolutionarily conserved NAD^+-dependent deacylases and have been implicated in both apoptosis and necroptosis (Ding and Hao, 2021; Kozako et al., 2018; Luo et al., 2019; Song et al., 2021; Xu et al., 2019). Sirtuins are able to modulate Akt activity by directly deacetylating the pleckstrin homology (PH) domain of Akt, enabling its localization to the cell membrane and subsequent activation (Sundaresan et al., 2011). SIRT2 is the predominantly cytoplasmic member of the sirtuin family, which directly binds to and is required for the full activation of Akt (Dan et al., 2012; Ramakrishnan et al., 2014). FLS-359 is a newly described allosteric SIRT2 modulator that inhibits the growth and spread of HCMV in cultured fibroblasts and mouse models of infection (Roche et al., 2023). In biochemical assays, the drug binds to SIRT2 and alters its thermal denaturation profile; it is selective for inhibition of SIRT2 deacetylation versus Sirt1 and Sirt3, the Sirts most closely related to SIRT2; and it is substrate selective, inhibiting SIRT2 deacetylation but not demyristoylation. The engagement of FLS-359 with SIRT2 was confirmed in an X-ray structure at 1.8 Å resolution; and its biological activity was confirmed by demonstrating that the drug induces hyperacetylation of the SIRT2 target, α-tubulin, and causes degradation of c-Myc, well-known consequences of SIRT2 inhibition (Jing et al., 2016; Liu et al., 2013; North et al., 2003).

We show here that inhibition of SIRT2 using a novel small-molecule inhibitor, FLS-379 (Roche et al., 2023), leads to the death of HCMV-infected monocytes via both the apoptotic and necroptotic pathways. The novel SIRT2 inhibitor exerted its proapoptotic effect through the Akt pathway by blocking HCMV-induced S473 Akt phosphorylation and preventing the downstream upregulation of Mcl-1. Concurrently, SIRT2 inhibition led to increased activation of MLKL, the executioner kinase of necroptosis, following HCMV infection. Taken together, these data support SIRT2 inhibition as a new strategy through which HCMV-infected monocytes can be eliminated by simultaneously counteracting virus-induced antiapoptotic and anti-necroptotic mechanisms.

2. Materials and methods

2.1. Human peripheral blood monocyte isolation and culture

Isolation of human peripheral blood monocytes was performed as previously described (Chan et al., 2010; Smith et al., 2004a; Yurochko and Huang, 1999). Blood was drawn from voluntary random donors by venipuncture, diluted in RPMI-1640 media (ATCC, Manassas, VA), and centrifuged through Ficoll-Paque cell separation medium (Cytiva, Uppsala, Sweden) to remove red blood cells and neutrophils. Mononuclear cells were collected and washed with saline to remove the platelets and then separated by centrifugation through a Percoll (GE Healthcare, Wilkes-Barre, PA) gradient (40% and 48.6%). More than 95% of isolated peripheral blood mononuclear cells were monocytes, as determined by $CD14^+$ or $CD16^+$ staining. The cells were washed with saline, resuspended in RPMI-1640 medium, and counted. All experiments were performed in 0%–0.5% human serum at 37 °C in a 5% CO_2 incubator, unless otherwise stated. SUNY Upstate Medical University Institutional Review Board and Health Insurance Portability and Accountability Act guidelines for the use of human subjects were followed for all experimental protocols in our study. For the inhibitor studies, the following reagents were used: FLS-359 and FLSX-008 (SIRT2 inhibitors from Evrys Bio) (Roche et al., 2023) and UM-116 (an Mcl-1 inhibitor from the Nikolovska-Coleska lab).

2.2. Virus preparation and infection

Human embryonic lung (HEL) 299 fibroblasts (CCL-137; American Type Culture Collection, Manassas, VA) were cultured in Dulbecco modified Eagle medium (DMEM) (Corning, Manassas, VA) with 100 U/mL Penicillin and 100 μg/mL Streptomycin (Life Technologies, Carlsbad, CA), 2.5 μg/mL Plasmocin (Invivogen, San Diego, CA), and 10%

fetal bovine serum (FBS) (Sigma). Upon reaching confluence, the fibroblasts were infected with HCMV (strain TB40/E) in DMEM supplemented with 4% FBS. Virus was purified from the supernatant on a 20% sorbitol cushion to remove cellular contaminants and resuspended in RPMI-1640 medium. A multiplicity of infection (MOI) of 5 was used for each experiment, as >99% of monocytes were infected with TB40E particles (Chan et al., 2009b). Mock infection was performed by adding an equivalent volume of RPMI-1640 medium to monocytes.

2.3. Flow cytometry

Monocytes were washed in phosphate-buffered saline (PBS) and stained with fluorescein isothiocyanate (FITC)-annexin V (Life Technologies) and propidium iodide (PI) stain (Life Technologies) to detect dead and dying cells. After staining, the cells were analyzed by flow cytometry using an LSRFortessa cell analyzer and BD FACSDiva software (BD Biosciences, Franklin Lakes, NJ). Our gating strategy on forward scatter (FSC)/side scatter (SSC) was set to include both cells in the early stages of apoptosis (decreased FSC and increased SSC compared to those for viable cells) and cells in the late stages of apoptosis (decreased FSC and decreased SSC compared to those of viable cells).

2.4. Sulforhodamine B (SRB) cytotoxicity assay

Monocytes were plated in 96-well plates and cultured in RPMI-1640 media supplemented with 0.1% human serum. Cytotoxicity was measured using an SRB assay (Abcam, Cambridge, UK). Briefly, the monocytes were fixed for 1 h (h) at 4 °C, the wells were gently washed 3 times with dH_2O, and the adherent cells were stained with SRB staining solution for 15 min protected from light. The stain was removed, and the wells were washed 4 times with washing solution. The protein-bound dye was solubilized with solubilization solution, and the absorbance was measured at 565 nm.

2.5. Western blot analysis

Monocytes were harvested in a modified radioimmunoprecipitation assay (RIPA) buffer (50 mM Tris-HCl [pH 7.5], 5 mM EDTA, 100 mM NaCl, 1% Triton X-100, 0.1% SDS, 10% glycerol) supplemented with protease inhibitor cocktail (Sigma) and phosphatase inhibitor cocktails 2 and 3 (Sigma) for 30 min (min) on ice. The lysates were cleared from the cell debris by centrifugation at 4 °C (5 min, 21130×*g*) and stored at −20 °C until further analysis. Protein samples were solubilized in Laemmli SDS-sample nonreducing (6×) buffer (Boston Bioproducts, Boston, MA) supplemented with β-mercaptoethanol (Amresco, Solon, OH) by incubating at 95 °C for 10 min. Equal amounts of total protein from each sample were loaded in each well, separated by SDS-polyacrylamide gel electrophoresis, and transferred to polyvinylidene difluoride membranes (Bio-Rad, Hercules, CA). Blots were blocked in 5% bovine serum albumin (BSA) (Fisher Scientific, Waltham, MA) for 1 h at room temperature (RT) and then incubated with primary antibodies overnight at 4 °C. The following antibodies were used: anti-Akt, anti-phospho (p)-Akt (S473), anti-p-Akt (T308), anti-Mcl-1, anti-RIP3, anti-p-RIP3, anti-MLKL, and anti-p-MLKL (Cell Signaling, Danvers, MA). The blots were then incubated with horseradish peroxidase (HRP)-conjugated secondary antibodies (Cell Signaling), and chemiluminescence was detected using the Amersham ECL Prime Western Blotting Detection reagent (GE Healthcare).

2.6. Immunoprecipitation

Monocytes were pretreated with a Mcl-1 inhibitor or DMSO vehicle for 1 h, and then infected with HCMV for 24 h. Monocyte lysates were harvested in NP-40 lysis buffer (1 mM DTT, 50 mM Tris-HCl [pH 7.4], 1 mM EDTA, 150 mM NaCl, 0.5% (v/v) NP-40) supplemented with protease inhibitor cocktail (Sigma-Aldrich) and phosphatase inhibitor cocktails 2 and 3 (Sigma-Aldrich) for 30 min on ice. The lysates were cleared from the cell debris by centrifugation at 4 °C (5 min, 21130×*g*). Input controls were collected and stored at −20 °C until further analysis. Lysates equivalent to 160 μg of total protein were incubated with 2 μg of antibody recognizing Mcl-1 (Invitrogen, Waltham, MA) or IgG isotype controls (Santa Cruz, Dallas, TX) overnight at 4 °C. Dynabeads protein G (Invitrogen) were added to the lysates and incubated at 4 °C for 4 h. The protein G beads with bound protein complexes were magnetically separated and washed with lysis buffer, followed by elution of the protein complexes. The samples were then prepared for SDS-polyacrylamide gel electrophoresis and analyzed by Western blot analysis.

2.7. Synthesis and characterization of UM-116

The UM-116 Mcl-1 inhibitor was synthesized through a presented route in Supplemental Fig. S1. Detailed chemistry and characterization are provided in the supplemental material and Supplemental Fig. S2.

2.8. Fluorescence polarization (FP) binding assay

Sensitive and quantitative FP-based binding assay was developed and optimized to determine the binding affinity of small-molecule inhibitors to the recombinant Mcl-1 protein. Fluorescent labeled Bid BH3-peptide, FAM-ϵ-Ahx-Bid peptide (QEDIIRNIARHLAQVGDSMDR), was used as a competitive probe. The assay buffer was 20 mM phosphate (pH 7.4), 50 mM NaCl, 1 mM EDTA, and 0.05% Pluronic F68 with a final DMSO concentration of 4%. All experiments were performed in a final volume of 125 μL using black 96-well plates (Corning no. 3792) and analyzed with Synergy H1 Hybrid BioTek plate reader at excitation and emission wavelengths of 485 nm and 530 nm, respectively, after incubation for 3 h at room temperature. Dissociation constant (K_d) of the FAM-BID was determined to be 5.99 ± 1.12 nM, demonstrating stable signal up to 24h (Fig. S3). Based on the K_d value, the concentration of the Mcl-1 protein used in the competitive binding experiments was 20 nM and the fluorescent probe, FAM-BID, was fixed at 2 nM. IC_{50} values were determined by nonlinear regression fitting of the competition curves (GraphPad Prism 7.0 Software) and converted into K_i values as previously described (Nikolovska-Coleska et al., 2004).

2.9. Bio-layer interferometry (BLI)

To confirm and determine the direct binding of UM-116 to Mcl-1 protein, the BLI experiments were performed as per our previous report (Kump et al., 2020) at room temperature on OctetRED96 (PALL/ForteBio) in black 96-well plates (Greiner bio-one, # 655209). The biotinylated Mcl-1 (10 μg/ml) was immobilized and saturated on Superstreptavidin (SSA) Biosensors (Sartorius, #18–5057) for 10 min. Association and dissociation cycles were fixed for 10 min. The same FP binding assay buffer (20 mM phosphate pH 7.4, 50 mM NaCl, 1 mM EDTA, and 0.05% Pluronic F68) was used for custom, baseline, and dissociation steps, while buffer containing serially diluted compound, UM-116 with final DMSO concentration of 4% DMSO was used for association. Association and dissociation cycles were fixed at 10 min each. Kinetic data were collected and processed with the Data Analysis software provided by ForteBio. All experiments were analyzed with referencing by subtraction of the buffer sensorgrams. Plotting the response nm values of the binding sensorgrams with the respective compound concentration was used for steady state analysis and calculation of the K_d value.

2.10. Immunofluorescence

Cell monolayers plated in glass-bottom plates were fixed for 15 min in 4% paraformaldehyde (PFA) (Sigma) in PBS, and then washed three times with PBS. Cell permeabilization and blocking of nonspecific

binding were performed by incubating the cells with 0.1% Triton X-100, 5% BSA, and 1:10 FcR blocking reagent (Miltenyi, Bergisch Gladbach, Germany) in PBS for 30 min at room temperature. The cells were then incubated overnight at 4 °C in a humidified chamber with an anti-LC3 antibody (Cell Signaling). Cells were washed in PBS and then incubated with an anti-rabbit secondary antibody conjugated to Alexa Fluor 488 (Cell Signaling) for 1 h, protected from light. Cells were washed in PBS and then incubated with Hoechst 33342 nuclear stain (Thermo Fisher) for 10 min before being analyzed on a Nikon Eclipse Ti80 epifluorescence microscope (Nikon, Melville, NY). Digitized images were resized, organized, thresholded, and labeled using ImageJ software, an open Java-based image processing program developed at the National Institutes of Health. Puncta per cell were counted from at least 30 unique cells per donor per treatment. The mean puncta per cell was then calculated.

2.11. Statistical analysis

All experiments were performed independently a minimum of 3 times using primary monocytes isolated from different blood donors. Survival data sets obtained from primary monocytes inherently have substantial variation due to donor variability. Consequently, data are displayed as matched experimental data points from individual donors in a side-by-side comparison. Data were analyzed using a two-way Student's *t*-test comparison or two-way ANOVA with GraphPad Prism software (GraphPad) and expressed as the mean ± the standard error of the mean (SEM). P values of less than 0.05 were considered statistically significant.

3. Results

3.1. Inhibition of SIRT2 triggers death of HCMV-infected monocytes

HCMV induces the survival of infected monocytes in the absence of viral lytic protein expression via viral glycoprotein binding to cellular surface receptors (Chan et al., 2010; Cojohari et al., 2016; Collins-McMillen et al., 2018; Collins-McMillen et al., 2015; Mahmud et al., 2020; Peppenelli et al., 2016; Peppenelli et al., 2018; Stevenson et al., 2014). This interaction triggers a noncanonical activation of the Akt signaling pathway, stimulating a preferential phosphorylation of Akt at S473 that is distinct from the T308/S473 phosphorylation ratio induced by normal myeloid growth factors (Cojohari et al., 2016; Mahmud et al., 2020; Peppenelli et al., 2018). HCMV-activated Akt leads to the upregulation of a unique subset of cellular antiapoptotic proteins (Cojohari et al., 2016; Mahmud et al., 2020; Peppenelli et al., 2018). SIRT2 directly binds and deacetylates Akt allowing for the phosphorylation and

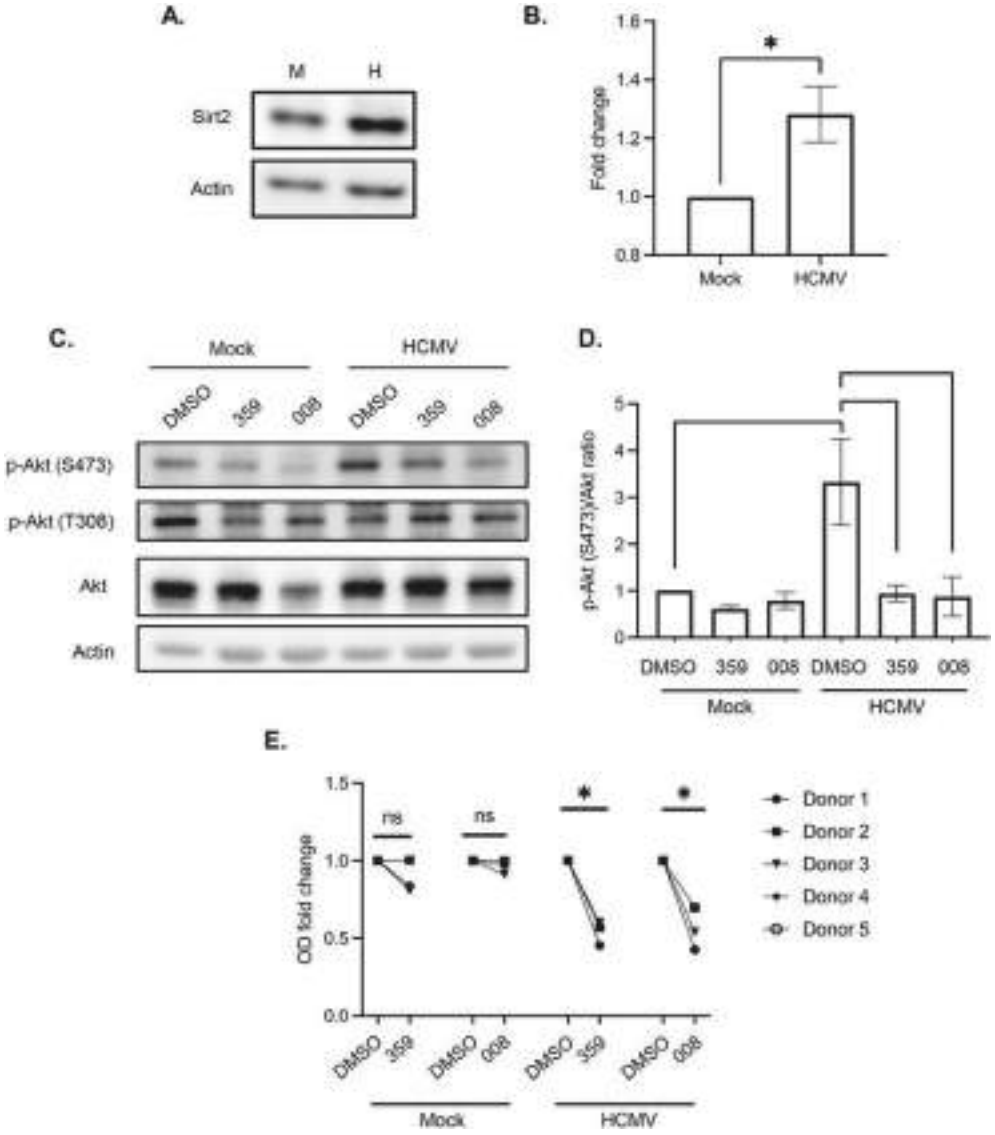

Fig. 1. Inhibition of SIRT2 promotes death of HCMV-infected monocytes. (A, B) Primary monocytes were harvested from peripheral blood and mock or HCMV infected for 24 h (h). Expression levels of SIRT2 were determined by immunoblotting. Membranes were probed for β-actin as a loading control. (C, D) Monocytes were treated with DMSO (vehicle control), 5 μM FLS-359 (359), or 5 μM FLSX-008 (008) (SIRT2 inhibitors) starting 1 h prior to infection, then mock or HCMV infected for 24 h. Expression levels of Akt and p-Akt were determined by immunoblotting. (E) Primary monocytes were mock infected or HCMV infected for 72 h and then treated with 5 μM FLS-359 or FLSX-008 at 1 dpi. Cells were subjected to an SRB cytotoxicity assay and the OD measured at 565 nm. The fold change in OD was normalized to the mock-infected DMSO-treated control. Data are representative of 3–5 independent blood donors. *, $p \leq 0.05$.

subsequent activation of Akt in several cell types, including cells of the myeloid lineage (Dan et al., 2012; Ramakrishnan et al., 2014). We found HCMV infection increased the expression of SIRT2 protein relative to mock infection at 24 h post infection (hpi), suggesting SIRT2 involvement in the activation of Akt within HCMV-infected monocytes (Fig. 1A and B). To investigate the role of SIRT2 in promoting the unique Akt activity induced by HCMV following infection of peripheral blood monocytes, we utilized a highly selective small-molecule inhibitor of SIRT2, FLS-359 (Roche et al., 2023). FLSX-008, another SIRT2 inhibitor, was also utilized in these studies to reduce the possibility that the effects of FLS-359 are due to off-target effects. We found that prophylactic treatment with SIRT2 inhibitors attenuated the HCMV-mediated Akt phosphorylation at S473 (Fig. 1C and D). HCMV infection did not stimulate T308 Akt phosphorylation, consistent with our previous findings (Cojohari et al., 2020), and the SIRT2 inhibitors had no effect on basal levels. Given the importance of Akt activity in the enhanced viability of HCMV-infected monocytes, we examined whether SIRT2-mediated Akt activation was necessary for the survival of infected cells. Monocytes were infected with HCMV immediately post-isolation from peripheral blood, followed by treatment with FLS-359, FLSX-008, or vehicle control at 1 dpi (day post-infection), when infected monocytes exhibit maximum viability (Chan et al., 2010; Chan et al., 2012a; Chan et al., 2012b; Collins-McMillen et al., 2015). At 3 dpi, we performed SRB viability assays and observed a significant increase in the death of HCMV-infected cells treated with the SIRT2 inhibitors and minimal death of uninfected cells (Fig. 1E). Taken together, these data indicate SIRT2 as a potential antiviral cellular target to selective eliminate quiescently HCMV-infected monocytes.

3.2. SIRT2 inhibition triggers apoptosis and necroptosis of HCMV-infected monocytes

In the absence of differentiation stimuli, peripheral blood monocytes rapidly undergo apoptosis after 48–72 h in the circulation (Patel et al., 2017; Whitelaw, 1966). When apoptosis is blocked, monocytes can initiate necroptosis as a "trapdoor" death pathway (Altman et al., 2020; Galluzzi et al., 2017; Ke et al., 2016; Lee et al., 2019). However, HCMV can block both pathways to ensure the survival of infected cells, and subsequently the systemic dissemination of the virus (Altman et al., 2020; Chan et al., 2010; Chan et al., 2012b; Cojohari et al., 2016; Collins-McMillen et al., 2018; Collins-McMillen et al., 2015; Peppenelli et al., 2016; Peppenelli et al., 2018; Reeves et al., 2012). Thus, we asked which death pathway were the SIRT2 inhibitors acting through to promote death of infected monocytes. Using annexin-V (AV) as a marker of apoptosis and propidium iodide (PI) as a marker for cell death, flow cytometry was performed to determine monocyte viability, as well as to differentiate between apoptotic and necroptotic cells. In agreement with our previous studies (Altman et al., 2020; Chan et al., 2010, 2012b;

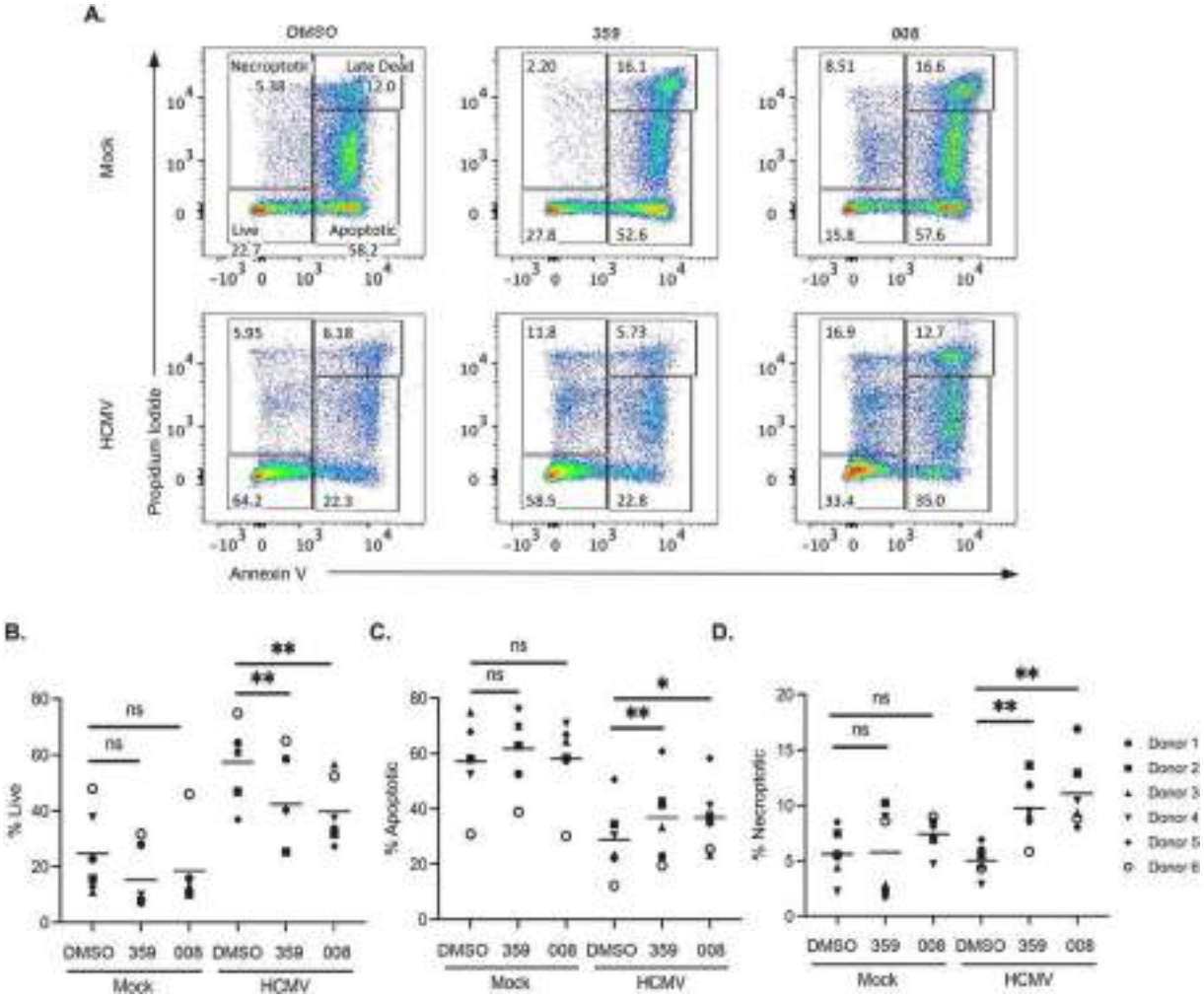

Fig. 2. Therapeutic treatment with SIRT2 inhibitors of HCMV-infected monocytes increases apoptosis and necroptosis. (A–D) Monocytes were mock infected or HCMV infected for 48 h and subsequently treated with DMSO, 5 μM FLS-359, or 5 μM FLSX-008 at 24 hpi. Monocytes were stained with annexin (AV)-FITC and propidium iodide (PI). Viability was analyzed by flow cytometry. Gates represent live (B), apoptotic (C), necroptotic (D), and late dead cell populations. (B–D) Horizontal lines indicate the mean result of the independent experiments. Data are representative of 6 independent blood donors. **, $p \leq 0.01$; *, $p \leq 0.05$.

Cojohari et al., 2016; Peppenelli et al., 2016, 2018), HCMV stimulated an increase in the percentage of live cells (AV negative, PI negative), thus also confirming infection of monocytes (Fig. 2). The inhibitors were then tested as a therapeutic treatment administered to infected monocytes at 24 hpi. Cells were treated with 5 μM of either inhibitor since this concentration abrogated SIRT2-mediated activation of Akt in HCMV-infected monocytes (Fig. 1C and D). Inhibition of SIRT2 shifted cells from the live cell population to both the "apoptotic" (AV positive, PI negative) and "necroptotic" (AV negative, PI positive) gates (Fig. 2A–D). With treatment post-infection, there was a reduction of ~30% of live infected cells in the presence of FLS-359 and FLSX-008 relative to the vehicle-treated control, indicating SIRT2 is necessary for the survival of HCMV-infected monocytes (Fig. 2B). Although uninfected cells appear to have some sensitivity to death induced by SIRT2 inhibition, the decrease in viability was highly variable and not statistically significant, which is likely due to uninfected monocytes already undergoing apoptosis in the absence of infection or activation stimuli (Fig. 2A). Consistent with the decrease in viability of infected monocytes, FLS-359 and FLSX-008 induced a ~1.4-fold increase in apoptosis and a ~2.3-fold increase in necroptosis of HCMV-infected cells (Fig. 2D). There was no significant effect on the levels of apoptosis or necroptosis of the mock-infected cells with SIRT2 inhibition (Fig. 2B–D). Next, we examined the effects of prophylactic treatment of the SIRT2 inhibitors on the viability of infected monocytes. Prophylactic SIRT2 inhibitor treatment reduced the frequency of live infected cells by ~40% (Fig. 3A and B). Concomitantly, FLS-359 and FLSX-008 increased the levels of apoptotic infected cells by ~1.5-fold and necroptotic infected cells by ~2.2-fold (Fig. 3C and D). Prophylactic treatment of mock-infected cells with both SIRT2 inhibitors did not increase apoptosis. However, we observed a significant (or trending towards significant) effect of SIRT2 inhibitors on the viability and necroptosis of mock-infected cells. In contrast to therapeutic treatments, where cells were treated with drugs at 2 dpi, prophylactically treated uninfected cells were given SIRT2 inhibitors immediately upon isolation from peripheral blood, suggesting that SIRT2 may accelerate death of young monocytes exiting the bone marrow but not aged monocytes already circulating in the blood. Regardless, our data clearly demonstrate that SIRT2 inhibitors have enhanced ability to induce death, via apoptosis and necroptosis, of HCMV-infected monocytes relative to uninfected cells under both therapeutic and prophylactic conditions.

To validate that both apoptotic and necroptotic pathways are being activated in HCMV-infected monocytes treated with SIRT2 inhibitors, we treated infected monocytes with UM-116 (an inhibitor of Mcl-1) as a control for stimulation of only the apoptotic pathway. Mcl-1 binds and sequesters proapoptotic members of the Bcl-2 family of proteins, preventing the proapoptotic effector proteins from oligomerizing and forming pores in the mitochondrial outer membrane (Giam et al., 2008; Willis et al., 2007). UM-116 is a novel small-molecule inhibitor that directly binds to Mcl-1 with a K_d value of 1.7 ± 0.2 μM determined by BLI and a IC_{50} value of 0.54 ± 0.11 μM in competitive FP based assay

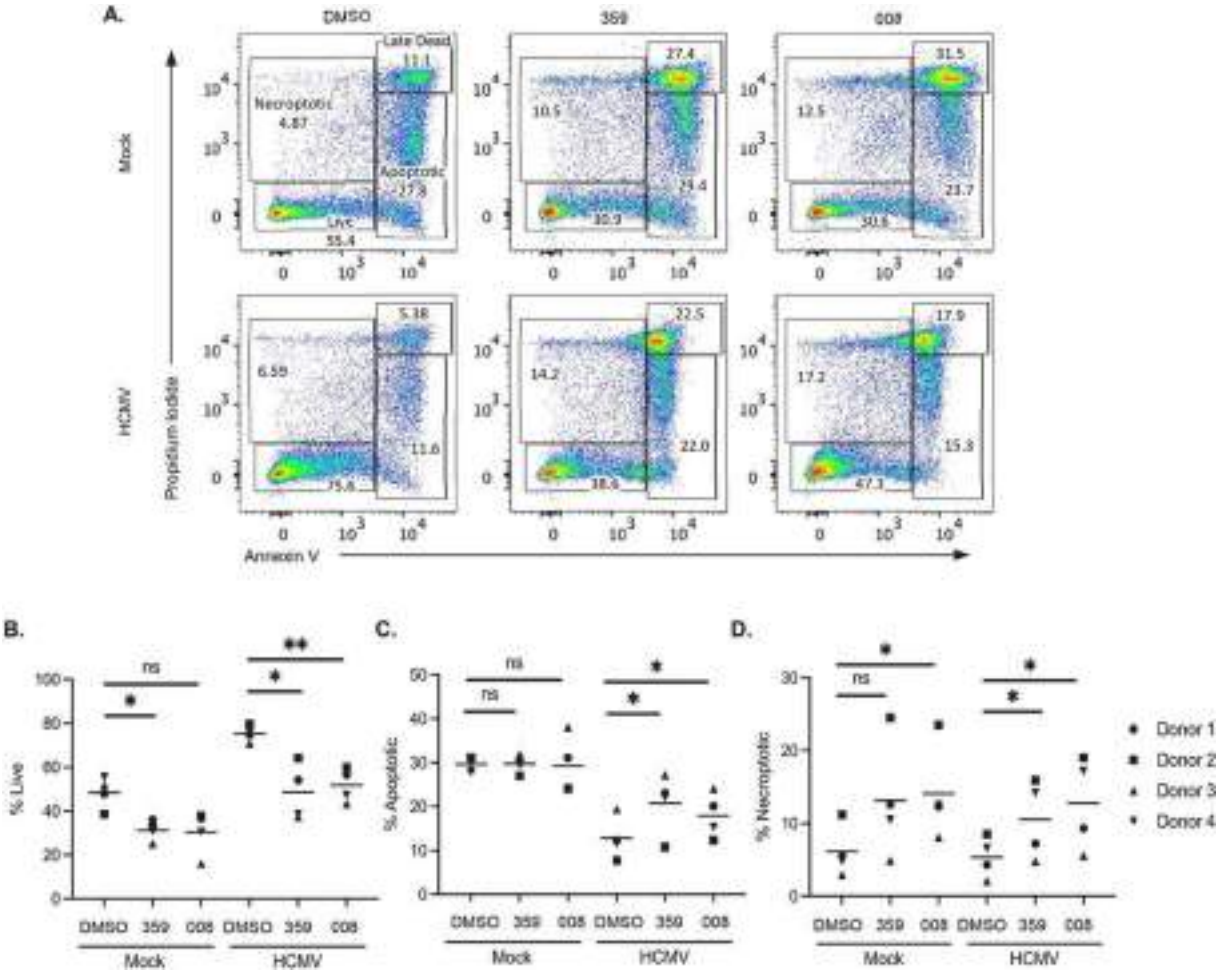

Fig. 3. Prophylactic treatment with SIRT2 inhibitors of HCMV-infected monocytes increases apoptosis and necroptosis. (A–D) Monocytes were pretreated with DMSO, 5 μM FLS-359, or 5 μM FLSX-008 starting 1 h prior to infection. Cells were then mock or HCMV infected for 48 h. Following infection, monocytes were stained with AV-FITC and PI. Viability was analyzed by flow cytometry. Gates represent live (B), apoptotic (C), necroptotic (D), and late dead cell populations. (B–D) Horizontal lines indicate the mean result of the independent experiments. Data are representative of 4 independent blood donors. **, $p \leq 0.01$; *, $p \leq 0.05$.

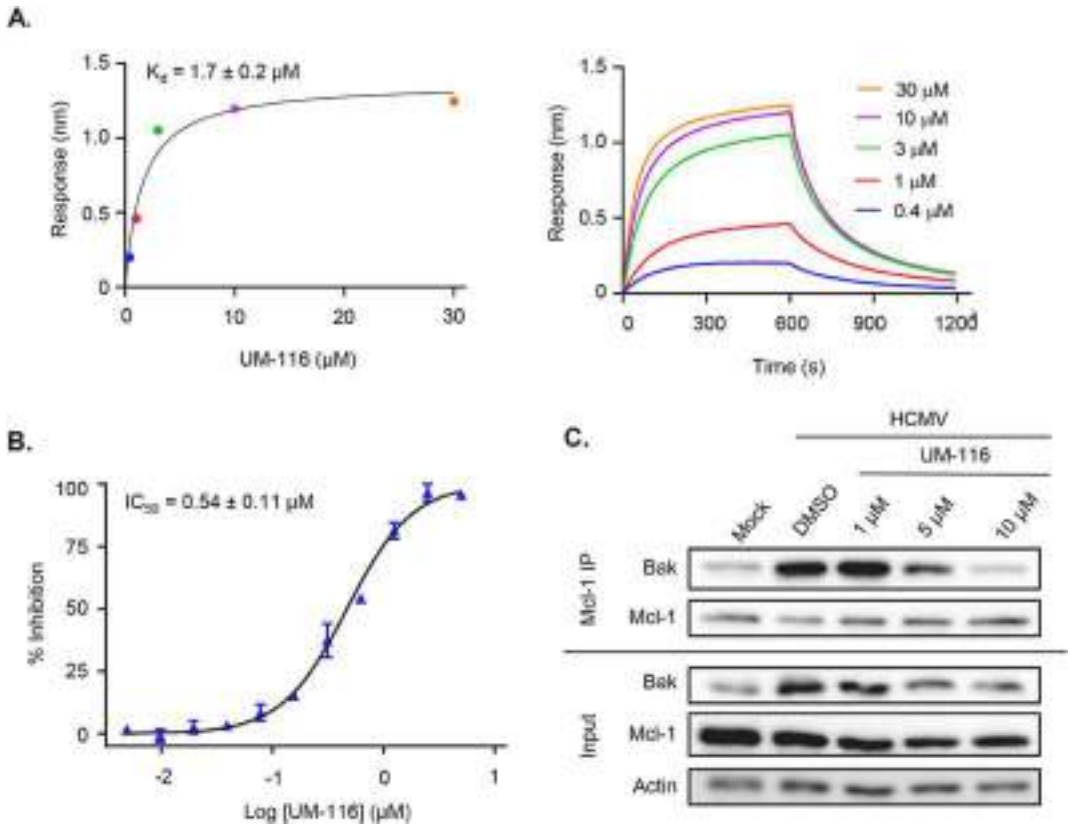

Fig. 4. UM-116 binds to Mcl-1 and disrupts protein-protein interactions with Bak in infected monocytes. (A) The binding affinity of UM-116 was determined by biolayer interferometry (BLI) with the presented sensorgrams of tested concentrations and (B) by competitive fluorescence polarization (FP) assay using fluorescent labeled Bid BH3 peptide. (C) Monocytes were treated with increasing concentrations of UM-116 (a Mcl-1 inhibitor) or DMSO for 1 h, followed by mock or HCMV infection for 24 h. Mcl-1 was immunoprecipitated using an anti-Mcl-1 antibody and the level of Bak bound to Mcl-1 was determined by immunoblotting. Membranes were probed for β-actin as a loading control. Data are representative of at least 3 independent blood donors.

(Fig. 4A and B). We confirmed that UM-116 inhibits Mcl-1 by competitively binding and blocking protein-protein interactions with its binding partner Bak in a dose dependent manner (Fig. 4C). Treatment with UM-116 confirmed that inhibiting Mcl-1 stimulated cell death strictly though apoptosis without a significant increase in necroptosis (Fig. 5). Taken together, our data indicate that SIRT2 inhibition may be a bona fide target to stimulate death of quiescently HCMV-infected monocytes via simultaneous activation of both the apoptotic and necroptotic pathways.

3.3. SIRT2 regulates apoptotic and necroptotic factors within HCMV-infected monocytes

Engagement of HCMV glycoproteins to cellular receptors modulate the phosphorylation ratio between Akt residues S473 and T308, which is known to regulate Akt substrate specificity (Jacinto et al., 2006; Yung et al., 2011), to increase the expression of select prosurvival proteins and the subsequent survival of infected monocytes (Altman et al., 2020; Chan et al., 2010, 2012b; Cojohari et al., 2016; Peppenelli et al., 2016, 2018). Mcl-1 is a critical Akt-dependent antiapoptotic protein that is upregulated following HCMV infection to a much greater extent than following treatment with normal myeloid growth factors (Chan et al., 2010; Peppenelli et al., 2016, 2018). Consequently, we examined whether SIRT2 inhibitors might be exerting their proapoptotic effect on infected monocytes by preventing the Akt-dependent upregulation of Mcl-1. As expected, HCMV infection increased Mcl-1 expression. However, treatment with FLS-359 and FLSX-008 dramatically attenuated the expression of Mcl-1 in HCMV-infected monocytes to levels observed in mock-infected cells (Fig. 6A and B). This abrogation of Mcl-1 expression indicates that SIRT2 inhibition may relieve the block on apoptosis in infected monocytes by preventing HCMV's Akt-dependent upregulation of Mcl-1.

HCMV's circumvention of apoptosis results in the inactivation of caspase 8, which then prompts infected monocytes to initiate necroptosis (Altman et al., 2020). Necroptosis is dependent on the sequential activation of RIPK1, RIPK3, and ultimately MLKL. MLKL acts as the final executioner kinase of the necroptosis pathway by undergoing phosphorylation, oligomerizing, and translocating to form pores in the plasma membrane (Cho et al., 2009). We have previously shown HCMV to stimulate cellular autophagy to block necroptosis between RIPK3 activation and the final MLKL activation steps, ensuring survival of infected monocytes (Altman et al., 2020). Since our data suggests SIRT2 inhibition leads to necroptosis, we examined if SIRT2 inhibition circumvents the blockage between RIPK3 and MLKL within infected monocytes. We confirmed that HCMV infection alone induced activation of RIPK3 relative to mock infection, indicating that infected monocytes have initiated the early steps of necroptosis (Fig. 6C and D). However, SIRT2 inhibition has no effect on RIPK3 activation in the context of infection, suggesting that the pro-necroptotic effect observed with the SIRT2 inhibitors occurs downstream of RIPK3. Indeed, treatment with the SIRT2 inhibitors FLS-359 and FLSX-008 enhanced the phosphorylation of MLKL in HCMV-infected monocytes without significantly affecting phosphorylation levels in mock-infected cells (Fig. 6E and F). Our data here supports a role for SIRT2 during HCMV infection in the regulation of apoptosis, via Akt-dependent expression of Mcl-1, and of necroptosis, via regulation of MLKL activation.

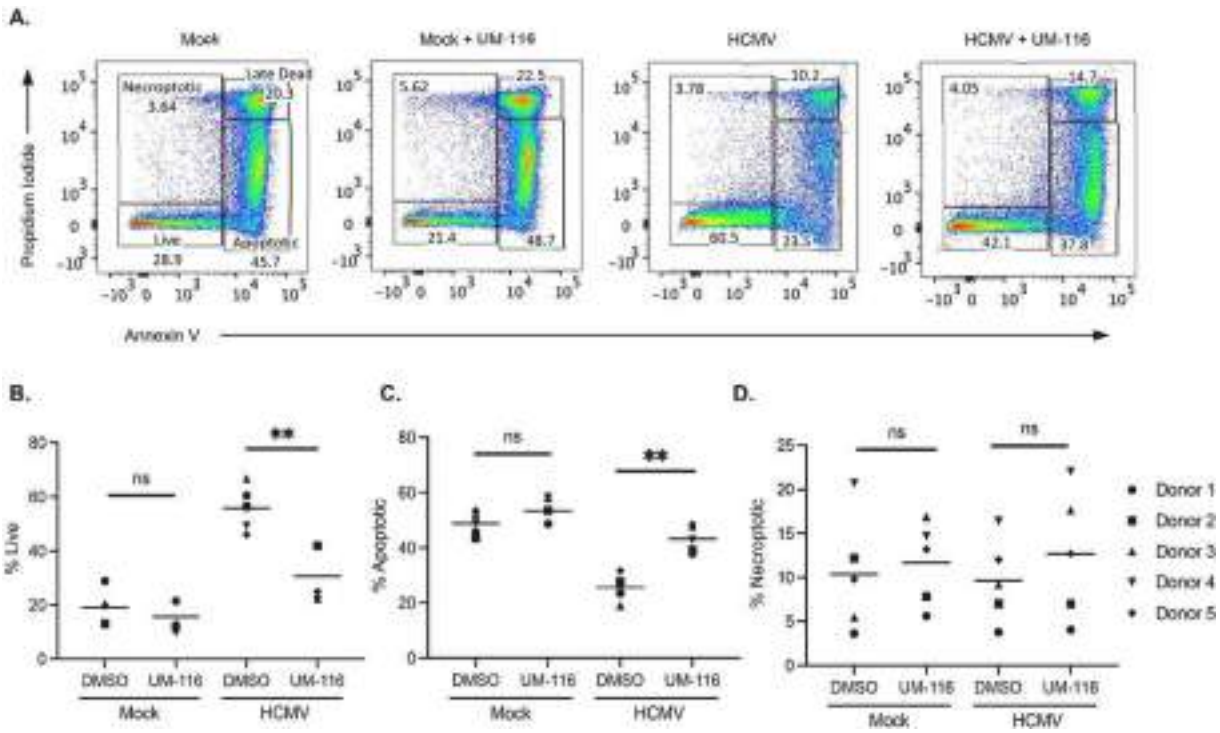

Fig. 5. Mcl-1 inhibition stimulates apoptosis, but not necroptosis, of HCMV-infected monocytes. (A–D) Monocytes were mock infected or HCMV infected for 48 h, followed by treatment with DMSO or 5 μM UM-116 for 24 h. Monocytes were stained with AV-FITC and PI. Cell viability was analyzed by flow cytometry. Gates represent live (B), apoptotic (C), necroptotic (D), and late dead cell populations. (B–D) Horizontal lines indicate the mean result of the independent experiments. Data are representative of 5 independent blood donors. **, $p \leq 0.01$; *, $p \leq 0.05$.

3.4. Formation of autophagosomes during HCMV infection is mediated by Akt

Our group has previously reported that HCMV infection stimulates the necroptotic pathway through RIPK3 phosphorylation, but concomitant induction of cellular autophagy, as determined by measuring autophagic flux and autophagosome accumulation, prevents activation of MLKL and the subsequent execution of necroptosis (Altman et al., 2020). We observed that SIRT2 inhibition promotes MLKL activation without affecting RIPK3 activity. Thus, we sought to determine whether reducing autophagosome accumulation is the mechanism through which the SIRT2 inhibitors relieve the block on necroptosis. After treating monocytes with SIRT2 inhibitors for 1 h and then infecting with HCMV for 2 h, we performed immunofluorescence analysis of LC3-II, a cytoplasmic protein that is lipidated and localized to autophagosomes during their maturation (Tanida et al., 2008). HCMV infection increased the mean number of puncta per cell by 85% relative to mock infection. Treatment with FLS-359 and FLSX-008 resulted in a 37.5% and 40.5% reduction of LC3-II puncta per cell, respectively, compared to the infected vehicle control, indicating a decrease in autophagosome accumulation following SIRT2 inhibition (Fig. 7A and B). Due to the central role that HCMV's unique activation of Akt plays in survival and many other cellular functions, we examined whether SIRT2's regulatory role in autophagosome formation could be mediated by Akt. Treatment with MK2206, an inhibitor of Akt, reduced the average number of LC3-II puncta per cell by 41.1%, mirroring treatment with the SIRT2 inhibitors (Fig. 7A and B). Our data here indicate that the unique activation of Akt by HCMV enhances cellular autophagosome accumulation and that preventing Akt activation, via SIRT2 inhibition, could lead to diminished autophagy resulting in necroptosis of infected monocytes.

4. Discussion

Monocytes are a key cell population responsible for hematogenous dissemination of HCMV, despite not being permissive to viral replication and having a short 48 h lifespan (Chan et al., 2012a; Manez et al., 1996; Patel et al., 2017; Taylor-Wiedeman et al., 1994). HCMV has evolved several mechanisms to prolong the survival of infected monocytes allowing for the differentiation of infected cells into replication permissive macrophages (Altman et al., 2020; Chan et al., 2010; Chan et al., 2012b; Cojohari et al., 2020; Cojohari et al., 2016; Collins-McMillen et al., 2015; Peppenelli et al., 2016; Peppenelli et al., 2018; Smith et al., 2004a). The primary route through which monocytes are programmed to die is apoptosis, which can be accelerated as part of an intrinsic antiviral defense response against the virus (Barber, 2001; Mangan et al., 1993). Monocytes also possess the molecular machinery necessary to shift course to an alternative antiviral cell death response pathway called necroptosis if apoptosis is impeded during a virus infection (Altman et al., 2020; Lee et al., 2019). Through long co-evolution with humans, HCMV appears to have developed mechanisms to counteract cell death pathways during infection of monocytes independent of *de novo* synthesized viral proteins. In this study, we demonstrate that HCMV utilizes the cellular deacetylase SIRT2 to simultaneously block both the apoptotic and necroptotic death pathways during quiescent infection of monocytes.

In our proposed model, SIRT2 acts as a central regulator of both apoptosis and necroptosis through modulation of Akt activity following HCMV infection of monocytes (Fig. 8). HCMV infection aberrantly modifies cellular signaling pathways in a manner reminiscent of cancer, with the PI3K/Akt pathway being a central pathway altered by the virus (Chan et al., 2008b, 2009a, 2010; Cojohari et al., 2016; Hoxhaj and Manning, 2020; Luo et al., 2003; Mahmud et al., 2020; Peppenelli et al., 2018; Smith et al., 2004b, 2007). Under canonical stimulation by normal myeloid growth factors, Akt is dually phosphorylated at residues S473 and T308 (Alessi et al., 1996; Cojohari et al., 2020; Mahmud et al., 2020; Peppenelli et al., 2016, 2018). In contrast, binding of HCMV glycoproteins to cellular receptors initiates a signaling cascade in monocytes that leads to a noncanonical Akt phosphorylation profile

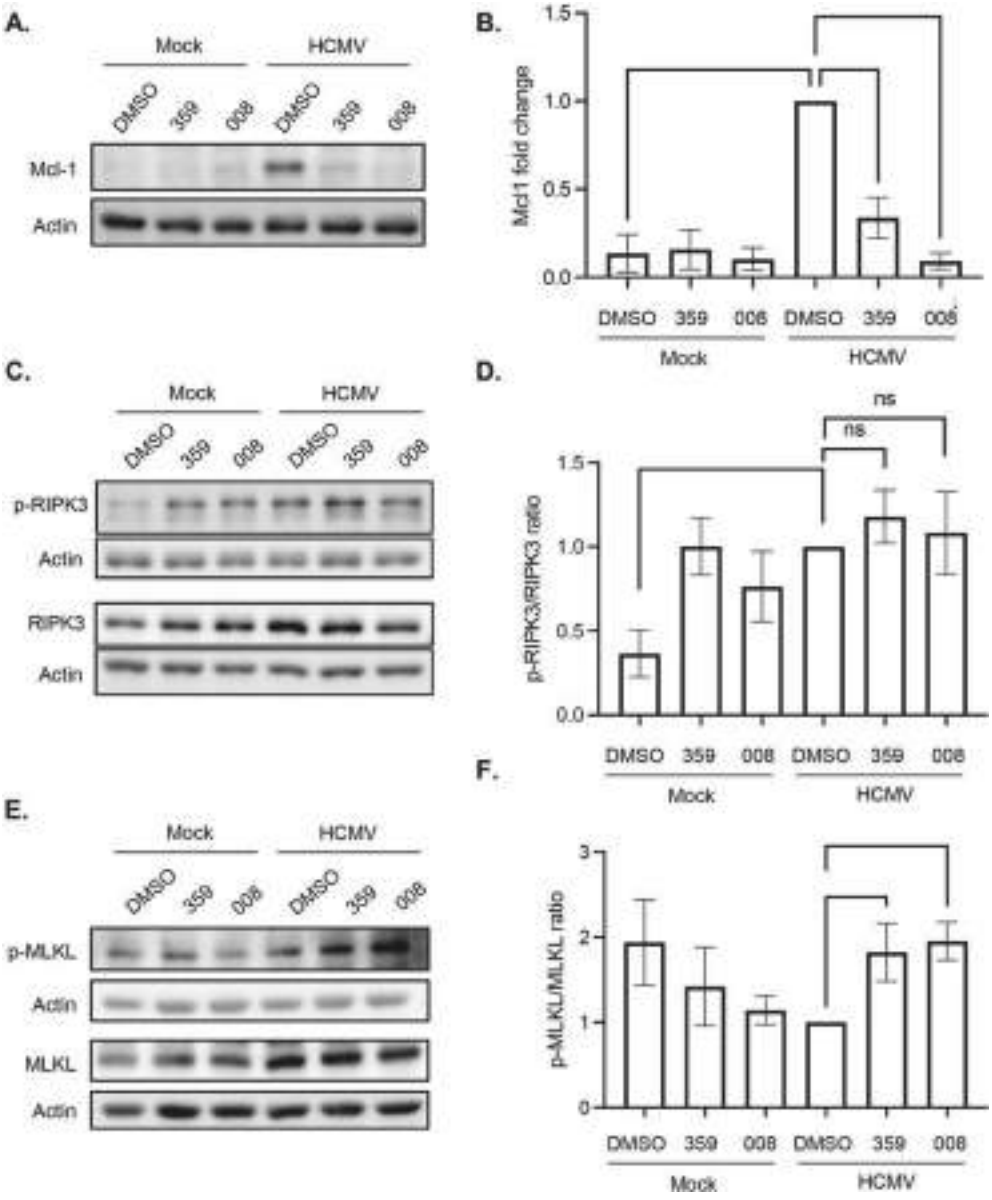

Fig. 6. SIRT2 regulates the expression and activity of factors involved in apoptosis and necroptosis. (A–F) Monocytes were treated with DMSO, 5 μM FLS-359, or 5 μM FLSX-008 1 h prior to infection. Cells were then mock infected or HCMV infected for 24 h. Expression levels of Mcl-1, RIPK3, p-RIPK3, MLKL, and p-MLKL were determined by immunoblotting. Membranes were probed for β-actin as a loading control. Data are representative of at least 4 independent blood donors. ***, $p \leq 0.001$; **, $p \leq 0.01$; *, $p \leq 0.05$.

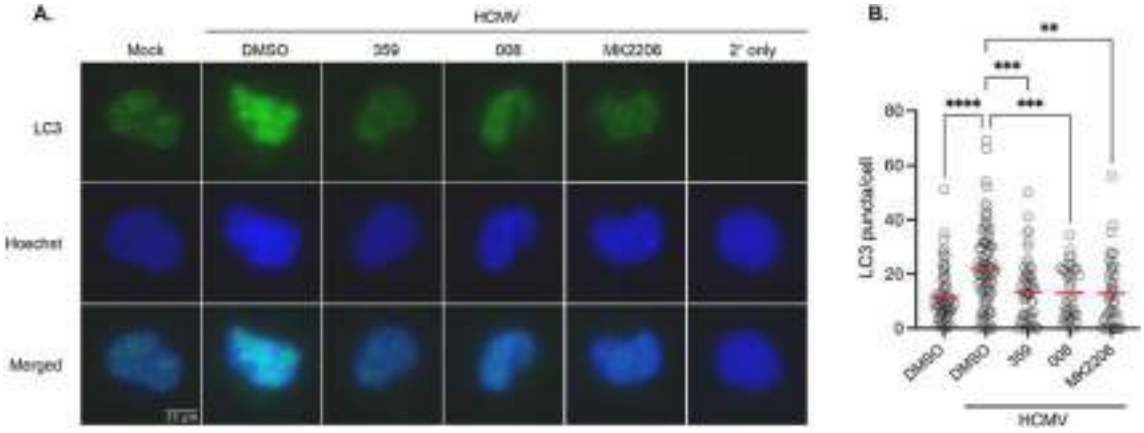

Fig. 7. SIRT2 and Akt are required for HCMV-induced autophagosome accumulation in infected monocytes. (A, B) Monocytes were treated with DMSO, 5 μM FLS-359, 5 μM FLSX-008, or 10 μM MK2206 (an Akt inhibitor) 1 h prior to infection. Cells were mock infected or HCMV infected for 2 h, followed by immunofluorescent analysis with an anti-LC3 antibody (green) and Hoechst staining (blue). (B) LC3 puncta per cell were counted using FIJI and plotted with the mean (red line). Data are representative of at least 3 independent blood donors. ****, $p \leq 0.0001$; ***, $p \leq 0.001$; **, $p \leq 0.01$; *, $p \leq 0.05$.

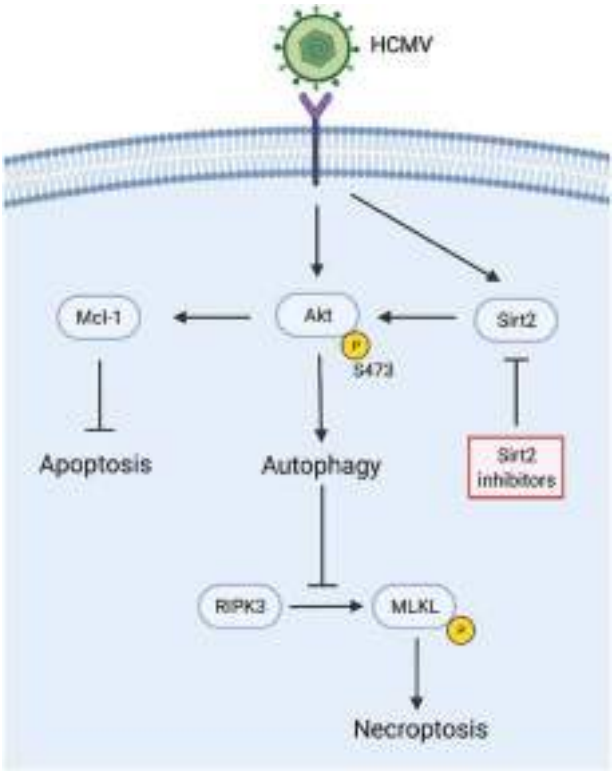

Fig. 8. Proposed model for SIRT2 regulation of apoptosis and necroptosis in HCMV-infected monocytes. In the absence of myeloid differentiation factors, monocytes undergo programmed cell death within 48 h after entering the peripheral circulation. Upon HCMV binding to cellular receptors, Akt is preferentially phosphorylated at S473 to trigger pro-survival pathways that circumvent apoptosis and necroptosis. The unique phosphorylation of Akt during HCMV infection leads to the increased expression of antiapoptotic proteins such as Mcl-1. HCMV-induced activation of Akt also enhances cellular autophagy, which blocks phosphorylation of MLKL during necroptosis. SIRT2-mediated deacetylation of Akt is required for HCMV's unique activation of Akt in monocytes. Inhibition of SIRT2 relieves the viral-induced blocks on both the apoptotic and necroptotic death pathways by reducing expression of Mcl-1 and by reducing autophagy to allow the activation of MLKL, thus promoting death of HCMV-infected monocytes through dual concurrent mechanisms.

wherein S473 is preferentially phosphorylated (Cojohari et al., 2020; Mahmud et al., 2020; Peppenelli et al., 2016, 2018), which also occurs in some cancers (Fernandes et al., 2013; Kerr, 2011; Opel et al., 2007; Tsurutani et al., 2006). SHIP1 normally acts as a negative regulator of Akt by opposing the action of PI3K, but in some transformed cells, SHIP1 amplifies Akt activity through the specific phosphorylation of S473 (Fernandes et al., 2013; Kerr, 2011). We have previously shown a similar dysregulation of SHIP1 during HCMV infection of monocytes where HCMV upregulates SHIP1, which then acts as a positive regulator of Akt by mediating the S473 site-specific phosphorylation (Cojohari et al., 2016). The distinct activation profile of Akt leads to a HCMV-specific transcriptomic landscape that includes the increased expression of a distinct subset of antiapoptotic proteins not upregulated during growth factor-induced signaling (Chan et al., 2008b, 2009a, 2010; Cojohari et al., 2016; Mahmud et al., 2020; Peppenelli et al., 2016, 2018). Here, we show HCMV-induced SIRT2 likely mediates deacetylation of Akt that permits HCMV's unique glycoprotein-initiated signaling to impart a distinctive Akt activation profile.

A primary function of HCMV-activated Akt is to prevent the intrinsic biological programming of monocytes to undergo apoptosis and the acceleration of apoptosis due to the initiation of antiviral defenses. The phosphorylation profile of Akt dictates its downstream substate specificity (Jacinto et al., 2006; Yung et al., 2011) and we have found that the preferential phosphorylation of S473 leads to the upregulation of a unique milieu of antiapoptotic proteins, including Mcl-1, HSP27, and XIAP (Chan et al., 2010, 2012b; Cojohari et al., 2016; Peppenelli et al., 2016, 2018). However, upon inhibition of apoptosis via blockage of procaspase 8 cleavage, the trapdoor cellular defensive death pathway necroptosis is opened (Altman et al., 2020; Galluzzi et al., 2017; Ke et al., 2016; Lee et al., 2019; Mocarski et al., 2011, 2015; Upton et al., 2008, 2010, 2012). We have shown infected monocytes initiate the early steps of necroptosis involving the phosphorylation of RIPK3 (Altman et al., 2020). However, HCMV rapidly blocks the progression of necroptosis preventing the activation of the final executioner protein MLKL (Altman et al., 2020). Inhibition of MLKL, and therefore necroptosis, is dependent on the HCMV-induced stimulation of cellular autophagy (Altman et al., 2020). Our current study now demonstrates that the HCMV-specific activation of Akt promotes autophagosome accumulation and that preventing the activation of Akt likely reduces HCMV-induced autophagy, leading to necroptosis. Based on SIRT2 acting as a gateway allowing HCMV glycoproteins to uniquely regulate Akt activity, our study supports the targeting of SIRT2 as a means of eliminating quiescently HCMV-infected monocytes via apoptosis and/or necroptosis.

Our study also identifies an unusual relationship between HCMV-activated Akt and autophagy. Traditionally, Akt has an inhibitory role in the regulation of cellular autophagy. Akt is directly implicated as a negative regulator of autophagy via phosphorylation of Beclin 1, a component of the Beclin 1-Vsp34-Vsp15 autophagy nucleation core complex (Kang et al., 2011; Wang et al., 2012). Additionally, Akt is thought to negatively regulate autophagy through activation of mTOR (Egan et al., 2011; Heras-Sandoval et al., 2014; Kim et al., 2011; Kim and Guan, 2015; Song et al., 2018), which we have shown to be rapidly activated in HCMV-infected monocytes following viral entry (Altman et al., 2019; Peppenelli et al., 2018). Yet, we found a positive relationship between Akt and autophagy, as abrogating Akt activity via direct or SIRT2-mediated inhibition attenuated autophagy. Why HCMV-activated Akt has the opposite effect on autophagy remains unknown. Aberrant microenvironments, such as those during cancer or viral infections, can have profound effect on the cellular signaling network leading to atypical biological outcomes. For example, AMPK traditionally negatively regulates mTOR activity, however HCMV infection uncouples the AMPK-mTOR signaling axis allowing both AMPK and mTOR to be activated simultaneously during both lytic and silent infections (Altman et al., 2019, 2020; Kudchodkar et al., 2007; Moorman et al., 2008). Another instance is the conversion of SHIP1 from a negative to positive regulator of AKT during HCMV infection (Cojohari et al., 2016). How HCMV modulates signaling and protein activities to allow Akt to promote autophagy during viral infection of monocytes is an important avenue of future studies.

Overall, our study demonstrates the potential utility of targeting SIRT2 as an antiviral strategy. Targeting host proteins as an antiviral strategy offers several advantages over targeting viral proteins, including limiting drug resistance and the potential for broad-spectrum antiviral activity (Kumar et al., 2020; Tripathi et al., 2021). The SIRT2 inhibitor FLS-359 has been shown to possess antiviral activity against a wide range of both DNA and RNA viruses, including members of the herpesvirus, flavivirus, orthomyxovirus, hepadnavirus, and coronavirus families (Roche et al., 2023). FLS-359 has been demonstrated to be well-tolerated in animal studies with no weight loss or adverse clinical signs (Roche et al., 2023). Unlike knockout mouse models of the other members of the Sirtuin family, SIRT2 knockout mice are viable without significant phenotypic abnormalities (Ciarlo et al., 2017; Finkel et al., 2009). SIRT2 inhibition has previously been shown to inhibit growth of HCMV during lytic infection in fibroblast cells (Mao et al., 2016; Roche et al., 2023). This study demonstrates that SIRT2 inhibition does not only inhibit HCMV lytic replication, but it also promotes death of quiescently infected monocytes. The lack of lytic viral protein expression in quiescently infected monocytes is an obstacle that has prevented

all the current direct-targeted antivirals from being fully effective against HCMV. In the case of transplant recipients, although the current HCMV antivirals have been highly efficacious at reducing HCMV disease in the most vulnerable first few months immediately post-transplantation, antiviral therapies must eventually be discontinued due to drug toxicities, leading to later rebound HCMV reactivation of virus from quiescently infected monocytes that have extravasated into peripheral organ tissue (Singh, 2005). An ideal antiviral regimen would target the virus in both cells with active viral replication and cells that are silently harboring the virus during dissemination. Thus, the ability of a single SIRT2 inhibitor to target both lytic and quiescent stages of the HCMV lifecycle could have major implications to prognosis of high-risk transplant recipients.

Declaration of competing interest

The authors declare that they have no known competing financial interests or personal relationships that could have appeared to influence the work reported in this paper.

Data availability

Data will be made available on request.

Acknowledgments

We thank Christine Burrer in the Department of Microbiology and Immunology at SUNY Upstate Medical University for technical support, maintenance of lab operations, and assistance with virus growth and isolation. This work was supported by grants National Institute of Allergy and Infectious Disease (R01AI141460) to G.C. Chan, National Heart, Lung, and Blood Institute (R01HL139824) to G.C. Chan, National Cancer Institute (R01CA217141) to Z. Nikolovska-Coleska and AACR Bayer Innovation and Discovery Award to Z. Nikolovska-Coleska.

Appendix A. Supplementary data

Supplementary data to this article can be found online at https://doi.org/10.1016/j.antiviral.2023.105698.

References

Alessi, D.R., Andjelkovic, M., Caudwell, B., Cron, P., Morrice, N., Cohen, P., Hemmings, B.A., 1996. Mechanism of activation of protein kinase B by insulin and IGF-1. EMBO J. 15, 6541–6551.

Altman, A.M., Mahmud, J., Nikolovska-Coleska, Z., Chan, G., 2019. HCMV modulation of cellular PI3K/AKT/mTOR signaling: new opportunities for therapeutic intervention? Antivir. Res. 163, 82–90. https://doi.org/10.1016/j.antiviral.2019.01.009.

Altman, A.M., Miller, M.J., Mahmud, J., Smith, N.A., Chan, G.C., 2020. Human cytomegalovirus-induced autophagy prevents necroptosis of infected monocytes. J. Virol. 94 https://doi.org/10.1128/jvi.01022-20.

Azevedo, L.S., Pierrotti, L.C., Abdala, E., Costa, S.F., Strabelli, T.M., Campos, S.V., Ramos, J.F., Latif, A.Z., Litvinov, N., Maluf, N.Z., Caiaffa Filho, H.H., Pannuti, C.S., Lopes, M.H., Santos, V.A., Linardi Cda, C., Yasuda, M.A., Marques, H.H., 2015. Cytomegalovirus infection in transplant recipients. Clinics 70, 515–523. https://doi.org/10.6061/clinics/2015(07)09.

Barber, G.N., 2001. Host defense, viruses and apoptosis. Cell Death Differ. 8, 113–126. https://doi.org/10.1038/sj.cdd.4400823.

Boeckh, M., Nichols, W.G., Papanicolaou, G., Rubin, R., Wingard, J.R., Zaia, J., 2003. Cytomegalovirus in hematopoietic stem cell transplant recipients: current status, known challenges, and future strategies. Biol. Blood Marrow Transplant. 9, 543–558. https://doi.org/10.1016/s1083-8791(03)00287-8.

Cannon, M.J., Schmid, D.S., Hyde, T.B., 2010. Review of cytomegalovirus seroprevalence and demographic characteristics associated with infection. Rev. Med. Virol. 20, 202–213. https://doi.org/10.1002/rmv.655.

Chan, G., Bivins-Smith, E.R., Smith, M.S., Smith, P.M., Yurochko, A.D., 2008a. Transcriptome analysis reveals human cytomegalovirus reprograms monocyte differentiation toward an M1 macrophage. J. Immunol. 181, 698–711.

Chan, G., Bivins-Smith, E.R., Smith, M.S., Yurochko, A.D., 2008b. Transcriptome analysis of NF-kappaB- and phosphatidylinositol 3-kinase-regulated genes in human cytomegalovirus-infected monocytes. J. Virol. 82, 1040–1046. https://doi.org/10.1128/JVI.00864-07.

Chan, G., Bivins-Smith, E.R., Smith, M.S., Yurochko, A.D., 2009a. NF-kappaB and phosphatidylinositol 3-kinase activity mediates the HCMV-induced atypical M1/M2 polarization of monocytes. Virus Res. 144, 329–333. https://doi.org/10.1016/j.virusres.2009.04.026.

Chan, G., Nogalski, M.T., Bentz, G.L., Smith, M.S., Parmater, A., Yurochko, A.D., 2010. PI3K-dependent upregulation of Mcl-1 by human cytomegalovirus is mediated by epidermal growth factor receptor and inhibits apoptosis in short-lived monocytes. J. Immunol. 184, 3213–3222. https://doi.org/10.4049/jimmunol.0903025.

Chan, G., Nogalski, M.T., Stevenson, E.V., Yurochko, A.D., 2012a. Human cytomegalovirus induction of a unique signalsome during viral entry into monocytes mediates distinct functional changes: a strategy for viral dissemination. J. Leukoc. Biol. 92, 743–752. https://doi.org/10.1189/jlb.0112040.

Chan, G., Nogalski, M.T., Yurochko, A.D., 2009b. Activation of EGFR on monocytes is required for human cytomegalovirus entry and mediates cellular motility. Proc. Natl. Acad. Sci. U. S. A. 106, 22369–22374. https://doi.org/10.1073/pnas.0908787106.

Chan, G., Nogalski, M.T., Yurochko, A.D., 2012b. Human cytomegalovirus stimulates monocyte-to-macrophage differentiation via the temporal regulation of caspase 3. J. Virol. 86, 10714–10723. https://doi.org/10.1128/JVI.07129-11.

Cho, Y.S., Challa, S., Moquin, D., Genga, R., Ray, T.D., Guildford, M., Chan, F.K., 2009. Phosphorylation-driven assembly of the RIP1-RIP3 complex regulates programmed necrosis and virus-induced inflammation. Cell 137, 1112–1123. https://doi.org/10.1016/j.cell.2009.05.037.

Ciarlo, E., Heinonen, T., Theroude, C., Herderschee, J., Mombelli, M., Lugrin, J., Pfefferle, M., Tyrrell, B., Lensch, S., Acha-Orbea, H., Le Roy, D., Auwerx, J., Roger, T., 2017. Sirtuin 2 deficiency increases bacterial phagocytosis by macrophages and protects from chronic staphylococcal infection. Front. Immunol. 8, 1037. https://doi.org/10.3389/fimmu.2017.01037.

Cobbs, C.S., Harkins, L., Samanta, M., Gillespie, G.Y., Bharara, S., King, P.H., Nabors, L. B., Cobbs, C.G., Britt, W.J., 2002. Human cytomegalovirus infection and expression in human malignant glioma. Cancer Res. 62, 3347–3350.

Cojohari, O., Mahmud, J., Altman, A.M., Peppenelli, M.A., Miller, M.J., Chan, G.C., 2020. Human cytomegalovirus mediates unique monocyte-to-macrophage differentiation through the PI3K/SHIP1/Akt signaling network. Viruses 12. https://doi.org/10.3390/v12060652.

Cojohari, O., Peppenelli, M.A., Chan, G.C., 2016. Human cytomegalovirus induces an atypical activation of Akt to stimulate the survival of short-lived monocytes. J. Virol. 90, 6443–6452. https://doi.org/10.1128/JVI.00214-16.

Collins-McMillen, D., Chesnokova, L., Lee, B.J., Fulkerson, H.L., Brooks, R., Mosher, B.S., Yurochko, A.D., 2018. HCMV Infection and Apoptosis: How Do Monocytes Survive HCMV Infection? https://doi.org/10.3390/v10100533 Viruses 10.

Collins-McMillen, D., Kim, J.H., Nogalski, M.T., Stevenson, E.V., Chan, G.C., Caskey, J.R., Cieply, S.J., Yurochko, A.D., 2015. Human cytomegalovirus promotes survival of infected monocytes via a distinct temporal regulation of cellular Bcl-2 family proteins. J. Virol. 90, 2356–2371. https://doi.org/10.1128/jvi.01994-15.

Crumpacker, C.S., 1992. Mechanism of action of foscarnet against viral polymerases. Am. J. Med. 92, 3s–7s. https://doi.org/10.1016/0002-9343(92)90329-a.

Dan, L., Klimenkova, O., Klimiankou, M., Klusman, J.H., van den Heuvel-Eibrink, M.M., Reinhardt, D., Welte, K., Skokowa, J., 2012. The role of sirtuin 2 activation by nicotinamide phosphoribosyltransferase in the aberrant proliferation and survival of myeloid leukemia cells. Haematologica 97, 551–559. https://doi.org/10.3324/haematol.2011.055236.

Ding, T., Hao, J., 2021. Sirtuin 2 knockdown inhibits cell proliferation and RAS/ERK signaling, and promotes cell apoptosis and cell cycle arrest in multiple myeloma. Mol. Med. Rep. 24 https://doi.org/10.3892/mmr.2021.12400.

Egan, D., Kim, J., Shaw, R.J., Guan, K.L., 2011. The autophagy initiating kinase ULK1 is regulated via opposing phosphorylation by AMPK and mTOR. Autophagy 7, 643–644. https://doi.org/10.4161/auto.7.6.15123.

Elder, E., Krishna, B., Williamson, J., Aslam, Y., Farahi, N., Wood, A., Romashova, V., Roche, K., Murphy, E., Chilvers, E., Lehner, P.J., Sinclair, J., Poole, E., 2019. Monocytes latently infected with human cytomegalovirus evade neutrophil killing. iScience 12, 13–26. https://doi.org/10.1016/j.isci.2019.01.007.

Emery, V.C., 2001. Investigation of CMV disease in immunocompromised patients. J. Clin. Pathol. 54, 84–88. https://doi.org/10.1136/jcp.54.2.84.

Fernandes, S., Iyer, S., Kerr, W.G., 2013. Role of SHIP1 in cancer and mucosal inflammation. Ann. N. Y. Acad. Sci. 1280, 6–10. https://doi.org/10.1111/nyas.12038.

Fiala, M., Heiner, D.C., Turner, J.A., Rosenbloom, B., Guze, L.B., 1977. Infectious mononucleosis and mononucleosis syndromes. West. J. Med. 126, 445–459.

Finkel, T., Deng, C.X., Mostoslavsky, R., 2009. Recent progress in the biology and physiology of sirtuins. Nature 460, 587–591. https://doi.org/10.1038/nature08197.

Fletcher-Etherington, A., Nobre, L., Nightingale, K., Antrobus, R., Nichols, J., Davison, A. J., Stanton, R.J., Weekes, M.P., 2020. Human cytomegalovirus protein pUL36: a dual cell death pathway inhibitor. Proc. Natl. Acad. Sci. U. S. A. 117, 18771–18779. https://doi.org/10.1073/pnas.2001887117.

Galluzzi, L., Kepp, O., Chan, F.K., Kroemer, G., 2017. Necroptosis: mechanisms and relevance to disease. Annu. Rev. Pathol. 12, 103–130. https://doi.org/10.1146/annurev-pathol-052016-100247.

Geisler, J., Touma, J., Rahbar, A., Soderberg-Naucler, C., Vetvik, K., 2019. A review of the potential role of human cytomegalovirus (HCMV) infections in breast cancer carcinogenesis and abnormal immunity. Cancers 11. https://doi.org/10.3390/cancers11121842.

Giam, M., Huang, D.C., Bouillet, P., 2008. BH3-only proteins and their roles in programmed cell death. Oncogene 27 (Suppl 1), S128–S136. https://doi.org/10.1038/onc.2009.50.

Hargett, D., Shenk, T.E., 2010. Experimental human cytomegalovirus latency in CD14+ monocytes. Proc. Natl. Acad. Sci. U. S. A. 107, 20039–20044. https://doi.org/10.1073/pnas.1014509107.

Heras-Sandoval, D., Perez-Rojas, J.M., Hernandez-Damian, J., Pedraza-Chaverri, J., 2014. The role of PI3K/AKT/mTOR pathway in the modulation of autophagy and the clearance of protein aggregates in neurodegeneration. Cell. Signal. 26, 2694–2701. https://doi.org/10.1016/j.cellsig.2014.08.019.

Hoxhaj, G., Manning, B.D., 2020. The PI3K-AKT network at the interface of oncogenic signalling and cancer metabolism. Nat. Rev. Cancer 20, 74–88. https://doi.org/10.1038/s41568-019-0216-7.

Jacinto, E., Facchinetti, V., Liu, D., Soto, N., Wei, S., Jung, S.Y., Huang, Q., Qin, J., Su, B., 2006. SIN1/MIP1 maintains rictor-mTOR complex integrity and regulates Akt phosphorylation and substrate specificity. Cell 127, 125–137. https://doi.org/10.1016/j.cell.2006.08.033.

Jacobson, M.A., 1992. Review of the toxicities of foscarnet. J. Acquir. Immune Defic. Syndr. 5 (Suppl 1), S11–S17.

Jing, H., Hu, J., He, B., Negron Abril, Y.L., Stupinski, J., Weiser, K., Carbonaro, M., Chiang, Y.L., Southard, T., Giannakakou, P., Weiss, R.S., Lin, H., 2016. A SIRT2-selective inhibitor promotes c-Myc oncoprotein degradation and exhibits broad anticancer activity. Cancer Cell 29, 297–310. https://doi.org/10.1016/j.ccell.2016.02.007.

Kang, R., Zeh, H.J., Lotze, M.T., Tang, D., 2011. The Beclin 1 network regulates autophagy and apoptosis. Cell Death Differ. 18, 571–580. https://doi.org/10.1038/cdd.2010.191.

Ke, X., Lei, L., Li, H., Li, H., Yan, F., 2016. Manipulation of necroptosis by Porphyromonas gingivalis in periodontitis development. Mol. Immunol. 77, 8–13. https://doi.org/10.1016/j.molimm.2016.07.010.

Kendle, J.B., Fan-Havard, P., 1998. Cidofovir in the treatment of cytomegaloviral disease. Ann. Pharmacother. 32, 1181–1192. https://doi.org/10.1345/aph.17312.

Kerr, W.G., 2011. Inhibitor and activator: dual functions for SHIP in immunity and cancer. Ann. N. Y. Acad. Sci. 1217, 1–17. https://doi.org/10.1111/j.1749-6632.2010.05869.x.

Kim, J., Kundu, M., Viollet, B., Guan, K.L., 2011. AMPK and mTOR regulate autophagy through direct phosphorylation of Ulk1. Nat. Cell Biol. 13, 132–141. https://doi.org/10.1038/ncb2152.

Kim, Y.C., Guan, K.L., 2015. mTOR: a pharmacologic target for autophagy regulation. J. Clin. Invest. 125, 25–32. https://doi.org/10.1172/JCI73939.

Kozako, T., Mellini, P., Ohsugi, T., Aikawa, A., Uchida, Y.I., Honda, S.I., Suzuki, T., 2018. Novel small molecule SIRT2 inhibitors induce cell death in leukemic cell lines. BMC Cancer 18, 791. https://doi.org/10.1186/s12885-018-4710-1.

Krishna, B.A., Poole, E.L., Jackson, S.E., Smit, M.J., Wills, M.R., Sinclair, J.H., 2017. Latency-associated expression of human cytomegalovirus US28 attenuates cell signaling pathways to maintain latent infection. mBio 8. https://doi.org/10.1128/mBio.01754-17.

Kudchodkar, S.B., Del Prete, G.Q., Maguire, T.G., Alwine, J.C., 2007. AMPK-mediated inhibition of mTOR kinase is circumvented during immediate-early times of human cytomegalovirus infection. J. Virol. 81, 3649–3651. https://doi.org/10.1128/JVI.02079-06.

Kumar, N., Sharma, S., Kumar, R., Tripathi, B.N., Barua, S., Ly, H., Rouse, B.T., 2020. Host-Directed antiviral therapy. Clin. Microbiol. Rev. 33 https://doi.org/10.1128/CMR.00168-19.

Kump, K.J., Miao, L., Mady, A.S.A., Ansari, N.H., Shrestha, U.K., Yang, Y., Pal, M., Liao, C., Perdih, A., Abulwerdi, F.A., Chinnaswamy, K., Meagher, J.L., Carlson, J.M., Khanna, M., Stuckey, J.A., Nikolovska-Coleska, Z., 2020. Discovery and characterization of 2,5-substituted benzoic acid dual inhibitors of the anti-apoptotic Mcl-1 and Bfl-1 proteins. J. Med. Chem. 63, 2489–2510. https://doi.org/10.1021/acs.jmedchem.9b01442.

Lee, A.C.Y., Zhang, A.J.X., Chu, H., Li, C., Zhu, H., Mak, W.W.N., Chen, Y., Kok, K.H., To, K.K.W., Yuen, K.Y., 2019. H7N9 influenza A virus activation of necroptosis in human monocytes links innate and adaptive immune responses. Cell Death Dis. 10, 442. https://doi.org/10.1038/s41419-019-1684-0.

Liu, P.Y., Xu, N., Malyukova, A., Scarlett, C.J., Sun, Y.T., Zhang, X.D., Ling, D., Su, S.P., Nelson, C., Chang, D.K., Koach, J., Tee, A.E., Haber, M., Norris, M.D., Toon, C., Rooman, I., Xue, C., Cheung, B.B., Kumar, S., Marshall, G.M., Biankin, A.V., Liu, T., 2013. The histone deacetylase SIRT2 stabilizes Myc oncoproteins. Cell Death Differ. 20, 503–514. https://doi.org/10.1038/cdd.2012.147.

Liu, Q., Qiu, J., Liang, M., Golinski, J., van Leyen, K., Jung, J.E., You, Z., Lo, E.H., Degterev, A., Whalen, M.J., 2014. Akt and mTOR mediate programmed necrosis in neurons. Cell Death Dis. 5, e1084 https://doi.org/10.1038/cddis.2014.69.

Luo, G., Jian, Z., Zhu, Y., Zhu, Y., Chen, B., Ma, R., Tang, F., Xiao, Y., 2019. Sirt1 promotes autophagy and inhibits apoptosis to protect cardiomyocytes from hypoxic stress. Int. J. Mol. Med. 43, 2033–2043. https://doi.org/10.3892/ijmm.2019.4125.

Luo, J., Manning, B.D., Cantley, L.C., 2003. Targeting the PI3K-Akt pathway in human cancer: rationale and promise. Cancer Cell 4, 257–262. https://doi.org/10.1016/s1535-6108(03)00248-4.

Maertens, J., Cordonnier, C., Jaksch, P., Poiré, X., Uknis, M., Wu, J., Wijatyk, A., Saliba, F., Witzke, O., Villano, S., 2019. Maribavir for preemptive treatment of cytomegalovirus reactivation. N. Engl. J. Med. 381, 1136–1147. https://doi.org/10.1056/NEJMoa1714656.

Mahmud, J., Miller, M.J., Altman, A.M., Chan, G.C., 2020. Human cytomegalovirus glycoprotein-initiated signaling mediates the aberrant activation of Akt. J. Virol. 94 https://doi.org/10.1128/JVI.00167-20.

Manez, R., Kusne, S., Rinaldo, C., Aguado, J.M., St George, K., Grossi, P., Frye, B., Fung, J.J., Ehrlich, G.D., 1996. Time to detection of cytomegalovirus (CMV) DNA in blood leukocytes is a predictor for the development of CMV disease in CMV-seronegative recipients of allografts from CMV-seropositive donors following liver transplantation. J. Infect. Dis. 173, 1072–1076. https://doi.org/10.1093/infdis/173.5.1072.

Mangan, D.F., Mergenhagen, S.E., Wahl, S.M., 1993. Apoptosis in human monocytes: possible role in chronic inflammatory diseases. J. Periodontol. 64, 461–466.

Mao, G., Li, H., Ding, X., Meng, X., Wang, G., Leng, S.X., 2016. Suppressive effects of sirtinol on human cytomegalovirus (hCMV) infection and hCMV-induced activation of molecular mechanisms of senescence and production of reactive oxygen species. Mech. Ageing Dev. 158, 62–69. https://doi.org/10.1016/j.mad.2015.12.005.

Matthews, T., Boehme, R., 1988. Antiviral activity and mechanism of action of ganciclovir. Rev. Infect. Dis. 10 (Suppl 3), S490–S494. https://doi.org/10.1093/clinids/10.supplement_3.s490.

McNamara, C.R., Ahuja, R., Osafo-Addo, A.D., Barrows, D., Kettenbach, A., Skidan, I., Teng, X., Cuny, G.D., Gerber, S., Degterev, A., 2013. Akt Regulates TNFalpha synthesis downstream of RIP1 kinase activation during necroptosis. PLoS One 8, e56576. https://doi.org/10.1371/journal.pone.0056576.

Min, C.K., Shakya, A.K., Lee, B.J., Streblow, D.N., Caposio, P., Yurochko, A.D., 2020. The differentiation of human cytomegalovirus infected-monocytes is required for viral replication. Front. Cell. Infect. Microbiol. 10, 368. https://doi.org/10.3389/fcimb.2020.00368.

Mocarski, E.S., Guo, H., Kaiser, W.J., 2015. Necroptosis: the Trojan horse in cell autonomous antiviral host defense. Virology 479–480, 160–166. https://doi.org/10.1016/j.virol.2015.03.016.

Mocarski, E.S., Upton, J.W., Kaiser, W.J., 2011. Viral infection and the evolution of caspase 8-regulated apoptotic and necrotic death pathways. Nat. Rev. Immunol. 12, 79–88. https://doi.org/10.1038/nri3131.

Moorman, N.J., Cristea, I.M., Terhune, S.S., Rout, M.P., Chait, B.T., Shenk, T., 2008. Human cytomegalovirus protein UL38 inhibits host cell stress responses by antagonizing the tuberous sclerosis protein complex. Cell Host Microbe 3, 253–262. https://doi.org/10.1016/j.chom.2008.03.002.

Nikitskaya, E., Lebedeva, A., Ivanova, O., Maryukhnich, E., Shpektor, A., Grivel, J.C., Margolis, L., Vasilieva, E., 2016. Cytomegalovirus-productive infection is associated with acute coronary syndrome. J. Am. Heart Assoc. 5 https://doi.org/10.1161/JAHA.116.003759.

Nikolovska-Coleska, Z., Wang, R., Fang, X., Pan, H., Tomita, Y., Li, P., Roller, P.P., Krajewski, K., Saito, N.G., Stuckey, J.A., Wang, S., 2004. Development and optimization of a binding assay for the XIAP BIR3 domain using fluorescence polarization. Anal. Biochem. 332, 261–273. https://doi.org/10.1016/j.ab.2004.05.055.

North, B.J., Marshall, B.L., Borra, M.T., Denu, J.M., Verdin, E., 2003. The human Sir2 ortholog, SIRT2, is an NAD+-dependent tubulin deacetylase. Mol. Cell 11, 437–444. https://doi.org/10.1016/s1097-2765(03)00038-8.

Opel, D., Poremba, C., Simon, T., Debatin, K.M., Fulda, S., 2007. Activation of Akt predicts poor outcome in neuroblastoma. Cancer Res. 67, 735–745. https://doi.org/10.1158/0008-5472.CAN-06-2201.

Patel, A.A., Zhang, Y., Fullerton, J.N., Boelen, L., Rongvaux, A., Maini, A.A., Bigley, V., Flavell, R.A., Gilroy, D.W., Asquith, B., Macallan, D., Yona, S., 2017. The fate and lifespan of human monocyte subsets in steady state and systemic inflammation. J. Exp. Med. 214, 1913–1923. https://doi.org/10.1084/jem.20170355.

Patel, R., Paya, C.V., 1997. Infections in solid-organ transplant recipients. Clin. Microbiol. Rev. 10, 86–124. https://doi.org/10.1128/CMR.10.1.86.

Patil, A.J., Sharma, A., Kenney, M.C., Kuppermann, B.D., 2010. Valganciclovir in the treatment of cytomegalovirus retinitis in HIV-infected patients. Clin. Ophthalmol. 4, 111–119. https://doi.org/10.2147/opth.s3248.

Peppenelli, M.A., Arend, K.C., Cojohari, O., Moorman, N.J., Chan, G.C., 2016. Human cytomegalovirus stimulates the synthesis of select Akt-dependent antiapoptotic proteins during viral entry to promote survival of infected monocytes. J. Virol. 90, 3138–3147. https://doi.org/10.1128/JVI.02879-15.

Peppenelli, M.A., Miller, M.J., Altman, A.M., Cojohari, O., Chan, G.C., 2018. Aberrant regulation of the Akt signaling network by human cytomegalovirus allows for targeting of infected monocytes. Antivir. Res. 158, 13–24. https://doi.org/10.1016/j.antiviral.2018.07.015.

Perrottet, N., Decosterd, L.A., Meylan, P., Pascual, M., Biollaz, J., Buclin, T., 2009. Valganciclovir in adult solid organ transplant recipients: pharmacokinetic and pharmacodynamic characteristics and clinical interpretation of plasma concentration measurements. Clin. Pharmacokinet. 48, 399–418. https://doi.org/10.2165/00003088-200948060-00006.

Rahman, M., Dastmalchi, F., Karachi, A., Mitchell, D., 2019. The role of CMV in glioblastoma and implications for immunotherapeutic strategies. OncoImmunology 8, e1514921. https://doi.org/10.1080/2162402X.2018.1514921.

Ramakrishnan, G., Davaakhuu, G., Kaplun, L., Chung, W.C., Rana, A., Atfi, A., Miele, L., Tzivion, G., 2014. SIRT2 deacetylase is a novel AKT binding partner critical for AKT activation by insulin. J. Biol. Chem. 289, 6054–6066. https://doi.org/10.1074/jbc.M113.537266.

Reeves, M.B., Breidenstein, A., Compton, T., 2012. Human cytomegalovirus activation of ERK and myeloid cell leukemia-1 protein correlates with survival of latently infected cells. Proc. Natl. Acad. Sci. U. S. A. 109, 588–593. https://doi.org/10.1073/pnas.1114966108.

Roche, K.L., Remiszewski, S., Todd, M.J., Kulp 3rd, J.L., Tang, L., Welsh, A.V., Barry, A. P., De, C., Reiley, W.W., Wahl, A., Garcia, J.V., Luftig, M.A., Shenk, T., Tonra, J.R., Murphy, E.A., Chiang, L.W., 2023. An allosteric inhibitor of sirtuin 2 deacetylase activity exhibits broad-spectrum antiviral activity. J. Clin. Invest. 133 https://doi.org/10.1172/JCI158978.

Rossetto, C.C., Tarrant-Elorza, M., Pari, G.S., 2013. Cis and trans acting factors involved in human cytomegalovirus experimental and natural latent infection of CD14 (+) monocytes and CD34 (+) cells. PLoS Pathog. 9, e1003366 https://doi.org/10.1371/journal.ppat.1003366.

Sinclair, J., Sissons, P., 1996. Latent and persistent infections of monocytes and macrophages. Intervirology 39, 293–301.
Singh, N., 2005. Late-onset cytomegalovirus disease as a significant complication in solid organ transplant recipients receiving antiviral prophylaxis: a call to heed the mounting evidence. Clin. Infect. Dis. 40, 704–708. https://doi.org/10.1086/427506.
Smith, M.S., Bentz, G.L., Alexander, J.S., Yurochko, A.D., 2004a. Human cytomegalovirus induces monocyte differentiation and migration as a strategy for dissemination and persistence. J. Virol. 78, 4444–4453. https://doi.org/10.1128/jvi.78.9.4444-4453.2004.
Smith, M.S., Bentz, G.L., Smith, P.M., Bivins, E.R., Yurochko, A.D., 2004b. HCMV activates PI(3)K in monocytes and promotes monocyte motility and transendothelial migration in a PI(3)K-dependent manner. J. Leukoc. Biol. 76, 65–76. https://doi.org/10.1189/jlb.1203621.
Smith, M.S., Bivins-Smith, E.R., Tilley, A.M., Bentz, G.L., Chan, G., Minard, J., Yurochko, A.D., 2007. Roles of phosphatidylinositol 3-kinase and NF-kappaB in human cytomegalovirus-mediated monocyte diapedesis and adhesion: strategy for viral persistence. J. Virol. 81, 7683–7694. https://doi.org/10.1128/JVI.02839-06.
Smith, N.A., Chan, G.C., O'Connor, C.M., 2021. Modulation of host cell signaling during cytomegalovirus latency and reactivation. Virol. J. 18, 207. https://doi.org/10.1186/s12985-021-01674-1.
Soderberg-Naucler, C., Streblow, D.N., Fish, K.N., Allan-Yorke, J., Smith, P.P., Nelson, J. A., 2001. Reactivation of latent human cytomegalovirus in CD14(+) monocytes is differentiation dependent. J. Virol. 75, 7543–7554. https://doi.org/10.1128/JVI.75.16.7543-7554.2001.
Song, G., Lu, H., Chen, F., Wang, Y., Fan, W., Shao, W., Lu, H., Lin, B., 2018. Tetrahydrocurcumininduced autophagy via suppression of PI3K/Akt/mTOR in nonsmall cell lung carcinoma cells. Mol. Med. Rep. 17, 5964–5969. https://doi.org/10.3892/mmr.2018.8600.
Song, S., Ding, Y., Dai, G.L., Zhang, Y., Xu, M.T., Shen, J.R., Chen, T.T., Chen, Y., Meng, G.L., 2021. Sirtuin 3 deficiency exacerbates diabetic cardiomyopathy via necroptosis enhancement and NLRP3 activation. Acta Pharmacol. Sin. 42, 230–241. https://doi.org/10.1038/s41401-020-0490-7.
Stevenson, E.V., Collins-McMillen, D., Kim, J.H., Cieply, S.J., Bentz, G.L., Yurochko, A.D., 2014. HCMV reprogramming of infected monocyte survival and differentiation: a Goldilocks phenomenon. Viruses 6, 782–807. https://doi.org/10.3390/v6020782.
Sundaresan, N.R., Pillai, V.B., Wolfgeher, D., Samant, S., Vasudevan, P., Parekh, V., Raghuraman, H., Cunningham, J.M., Gupta, M., Gupta, M.P., 2011. The deacetylase SIRT1 promotes membrane localization and activation of Akt and PDK1 during tumorigenesis and cardiac hypertrophy. Sci. Signal. 4, ra46. https://doi.org/10.1126/scisignal.2001465.
Tanida, I., Ueno, T., Kominami, E., 2008. LC3 and autophagy. Methods Mol. Biol. 445, 77–88. https://doi.org/10.1007/978-1-59745-157-4_4.
Taylor-Wiedeman, J., Sissons, P., Sinclair, J., 1994. Induction of endogenous human cytomegalovirus gene expression after differentiation of monocytes from healthy carriers. J. Virol. 68, 1597–1604. https://doi.org/10.1128/JVI.68.3.1597-1604.1994.
Tripathi, D., Sodani, M., Gupta, P.K., Kulkarni, S., 2021. Host directed therapies: COVID-19 and beyond. Curr Res Pharmacol Drug Discov 2, 100058. https://doi.org/10.1016/j.crphar.2021.100058.
Tsurutani, J., Fukuoka, J., Tsurutani, H., Shih, J.H., Hewitt, S.M., Travis, W.D., Jen, J., Dennis, P.A., 2006. Evaluation of two phosphorylation sites improves the prognostic significance of Akt activation in non-small-cell lung cancer tumors. J. Clin. Oncol. 24, 306–314. https://doi.org/10.1200/jco.2005.02.4133.
Upton, J.W., Chan, F.K., 2014. Staying alive: cell death in antiviral immunity. Mol. Cell 54, 273–280. https://doi.org/10.1016/j.molcel.2014.01.027.
Upton, J.W., Kaiser, W.J., Mocarski, E.S., 2008. Cytomegalovirus M45 cell death suppression requires receptor-interacting protein (RIP) homotypic interaction motif (RHIM)-dependent interaction with RIP1. J. Biol. Chem. 283, 16966–16970. https://doi.org/10.1074/jbc.C800051200.
Upton, J.W., Kaiser, W.J., Mocarski, E.S., 2010. Virus inhibition of RIP3-dependent necrosis. Cell Host Microbe 7, 302–313. https://doi.org/10.1016/j.chom.2010.03.006.
Upton, J.W., Kaiser, W.J., Mocarski, E.S., 2012. DAI/ZBP1/DLM-1 complexes with RIP3 to mediate virus-induced programmed necrosis that is targeted by murine cytomegalovirus vIRA. Cell Host Microbe 11, 290–297. https://doi.org/10.1016/j.chom.2012.01.016.
Verghese, P.S., Schleiss, M.R., 2013. Letermovir treatment of human cytomegalovirus infection antiinfective agent. Drugs Future 38, 291–298. https://doi.org/10.1358/dof.2013.038.05.1946425.
Wagenknecht, N., Reuter, N., Scherer, M., Reichel, A., Muller, R., Stamminger, T., 2015. Contribution of the major ND10 proteins PML, hDaxx and Sp100 to the regulation of human cytomegalovirus latency and lytic replication in the monocytic cell line THP-1. Viruses 7, 2884–2907. https://doi.org/10.3390/v7062751.
Wang, R.C., Wei, Y., An, Z., Zou, Z., Xiao, G., Bhagat, G., White, M., Reichelt, J., Levine, B., 2012. Akt-mediated regulation of autophagy and tumorigenesis through Beclin 1 phosphorylation. Science 338, 956–959. https://doi.org/10.1126/science.1225967.
Whitelaw, D.M., 1966. The intravascular lifespan of monocytes. Blood 28, 455–464.
Willis, S.N., Fletcher, J.I., Kaufmann, T., van Delft, M.F., Chen, L., Czabotar, P.E., Ierino, H., Lee, E.F., Fairlie, W.D., Bouillet, P., Strasser, A., Kluck, R.M., Adams, J.M., Huang, D.C., 2007. Apoptosis initiated when BH3 ligands engage multiple Bcl-2 homologs, not Bax or Bak. Science 315, 856–859. https://doi.org/10.1126/science.1133289.
Xu, D., Jiang, X., He, H., Liu, D., Yang, L., Chen, H., Wu, L., Geng, G., Li, Q., 2019. SIRT2 functions in aging, autophagy, and apoptosis in post-maturation bovine oocytes. Life Sci. 232, 116639. https://doi.org/10.1016/j.lfs.2019.116639.
Yung, H.W., Charnock-Jones, D.S., Burton, G.J., 2011. Regulation of AKT phosphorylation at Ser473 and Thr308 by endoplasmic reticulum stress modulates substrate specificity in a severity dependent manner. PLoS One 6, e17894. https://doi.org/10.1371/journal.pone.0017894.
Yurochko, A.D., Huang, E.S., 1999. Human cytomegalovirus binding to human monocytes induces immunoregulatory gene expression. J. Immunol. 162, 4806–4816.
Yurochko, A.D., Hwang, E.S., Rasmussen, L., Keay, S., Pereira, L., Huang, E.S., 1997. The human cytomegalovirus UL55 (gB) and UL75 (gH) glycoprotein ligands initiate the rapid activation of Sp1 and NF-kappaB during infection. J. Virol. 71, 5051–5059. https://doi.org/10.1128/JVI.71.7.5051-5059.1997.
Yurochko, A.D., Liu, D.Y., Eierman, D., Haskill, S., 1992. Integrins as a primary signal transduction molecule regulating monocyte immediate-early gene induction. Proc. Natl. Acad. Sci. U. S. A. 89, 9034–9038.
Zuhair, M., Smit, G.S.A., Wallis, G., Jabbar, F., Smith, C., Devleesschauwer, B., Griffiths, P., 2019. Estimation of the worldwide seroprevalence of cytomegalovirus: a systematic review and meta-analysis. Rev. Med. Virol. 29, e2034 https://doi.org/10.1002/rmv.2034.

Evrys Bio, LLC

Unaudited Financial Statements

STATEMENT OF INCOME

	Twelve months ended December 31,		
	2023	2022	2021
Revenues			
Government Grants	$ 758,201	$ 176,727	$ 2,259,470
Research Contracts	$ 5,483,792	$ 3,622,475	$ 920,153
Other Income *	$ 65,205	$ 8,277	$ 208,216
Total Revenue	$ 6,307,199	$ 3,807,479	$ 3,387,839
Operating Expenses			
Research and Development	$ 5,646,831	$ 4,497,631	$ 2,958,970
General and Administrative	$ 1,459,202	$ 1,212,498	$ 1,043,336
Total Operating Expenses	$ 7,106,032	$ 5,710,129	$ 4,002,305
Net Income (Loss)	$ (798,833)	$ (1,902,650)	$ (614,467)

* *Other Income 2021 is from sale of Tax Credits*

Evrys Bio, LLC

Unaudited Financial Statements

STATEMENT OF FINANCIAL POSITION

	December 31, 2023	December 31, 2022	December 31, 2021
Assets			
Cash	$ 2,200,510	$ 2,736,485	$ 1,015,272
Accounts Receivable	$ 746,317	$ 273,884	$ 405,826
Other Current Assets	$ 110,742	$ 84,208	$ 162,043
Total current assets	$ 3,057,568	$ 3,094,577	$ 1,583,141
Property and equipment	$ 99,805	$ 127,025	$ -
Total Assets	$ 3,157,374	$ 3,221,602	$ 1,583,141
Liabilities and Members' Equity			
Current Liabilities			
Accounts Payable	$ 588,210	$ 350,542	$ 119,824
Other Current Liabilities	$ 620,877	$ 97,643	$ 405,743
Total Current Liabilities	$ 1,209,087	$ 448,185	$ 525,567
Long Term Liabilities	$ 83,882	$ 110,179	$ -
Total Liabilities	$ 1,292,969	$ 558,364	$ 525,567
Members' Equity			
Members' Equity	$ 2,663,238	$ 4,565,888	$ 1,672,041
Net Income	$ (798,833)	$ (1,902,650)	$ (614,467)
Total Member's Equity (deficit)	$ 1,864,405	$ 2,663,238	$ 1,057,575
Total Liabilities and Members' Equity (deficit)	$ 3,157,374	$ 3,221,602	$ 1,583,141

Evrys Bio, LLC
Summary Capitalization Table as of 12/31/2023

		Shares	Percent
Primary			
Class 1 Stock		6,150,417	76.95%
Class 2 Stock		937,315	11.73%
Class 3 Stock		904,635	11.32%
	Total	7,992,367	100.00%
Fully Diluted			
Class 1 Stock		6,150,417	28.02%
Class 2 Stock		937,315	4.27%
Class 3 Stock		904,635	4.12%
Class A Convertible Preferred Stock		4,500,000	20.50%
Class A-1 Convertible Preferred Stock		4,360,142	19.86%
Warrants Pfd A-1		1,591,976	7.25%
Total A-1		5,952,118	27.12%
Series B Convertible Preferred Stock		1,652,993	7.53%
Series B-1 Convertible Preferred Stock		706,755	3.22%
Class 3 Stock			
Warrants		45,977	0.21%
Stock Options		1,099,690	5.01%
	Total	21,949,900	100.00%